Molecular Mechanisms of Kinetochore Microtubule Attachment

ARCHIVES
MASSACHUSETTS INSTITUTE OF TECHNOLOGY
AUG 0 1 2012
LIBRARIES

Jens C. Schmidt

Diplom in Biochemistry
Freie Universität Berlin
2007

Submitted to the Department of Biology in partial fulfillment
of the requirements for the degree of

Doctor of Philosophy in Biology
Massachusetts Institute of Technology

© 2012 Jens C. Schmidt. All rights reserved.

The author hereby grants to MIT permission to reproduce
and to distribute publicly paper and electronic
copies of this thesis document in whole or in part
in any medium known or hereafter created.

Signature of the author: _____
Department of Biology
August 6, 2012

Certified by: _____
Iain M. Cheeseman
Professor in Biology
Thesis Supervisor

Certified by: _____
Robert T. Sauer
Professor in Biology
Chair, Committee for Graduate Students

Molecular Mechanisms of Kinetochore Microtubule Attachment

Jens C. Schmidt

Submitted to the Department of Biology on August 8th, 2012 in partial fulfillment of the requirements for the degree of Doctor of Philosophy in Biology

Abstract

To ensure equal chromosome segregation during mitosis, the macromolecular kinetochore must remain attached to depolymerizing microtubules, which drive poleward chromosome movement. Microtubules are highly dynamic structures that undergo dramatic structural changes during depolymerization. The results presented in this thesis define essential functions of the Astrin-SKAP-LC8 and Ska1 complexes at the kinetochore-microtubule interface. First, we demonstrate that the Astrin-SKAP-LC8 complex localizes preferentially to kinetochores of bi-oriented sister chromatids. Localization of the Astrin-SKAP-LC8 complex to kinetochores is controlled by a key regulator of kinetochore-microtubule attachments, Aurora B kinase. The Astrin-SKAP-LC8 complex is essential for mitotic progression and directly associates with microtubules. Furthermore, the microtubule polymerization factor CLASP requires the Astrin-SKAP-LC8 complex to localize to kinetochores. Second, we demonstrate that the Ska1 complex has many of the biochemical and biophysical properties of a molecular machine that can couple microtubule depolymerization to chromosome movement. The Ska1 complex diffuses on and tracks with depolymerizing microtubules and its microtubule binding activity is necessary to maintain kinetochore-fibers and power chromosome oscillations during metaphase. Importantly, we demonstrate that the Ska1 complex directly interacts with the peeling protofilaments present at the depolymerizing microtubule end, suggesting a unique mechanism by which the Ska1 complex remains attached to depolymerizing microtubules. Finally, we demonstrate that the Ska1 microtubule-binding domain has two conserved basic regions that are required for microtubule binding and are subject to regulation by Aurora B kinase. In total, we define essential properties of the Astrin-SKAP-LC8 and Ska1 complex required for the formation of kinetochore microtubule attachments.

Thesis Supervisor: Iain M. Cheeseman, Associate Professor of Biology

Acknowledgements

I have had the privilege of being the first graduate student in the Cheeseman Lab. I could not imagine a better environment to carry out my grad school research. Iain thank you for being an amazing mentor. The positive energy you bring to the lab, the constants encouragement and your unbelievable excitement, even about the most insignificant IF experiments, is truly inspiring. I have learned a lot from you about all aspects of scientific life and the trust you put in me to try whatever I wanted to is very much appreciated. If I ever run my own lab my goal will be to create an environment that is as positive and productive as it is in the Cheeseman Lab and I will try my best to pass on all the things I have learned from you, especially your sophisticated biochemical knowledge.

To my wife Chrissy. Thank you for your support and encouragement, although pipetting clear liquids from one tube into another seems boring. And most importantly thank you for understanding that an experiment that is supposed to take an hour, most likely takes two. I could not have done this without you and I would have never came to MIT in the first place, if it wasn't for you. I love you and I am very fortunate to have you by my side.

To my parents and my siblings. I am very fortunate to have such an amazing family. Thank you for your support and understanding of me moving far away to pursue my goals and dreams. And most importantly thank you for teaching me that you cannot be successful without working hard. I miss you all.

Thank you to all the members of the Cheeseman Lab. Karen, Tomomi, and Julie thank you for sharing your knowledge, always being open for discussions and being great examples for how to work efficiently. And most importantly, thank you for not constantly flashing your millions of Postdoc Dollars in my face. Chelsea, thank you for being the wizard behind the scenes. The lab would not run without you. So many of the reagents I use I look at and think "Oh yeah, Chelsea made that!". David, thank you for ganging up on Iain with me. Some day biochemistry will be ... Oh wait, never mind. Florencia and Kara, thanks for taking two of my four benches, making me listen to "Call me maybe" over and over again and once in a great while listening to "techno" music with me. I have had a great time with all of you and if I had to tell you one final thing I would say "Do more controls!", since Iain wont.

To my thesis committee members Angelika, Thomas, and Sam – thank your for your input and advice. I really appreciate you taking the time to help me throughout my time at MIT.

Table of Contents

Chapter I: Introduction

Mitosis

Development and tissue maintenance for multicellular organisms requires cell division. Approximately 10,000 trillion cell divisions occur during the lifetime of a human. During mitosis, the replicated genomic material is equally segregated generating two identical daughter cells. Faithfull chromosome segregation is essential because errors during this process are usually fatal for the daughter cells. Furthermore, non-diploid chromosome content, termed aneuploidy, can result from chromosome mis-segregation and is a hallmark of most cancers in humans (reviewed in (Gordon et al., 2012)).

Mitosis can be divided into five phases: Prophase, Prometaphase, Metaphase, Anaphase, and Telophase (Fig. 1). During prophase, replicated sister chromatids condense, forming compact structures, the bipolar mitotic spindle forms, and the nuclear envelope breaks down allowing the mitotic spindle to access the chromosomes. Prophase is followed by prometaphase, during which the bipolar mitotic spindle captures sister chromatids and drives chromosome movement to the spindle equator, also called the metaphase plate. To ensure proper chromosome segregation, replicated sister-chromatids must attach to microtubules emanating from opposite poles of the mitotic spindle at a single site on each chromosome, termed the kinetochore. The kinetochore is a large multi-protein complex that assembles on centromeric chromatin.

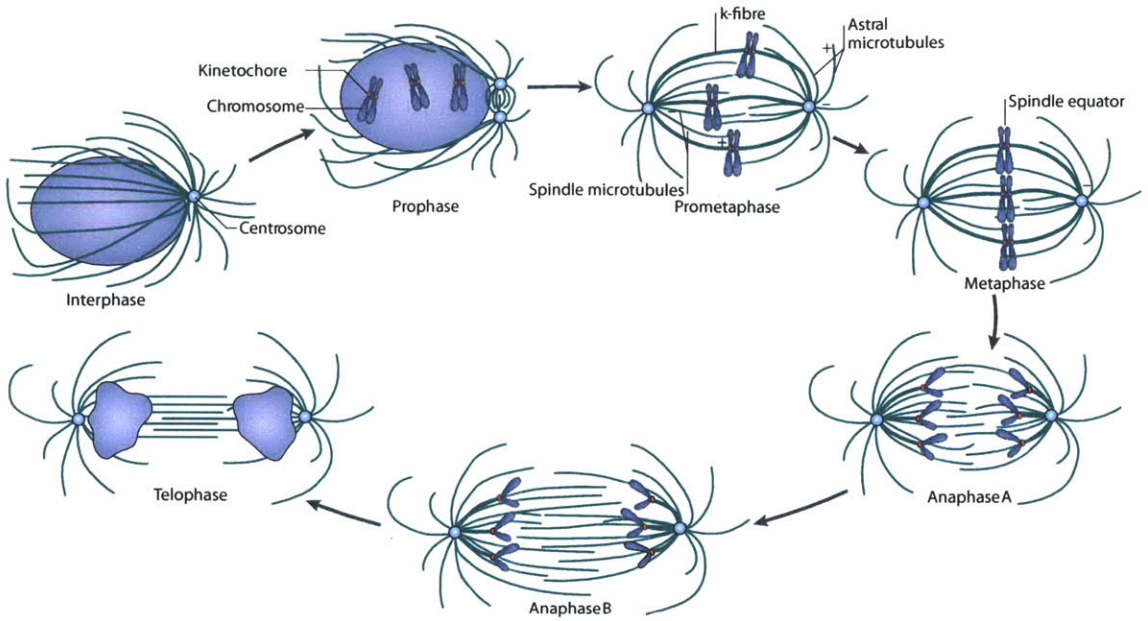

Figure 1. Structure of the mitotic spindle throughout mitosis. (Reproduced from (Walczak et al., 2010), Copyright © 2010 with permission from Nature Publishing Group) Diagram, showing mitotic spindle and chromosome morphology throughout the different stages of mitosis. During prophase chromosomes condense and the nuclear envelope breaks down. The bipolar spindle assembles and chromosomes congress to the metaphase plate during prometaphase. All chromosome are aligned at the metaphase plate and spindle assembly checkpoint is satisfied during metaphase. Chromosome segregation is triggered at the onset of anaphase, which proceeds by shortening of K-fibers during anaphase A, and central spindle elongation and movement of the spindle poles towards the cell cortex in anaphase B. During telophase chromosomes decondense, the nuclear envelope reforms and mitosis concludes with the formation of two daughter cells during cytokinesis.

The primary function of the kinetochore is to form the connection between the mitotic spindle-microtubules and the chromosome-DNA (reviewed in (Cheeseman and Desai, 2008)).

During chromosome congression to the metaphase plate, chromosome movement is powered in a variety of ways. Molecular motors such as the kinesin CENP-E and dynein, which bind laterally to microtubules, localize to the

kinetochore and power both plus and minus end directed movement of chromosomes along microtubule tracks. In addition, force generated by microtubule depolymerization plays a crucial role in chromosome movement throughout mitosis. To utilize microtubule depolymerization as an energy source for chromosome movement, the microtubule plus-end is positioned directly at the kinetochore through an end-on attachment (reviewed in (Kops et al., 2010)).

After chromosome congression is completed during prometaphase and all chromosomes are aligned, this phase of mitosis is termed metaphase. The spindle assembly checkpoint (SAC) monitors the attachment of kinetochores to the mitotic spindle and prevents the progression into the next stage of the cell cycle until all chromosomes are bi-oriented, such that the kinetochores from the sister-chromatid are bound to microtubules emanating from opposing spindle poles. Once all chromosomes are correctly bi-oriented, the SAC is "satisfied" and no longer inhibits the progression of the cell cycle. The Anaphase Promoting Complex then degrades cyclin-B and securin, the inhibitor of the protease separase. Separase in turn triggers chromosome separation by the cleavage of the centromeric cohesin molecules that connect the sister chromatids, resulting in anaphase (reviewed in (Musacchio and Salmon, 2007)).

Anaphase proceeds in two distinct steps. During anaphase A, the microtubules connecting the spindle pole and the kinetochore shorten, pulling the chromosomes towards the spindle poles. During anaphase B, the spindle midzone elongates and spindle poles are pulled towards the cell cortex, further

separating the sister chromatids. Anaphase B is mediated by pulling forces exerted by cortically localized dynein motors that pull on the astral microtubules connecting the spindle poles and the cell cortex, and by motors at the spindle midzone that slide the two half spindles apart (reviewed in (Walzcak et al., 2010)).

Mitosis concludes with telophase, during which the nuclear envelope reforms and chromosomes de-condense. The two daughter cells are formed by contraction of an actin and myosin ring at the cleavage furrow, which assembles on the plasma membrane around the spindle-midzone, between the chromosome masses, in a process that is termed cytokinesis (reviewed in (Fededa and Gerlich, 2012)).

Although many molecular details of mitosis are well understood, the forces that govern chromosome movements and the molecular players involved in this process are poorly defined. In this introduction, I will focus on the molecular players and mechanisms that allow kinetochores to utilize microtubule-depolymerization derived forces to drive chromosome segregation and ensure proper chromosome bi-orientation by generating tension between sister-chromatids.

Microtubules and their dynamic properties

The main component of the mitotic spindle is microtubules. Microtubules are composed of alpha/beta-tubulin heterodimers, which form a cylindrical tube by

lateral association of 13-15 linear tubulin polymers called protofilaments (Fig. 2). Due to the asymmetry of the tubulin-heterodimer, microtubules are polar with a fast growing plus end that associates with the kinetochore and a slower growing minus end located at the spindle pole (reviewed in (Desai and Mitchison, 1997)).

Microtubule assembly is driven by the hydrolysis of GTP. Both alpha- and beta-tubulin can bind GTP, and only the GTP bound tubulin-heterodimers can be incorporated into microtubules. Upon incorporation into the microtubule lattice, GTP in the beta-tubulin subunit is rapidly hydrolyzed to GDP and phosphate. Importantly, the GDP bound tubulin-heterodimer has a slightly kinked conformation relative to GTP bound heterodimers (Wang and Nogales, 2005), but is forced into a straight conformation in the context of the microtubule lattice (Fig. 2A). Thus, microtubules store potential energy derived from the hydrolysis of GTP. As a consequence microtubules display a characteristic property called dynamic instability. During microtubule polymerization, the tubulin-heterodimers at the growing end are GTP-bound, forming a stabilizing GTP-cap. When GTP hydrolysis occurs more rapidly than heterodimer incorporation or when other errors occur during microtubule polymerization, GDP-bound tubulin-heterodimers are exposed at the microtubule end and are free to assume their curved conformation as they are no longer constrained by the lateral contacts in the microtubule lattice. This conformational change generates a powerstroke of around 5 pN of force per protofilament (Grishchuk et al., 2005b). This transition is called catastrophe and leads to rapid depolymerization of the microtubule and the

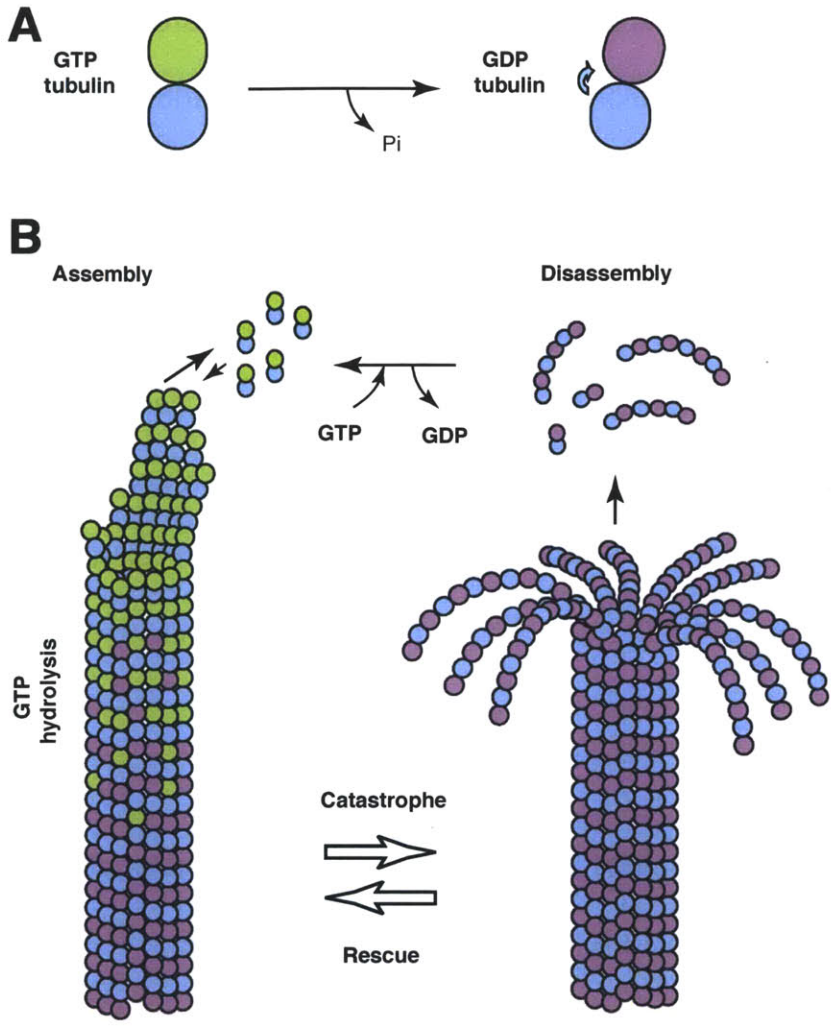

Figure 2. Structure and dynamics of microtubules. (Reproduced from (Al-Bassam and Chang, 2011), Copyright © 2011 with permission from Elsevier) (*A*) The structure of the tubulin dimer is influenced by the nucleotide state. The GTP-bound tubulin dimer has a straight conformation, while the GDP-bound tubulin dimers is slightly kinked. (*B*) GTP-bound tubulin dimers are incorporated into the growing microtubule and form a stabilizing GTP-cap, before hydrolyzing GTP to GDP in the context of the microtubule lattice, forcing the kinked GDP-bound tubulin dimer into a straight conformation. Catastrophe occurs when GDP-bound tubulin subunits are exposed at the microtubule end, allowing the GDP-bound tubulin dimers to assume their curved conformation, leading to the formation of characteristic rams horn structures and rapid microtubule depolymerization.

formation of characteristic bent protofilaments at the depolymerizing microtubule end. A depolymerizing microtubule can switch back into a polymerizing state by a

rescue step. The molecular details of this transition are poorly understood, but may involve re-association of GTP bound tubulin-heterodimers at the microtubule end. Thus, microtubules undergo cycles of polymerization, catastrophe, depolymerization, and rescue, together are termed dynamic instability. The rates and frequencies of these different steps are modulated in cells by a diverse set of enzymes. Kinesins such as the kinesin-13 MCAK can promote microtubule catastrophe and depolymerization, while TOG domain containing proteins such as XMAP215/Stu2p or CLASP can accelerate polymerization or promote rescue (Al-Bassam et al., 2010; Brouhard et al., 2008; Wordeman et al., 2007).

The mitotic spindle

To facilitate chromosomes segregation to the two daughter cells a bi-polar array of microtubules termed the mitotic spindle must form (Fig. 1). The mitotic spindle is a symmetric, antiparallel array of microtubules emanating from two spindle poles. At the core of each spindle pole is the centrosome, which is present in two copies before the onset of prophase. Like chromosomes, centrioles, the core component of centrosomes, duplicate once and only once per cell cycle in a semiconservative fashion, assuring that exactly two spindle poles are present during mitotic spindle assembly. Centrioles recruit the pericentriolar material that includes many factors that drive microtubule nucleation and growth. The gamma-tubulin ring complex (gamma-TuRC), for instance, is recruited to centrosomes and nucleates microtubules with their plus ends away from the spindle pole and

their minus ends anchored at the centrosome. Before the onset of mitosis, the two centrosomes are closely associated at the outer face of the nucleus. To form the bi-polar mitotic spindle, the spindle poles must separate. This separation is achieved by a combination of the dynein motor focusing microtubules at the spindle pole and the tetrameric kinesin Eg-5 pushing the spindle poles apart by generating anti-parallel sliding forces on microtubules emanating from the opposing spindle poles. The resulting structure is a football-shaped array of anti-parallel microtubules, with the plus ends of the microtubule pointing away from the spindle poles. Astral microtubules anchor the spindle poles to the cell cortex and position the spindle within the cell. This arrangement allows the chromosomes to attach to microtubule plus ends, which in turn can drive chromosome congression during prometaphase and chromosome segregation during anaphase (reviewed in (Walczak and Heald, 2008)).

Kinetochore architecture and assembly

The kinetochore is a large multi-protein complex that is assembled on centromeric DNA and mediates the connection between the mitotic spindle and the chromosomes (Fig. 3, (Cheeseman and Desai, 2008)). In addition to structural roles, the kinetochore serves an important regulatory role. Key components of the SAC localize to kinetochores to monitor kinetochore-microtubule attachment (Musacchio and Salmon, 2007). The kinetochore can be subdivided into two general regions, visible as separate bar shaped structures in

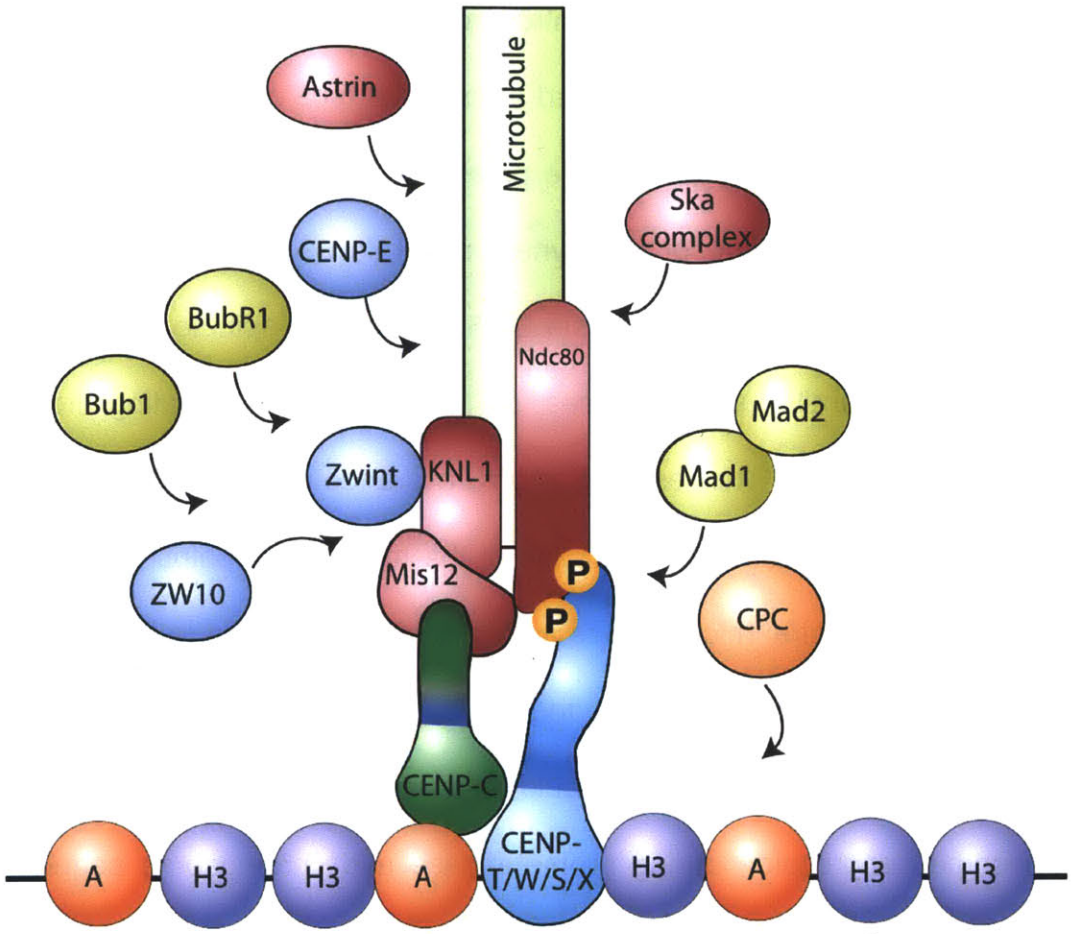

Figure 3. Composition of the vertebrate kinetochore. The histone H3 variant CENP-A is incorporated into centromeric chromatin and is necessary for kinetochore assembly. The inner kinetochore contains the CCAN, including the CENP-A binding partner CENP-C and the histone like CENP-T/W/S/X complex, which directly binds to DNA. In addition, the chromosomal passenger complex (CPC) localizes to the inner centromere and contains Aurora B kinase. The conserved KMN-network is the core component of the outer kinetochore and recruits SAC proteins as well as the Ska1 complex to kinetochores. Microtubule-binding, the key activity of the kinetochore, is carried out by the Ndc80 and Ska1 complexes.

conventional electron microscopy: an inner-kinetochore that directly contacts centromeric DNA, and an outer kinetochore that binds to spindle-microtubules. To date more than 100 different kinetochore components have been identified in

human cells, many of which are functionally poorly characterized (Cheeseman and Desai, 2008; Santaguida and Musacchio, 2009).

The inner kinetochore and the Constitutive Centromere Associated Network (CCAN)

The inner kinetochore mediates the direct connection between the kinetochore and the chromosomal DNA. The main components of the inner kinetochore is the constitutive centromere associated network (CCAN), which is localized to centromeric DNA throughout the cell cycle and forms a platform for outer-kinetochore assembly (Gascoigne and Cheeseman, 2011). The location of kinetochore assembly is epigenetically specified by the incorporation of the histone H3 variant CENP-A into centromeric histones (Dalal and Bui, 2010). In most cases in humans, the site of CENP-A assembly coincides with highly repetitive DNA sequences called alpha-satellite repeats. In human cells, the presence of CENP-A is necessary, but not sufficient for kinetochore assembly, with other unknown factors further contributing to centromere specification (Van Hooser et al., 2001). In addition to CENP-A, the histone-like, tetrameric CENP-S/X/T/W complex also has DNA binding activity and is necessary for proper kinetochore assembly (Nishino et al., 2012). CENP-C, which directly associates with CENP-A, and CENP-T are required to recruit all known outer kinetochore components (Gascoigne et al., 2011). Importantly, CENP-A, CENP-C and CENP-T localize to centromeric DNA throughout the cell cycle, whereas outer

kinetochore components do not assemble until entry into mitosis (Gascoigne and Cheeseman, 2011). This regulation is facilitated by phosphorylation of CENP-T and potentially other kinetochore components by CDK-cyclin B, upon entry into mitosis, allowing them to associate with their outer kinetochore binding partners (Gascoigne et al., 2011).

The outer kinetochore

Whereas the inner kinetochore facilitates the association of the kinetochore with centromeric DNA, the outer kinetochore mediates kinetochore-microtubule interactions and SAC signaling functions, as well as binding to other factors that regulate microtubule dynamics. The central and highly conserved component of the outer kinetochore is the Knl-1/Mis12-complex/Ndc80-complex (KMN) network, which forms a stable nine-protein assembly (Cheeseman et al., 2006; Cheeseman et al., 2004). The four-protein Mis12 complex is the central hub of the KMN network and is recruited to kinetochores via a direct interaction with CENP-C (Kline et al., 2006; Screpanti et al., 2011). The Mis12 complex directly binds to Knl1 and the Ndc80 complex (Cheeseman et al., 2006). Knl-1 is a large extended protein, which recruits the SAC components Bub1 and BubR1 to kinetochores as well as the protein phosphatase PP1gamma (Kiyomitsu et al., 2007; Liu et al., 2010), which is crucial for the formation of stable kinetochore-microtubule attachments. The final component of the KMN network is the four-protein Ndc80 complex, which binds microtubules directly via its chalponin

homology domain and its unstructured, charged, 80 amino-acid N-terminal tail (Cheeseman et al., 2006; Ciferri et al., 2008; Deluca et al., 2006). Furthermore, the Ndc80 complex is thought to be important for the recruitment of SAC components such as the Rod, ZW10, Zwilch (RZZ) complex and Mad1/2 (Musacchio and Salmon, 2007). Recent work has suggested that there are two independent pathways by which the Ndc80 complex is recruited to kinetochores. First, the Ndc80 complex associates with kinetochores as a component of the KMN network via a direct interaction with the Mis12 complex (Cheeseman et al., 2004). Second, the Ndc80 complex interacts with CENP-T in a manner that is dependent on prior phosphorylation of CENP-T by CDK/Cyclin B (Gascoigne et al., 2011).

Kinetochore-microtubule attachment

The central function of the kinetochore is to mediate the attachment of chromosomes to the mitotic spindle. To ensure equal chromosome segregation, sister-chromatids must bi-orient and remain attached to the mitotic spindle throughout mitosis. Spindle microtubules are highly dynamic structures, but they are stabilized at the kinetochore and form bundles of 15-20 microtubules termed kinetochore fibers (K-fibers) (McEwen et al., 1997). Depolymerization of K-fibers powers chromosome segregation in anaphase and provides the force to develop tension across sister-chromatids, which is necessary to ensure bi-orientation (McIntosh et al., 2010). However, thus far only two protein complexes have been

identified in human cells that localize to kinetochores, bind to microtubules, and are necessary for chromosome segregation; the Ndc80 complex and the Ska1 complex (Cheeseman et al., 2006; Deluca et al., 2006; Hanisch et al., 2006a; Hanisch et al., 2006b). Additional microtubule binding proteins localize to kinetochores to drive chromosome congression and the regulation of microtubule dynamics. These include the kinesin CENP-E, mitotic centromere associated kinesin (MCAK), and cytoplasmic dynein (Andrews et al., 2004; Howell et al., 2001; Kapoor et al., 2006; Pfarr et al., 1990; Wordeman and Mitchison, 1995; Yen et al., 1991).

The Ndc80 complex

The Ndc80 complex is a four-protein complex composed of Hec1 (Ndc80), Nuf2, Spc24 and Spc25 that is conserved throughout eukaryotes and is essential for kinetochore-microtubule attachment (Fig. 4A, (Cheeseman et al., 2006)). The Ndc80 complex has an extended coiled-coil region that includes the tetramerization interface. Within the coiled-coil of Ndc80, there is a 40 amino acid insertion that interrupts the coiled-coil and generates a flexible hinge region (Wang et al., 2008). In total, the complex spans a distance of approximately 55 nm (Wang et al., 2008). Spc24 and Spc25 form a globular RWD (RING finger-, WD-repeat, and DEAD-like proteins) domain, mediating interactions with both CENP-T and the Mis12 complex (Ciferri et al., 2008). The N-terminal regions of both Ndc80 and Nuf2 fold into chalponin homology domains, which directly

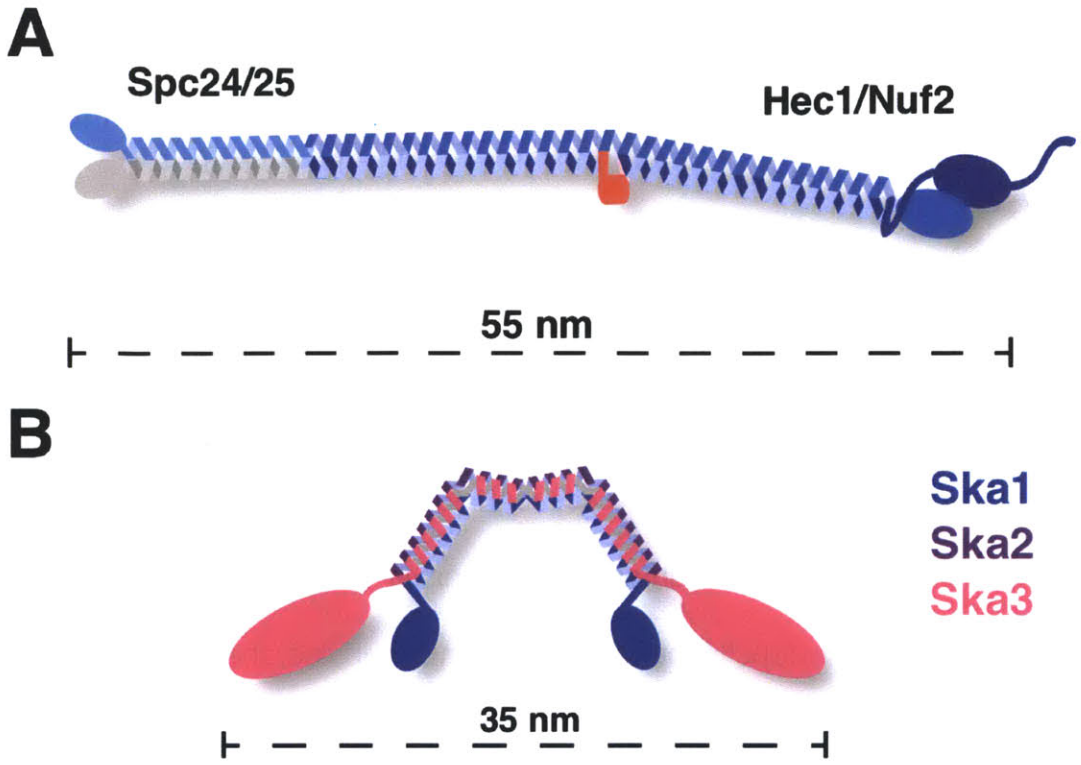

Figure 4. Composition of the Ndc80 and Ska1 complexes. (*A*) The four protein Ndc80 complex spans a total of 55 nm. Spc24/25 is responsible for kinetochore binding of the Ndc80 complex. Hec1/Nuf2 harbor the microtubule binding chalponin homology domain and disordered N-terminal tail. A 50 amino acids insertion (red) in the coiled-coil of Hec1 forms a loop and a flexible hinge region in the coiled-coil. (*B*) The three protein Ska1 complex forms a dimer of trimers. Ska2 together with the N-terminal 100 amino acids of Ska1 and Ska3 form a trimeric kinked coiled-coil. Based on static angle light scattering experiments to total complex spans about 35 nm (Jeyaprakash et al., 2012).

contact the microtubule lattice (Ciferri et al., 2008). In addition to binding to tubulin via its chalponin homology domain, Ndc80 also has an unstructured N-terminal tail of approximately 80 amino acids that directly interacts with microtubules (Guimaraes et al., 2008; Miller et al., 2008). The N-terminal tail contains several serine and threonine residues that are substrates for Aurora B

kinase (Cheeseman et al., 2006; Deluca et al., 2006). Phosphorylation of these residues reduces the microtubule binding affinity of the complex and is crucial to eliminate incorrect kinetochore-microtubule attachments (Cheeseman et al., 2006).

The Ska1 complex

Like the Ndc80 complex, the Ska1 complex localizes to kinetochores, binds to microtubules directly, and is necessary for the formation of kinetochore-microtubule interactions in human cells (Hanisch et al., 2006a; Welburn et al., 2009). In addition to directly interacting with microtubules, the Ska1 complex has been proposed to act as the coupler that allows kinetochores to remain attached to depolymerizing microtubules. Microspheres coated with Ska1 complex molecules are capable of tracking processively with depolymerizing microtubules in vitro (Welburn et al., 2009). The Ska1 complex is present in all vertebrates, but is absent in fungi and *Drosophila melanogaster*, although it is present in other insects. In human cells, the Ska1 complex is composed of three subunits, Ska1, Ska2, and Ska3 (Fig. 4B, (Welburn et al., 2009)).

Recently, a structure of the portion of the three proteins responsible for complex formation was solved, demonstrating that Ska2 together with the first 100 amino acids of Ska1 and Ska3 form a trimeric parallel coiled-coil that is kinked at approximately a sixty-degree angle after the first 30 amino acids (Fig. 4B, (Jeyaprakash et al., 2012)). Furthermore, the structure indicates that two

such coiled-coil trimers can dimerize into a hexamer, consistent with previous analyses by gel-filtration and sucrose gradient centrifugation. Importantly, the microtubule binding activity of the Ska1 complex is harbored in the sequences of the Ska1 complex that are not present in the structure that was solved.

Similarly to the Ndc80 complex, the Ska1 complex is a substrate for Aurora B kinase, with three phosphorylation sites on Ska3 and four phosphorylation sites on Ska1 (Chan et al., 2012). Phosphorylation of these sites is important for error correction, but also negatively regulates the recruitment of the Ska1 complex to kinetochores (Chan et al., 2012). The Ndc80 complex is directly required for the recruitment of the Ska1 complex the kinetochore, and the Ndc80 complex has therefore been proposed to be a direct binding partner of the Ska1 complex (Chan et al., 2012; Welburn et al., 2009; Zhang et al., 2012).

To define the mechanistic contribution of the Ska1 complex to coupling microtubule depolymerization to chromosome movement, it is critical to determine the biochemical and biophysical microtubule binding properties of the Ska1 complex. Importantly, in the context of the kinetochore, the microtubule binding activities of the Ndc80 and Ska1 complexes have to be coordinated. Thus, it is crucial to not only analyze the Ska1 and Ndc80 complexes in isolation, but also the combined activities of these proteins.

Astrin

Astrin was first identified as a mitotic spindle associated protein using mass-spectrometry (Mack and Compton, 2001). Astrin localizes to the mitotic spindle and kinetochores and is essential for mitotic progression (Gruber et al., 2002; Thein et al., 2007). Astrin is a dimer of 1193 amino acids with a N-terminal globular domain and two extended coiled-coil regions, which are interrupted by a short globular domain (Gruber et al., 2002). The precise functional role of Astrin in mitosis has yet to be established, although it has been implicated in the maintenance of centromeric cohesion (Thein et al., 2007). Since Astrin localizes to the mitotic spindle and was identified as a microtubule interacting protein, it is likely to interact directly or indirectly with microtubules and could contribute to kinetochore microtubule attachment.

Regulation of kinetochore microtubule attachment

For proper chromosome segregation to occur, sister chromatids must be correctly bi-oriented on the mitotic spindle. Frequent errors occur during the process. For example, both sister-kinetochores can attach to the same spindle pole, a state called mono-orientation. Alternatively, a single kinetochore can bind microtubules from both spindle poles, a state called merotelic attachment. Both of these erroneous attachment states differ from bi-oriented attachments in that no tension can be established between sister-kinetochores, i.e. the kinetochores can't be pulled apart by the forces applied towards the opposite spindle poles. As

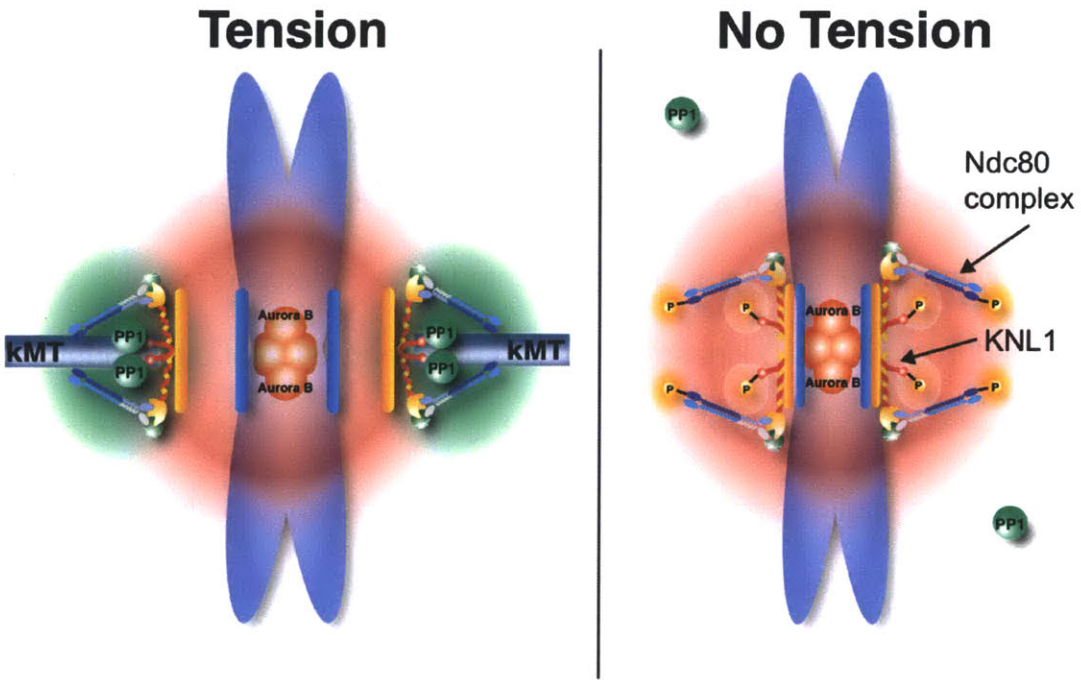

Figure 5. Tension dependent regulation of kinetochore-microtubule attachment by Aurora B kinase and protein phosphatase 1 gamma. (Adapted from (Liu et al., 2010)) Aurora B kinase localizes to the inner centromere, a region located between sister-kinetochores. When tension is low (left) the outer kinetochore targets of Aurora B kinase are within the range of the phosphorylation gradient (red). Phosphorylation of the KMN network reduces its the microtubule binding affinity, allowing incorrect kinetochore-microtubule attachments to be corrected. When tension is established (right), the outer kinetochore is spatially removed from Aurora B kinase, allowing protein phosphatase 1 gamma to associate with KNL-1, reversing Aurora B phosphorylation, and thereby stabilizing kinetochore-microtubule attachments of bi-oriented sister-chromatids.

a consequence, the distance between the sister-kinetochores is greater in bi-oriented chromosomes than incorrectly attached chromosomes. In addition, each kinetochore itself is deformed by spindle forces separating the inner and outer kinetochores. These spatial differences are crucial for the selective destabilization of incorrect kinetochore-microtubule attachments. Aurora B kinase

directly phosphorylates the KMN network, the Ska1 complex and other targets to destabilize kinetochore-microtubule attachments. Aurora B kinase is localized to the inner centromere region, distal to the outer kinetochore and between sister-kinetochores. Thus, when a sister kinetochore pair is under tension, which only occurs when they are properly bi-oriented, the kinetochores are spatially separated from Aurora B kinase preventing phosphorylation of outer kinetochore substrates. When an incorrect attachment is formed, no tension is established and thus the outer kinetochore substrates of Aurora B kinase can be phosphorylated. These erroneous attachments are selectively destabilized, allowing new potentially correct attachments to form (Fig. 5, reviewed in (Lampson and Cheeseman, 2011)).

The key substrates for Aurora B kinase in the KMN network are Ndc80 and KNL1. The N-terminal tail of Ndc80 contains multiple Aurora B phosphorylation sites, which decrease the affinity of the Ndc80 complex for microtubules when phosphorylated, allowing incorrect microtubule attachments to be released (Cheeseman et al., 2006; Deluca et al., 2006). The phosphorylation site on KNL1 has a different function with the same ultimate consequence. When KNL1 is phosphorylated by Aurora B, its affinity for protein phosphatase 1 gamma (PP1gamma) is strongly reduced (Liu et al., 2010). PP1gamma reverses Aurora B phosphorylation, thus stabilizing kinetochore microtubule attachment. When an incorrect attachment is formed, KNL1 is phosphorylated and thus can't recruit PP1gamma to stabilize microtubule attachment. In case of properly bi-

oriented sister-chromatids, KNL1 is not phosphorylated and recruits PP1gamma to stabilize kinetochore microtubule attachment. Recently, the Ska1 complex has also been implicated as a relevant Aurora B target to facilitate error correction. When the Ska1 complex is phosphorylated, it no longer localizes to kinetochore and therefore can't contribute to microtubule attachment, destabilizing incorrect attachments (Chan et al., 2012). This highlights a second mechanism by which Aurora B can regulate the stability of kinetochore-microtubule attachments. In addition to changing the biochemical properties of its targets, Aurora B can regulate the localizing of proteins to the kinetochore in a tension dependent manner. Stabilizing factors can thereby be excluded from the kinetochore when tension is low, allowing incorrect attachments to turn over. In contrast, when tension is established these stabilizing factors can localize to the kinetochore specifically reinforcing correct attachments.

Although many of the relevant targets for Aurora B in error correction are known, the spatio-temporal mechanism and the relative contribution of the different Aurora B targets remains to be determined.

The spindle assembly checkpoint

To assure equal chromosome segregation, anaphase onset must only occur when all sister-chromatids are properly bi-oriented at the metaphase plate. Anaphase onset is trigger by the degradation of securin, the inhibitor of separase, and cyclin B by the proteasome. Securin and cyclin B are targeted for

degradation by the E3 ubiquitin ligase anaphase promoting complex (APC), which requires the subunit cdc20 to be active. The spindle assembly checkpoint (SAC) sequesters cdc20 in an inactive state until all chromosomes are properly attached to the mitotic spindle.

To inactivate cdc20 the SAC components Bub3, BubR1 and Mad2 directly associate with cdc20 forming the mitotic checkpoint complex (MCC). Importantly, the formation of this complex is directed by kinetochores, which are not associated with microtubules. Cytosolic Mad2 is converted into a conformation capable of associating with cdc20 by a second pool of Mad2, which associates with kinetochores that are not attached to the spindle microtubules. Once a kinetochore becomes attached to microtubules Mad2 is removed, preventing the generation of MCC. Thus, the SAC senses the attachment state of the kinetochore. But since only bi-oriented sister-kinetochores stably associate with the mitotic spindle, only correctly attached sister-chromatids silence the MCC signal derived from the kinetochore. Therefor, the combination of the SAC and the error correction machinery assure that anaphase onset is only trigger when all chromosomes are properly bi-oriented (reviewed in (Musacchio and Salmon, 2007)).

Force generation by microtubule depolymerization

Microtubules store potential energy derived from GTP hydrolysis. When microtubules depolymerize, the protofilaments at the depolymerizing microtubule

end undergo a dramatic conformational change and assume a curved "rams-horn" like conformation. It has been shown that these peeling protofilaments can do mechanical work on the order of ~5 pN, comparable to an individual kinesin motor (Grishchuk et al., 2005a). The combination of all the 13-15 protofilaments in a microtubule can therefore generate a force of up to 60 pN, a substantial force on a molecular scale. Classic experiments by Bruce Niklas demonstrated that the combined action of the 15-20 microtubules attached to a kinetochore can generate up to 700 pN of force (Nicklas, 1983). The kinetochore therefore has the challenging task of remaining attached to the depolymerizing microtubule ends, which generate large forces and undergo dramatic conformational changes in the process. Two different models have been proposed to explain the physics of a coupler that can link microtubule depolymerization to chromosome movement; biased diffusion and forced walk models (Efremov et al., 2007; Hill, 1985).

Biased diffusion

Hill proposed a model to explain how a kinetochore could remain attached to a depolymerizing microtubule in the mid-80's based solely on theoretical considerations (Hill, 1985). He postulated that the kinetochore could form a large number of low affinity interactions with the microtubule, allowing the individual molecular linkers to diffuse along the microtubule lattice. Maximizing the number of interactions would minimize the total free energy of the system. As a

microtubule depolymerizes, interactions would be lost and the kinetochore would move along with the microtubule to establish a minimum energy state (Fig. 6A).

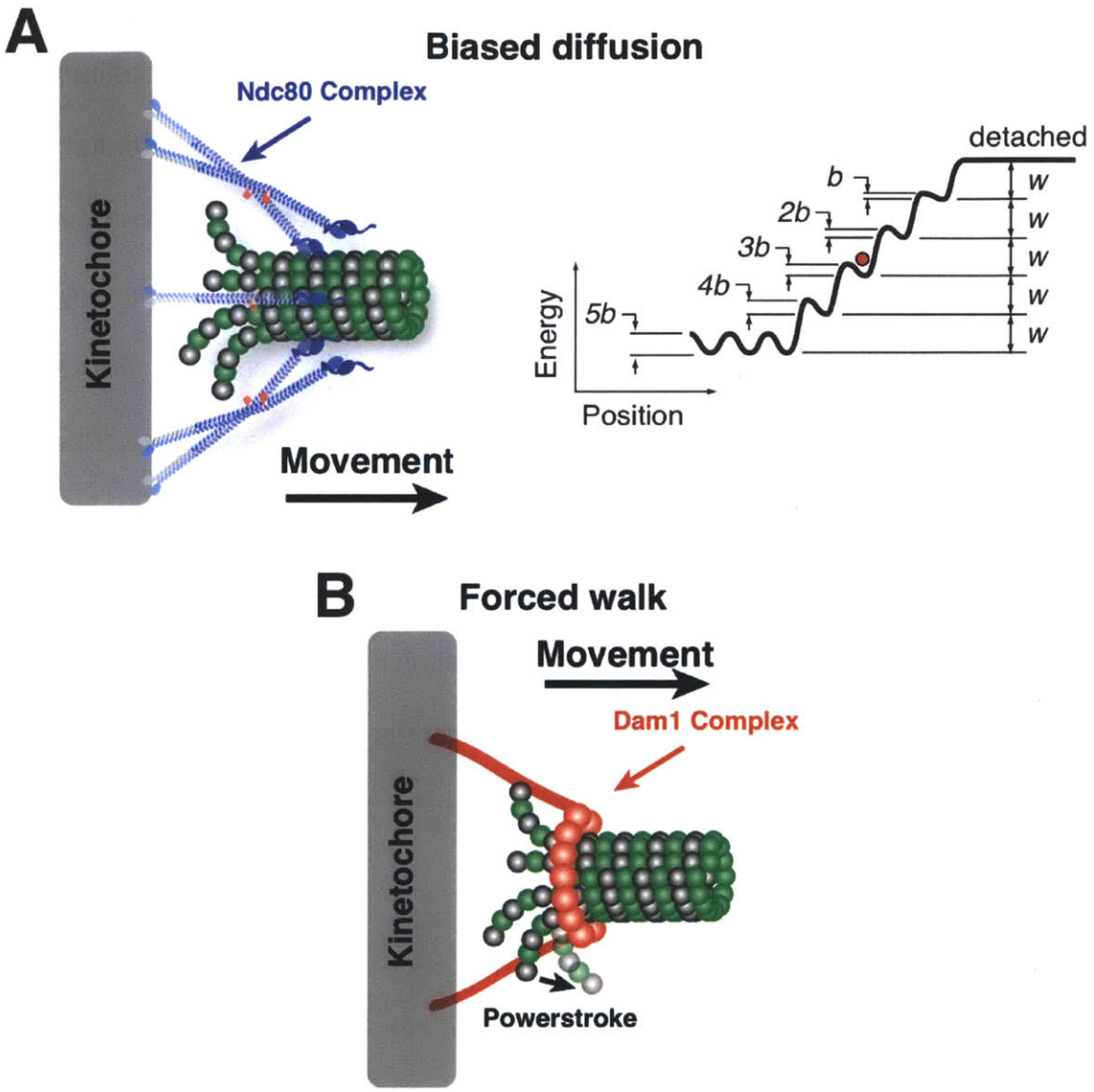

Figure 6. Models of coupling microtubule depolymerization to chromosome movement. (Adapted from (Santaguida and Musacchio, 2009)) (*A*) Biased diffusion models assume that the kinetochore forms many low affinity interactions with the microtubule. Dissociation of many weak interactions poses a significant energy barrier (right), allowing the kinetochore to remain attached to depolymerizing microtubules, and thereby biasing the diffusion of the kinetochore towards the microtubule minus end. The Ndc80 complex has been proposed to track with depolymerizing microtubules by biased diffusion, when artificially oligomerized (Powers et al., 2009). (*B*) Forced walk models require a coupler

which is tightly associated with the microtubule lattice and thus does not easily diffuse, such as the Dam1 ring complex. The coupler is displaced by the powerstroke of depolymerizing microtubule protofilaments and thereby moves towards the microtubule minus-end.
To completely lose its attachment to the microtubule, a large number of small interactions would have to be broken, presenting a substantial energy barrier, allowing the kinetochore to remain attached to the depolymerizing microtubule. The Ndc80 complex, which can track with depolymerizing microtubules, when artificially oligomerized by the addition of an antibody, or on the surface of a microsphere, has been proposed to act by a biased-diffusion mechanism (Powers et al., 2009).

Forced walk

In contrast to biased diffusion, forced walk models are based on the assumption that rather than diffusing passively on microtubules, the coupler is tightly bound to the microtubule lattice and can't easily diffuse. As a microtubule depolymerizes, the powerstroke of the peeling protofilaments would displace the coupler along the depolymerizing microtubule. The Dam1 complex, which is present only in fungi, can form a ring around microtubules and has been proposed to track the plus-ends of depolymerizing microtubules using a forced walk mechanism (Fig. 6B, (Efremov et al., 2007; Grishchuk et al., 2008a; Grishchuk et al., 2008b)).

Importantly, the biased diffusion and forced walk mechanisms are not mutually exclusive. These models have been driven by the observations made studying potential molecular players that have been proposed to carry out this coupling function in cells. In human cells, the Ndc80 and Ska1 complexes have been shown to be essential for microtubule attachment, but the mechanism by which these molecules couple chromosome movement to microtubule depolymerization remains unclear.

Findings presented in this thesis

During my graduate work, I identified the small kinetochore associated protein (SKAP) and dynein light chain 1 (LC8) as direct interaction partners of Astrin. Here, I demonstrate that the Astrin/SKAP/LC8 complex localizes only to aligned kinetochores and that kinetochore localization of the complex is antagonized by Aurora B kinase. Furthermore, SKAP directly associates with microtubules and the Astrin/SKAP/LC8 is directly required for CLASP localization to kinetochores. CLASP can therefore carry out its microtubule stabilizing functions at bi-oriented kinetochores, promoting maintenance of correct kinetochore-microtubule attachments.

In addition, I conducted a detailed molecular dissection of the Ska1 complex microtubule binding activity, identifying and characterizing the microtubule binding domain of the Ska1 complex. Importantly, I demonstrate that the Ska1 complex can track with depolymerizing microtubules and can confer this

activity to the Ndc80 complex. Surprisingly, I found that the Ska1 complex, but not the Ndc80 complex, can directly interact with the curved protofilament structures, present at depolymerizing microtubule ends. Together, these observations lead to a detailed model describing how the Ska1 complex and Ndc80 complex are coordinated to form an integrated coupler, capable of remaining associated with depolymerizing microtubules.

References

Al-Bassam, J., and F. Chang. 2011. Regulation of microtubule dynamics by TOG-domain proteins XMAP215/Dis1 and CLASP. *Trends Cell Biol.* 21:604-614.

Al-Bassam, J., H. Kim, G. Brouhard, A. van Oijen, S.C. Harrison, and F. Chang. 2010. CLASP promotes microtubule rescue by recruiting tubulin dimers to the microtubule. *Dev Cell.* 19:245-258.

Andrews, P.D., Y. Ovechkina, N. Morrice, M. Wagenbach, K. Duncan, L. Wordeman, and J.R. Swedlow. 2004. Aurora B regulates MCAK at the mitotic centromere. *Dev Cell.* 6:253-268.

Brouhard, G.J., J.H. Stear, T.L. Noetzel, J. Al-Bassam, K. Kinoshita, S.C. Harrison, J. Howard, and A.A. Hyman. 2008. XMAP215 is a processive microtubule polymerase. *Cell.* 132:79-88.

Chan, Y.W., A.A. Jeyaprakash, E.A. Nigg, and A. Santamaria. 2012. Aurora B controls kinetochore-microtubule attachments by inhibiting Ska complex-KMN network interaction. *The Journal of cell biology.* 196:563-571.

Cheeseman, I.M., J.S. Chappie, E.M. Wilson-Kubalek, and A. Desai. 2006. The conserved KMN network constitutes the core microtubule-binding site of the kinetochore. *In* Cell. Vol. 127. 983-997.

Cheeseman, I.M., and A. Desai. 2008. Molecular architecture of the kinetochore-microtubule interface. *In* Nat Rev Mol Cell Biol. Vol. 9. 33-46.

Cheeseman, I.M., S. Niessen, S. Anderson, F. Hyndman, J.R. Yates, K. Oegema, and A. Desai. 2004. A conserved protein network controls assembly of the outer kinetochore and its ability to sustain tension. *In* Genes Dev. Vol. 18. 2255-2268.

Ciferri, C., S. Pasqualato, E. Screpanti, G. Varetti, S. Santaguida, G. Dos Reis, A. Maiolica, J. Polka, J.G. De Luca, P. De Wulf, M. Salek, J. Rappsilber, C.A. Moores, E.D. Salmon, and A. Musacchio. 2008. Implications for kinetochore-microtubule attachment from the structure of an engineered Ndc80 complex. *In* Cell. Vol. 133. 427-439.

Dalal, Y., and M. Bui. 2010. Down the rabbit hole of centromere assembly and dynamics. *Current opinion in cell biology.* 22:392-402.

Deluca, J.G., W.E. Gall, C. Ciferri, D. Cimini, A. Musacchio, and E.D. Salmon. 2006. Kinetochore microtubule dynamics and attachment stability are regulated by Hec1. *In* Cell. Vol. 127. 969-982.

Desai, A., and T.J. Mitchison. 1997. Microtubule polymerization dynamics. *In* Annu Rev Cell Dev Biol. Vol. 13. 83-117.

Efremov, A., E.L. Grishchuk, J.R. McIntosh, and F.I. Ataullakhanov. 2007. In search of an optimal ring to couple microtubule depolymerization to processive chromosome motions. *In* Proc Natl Acad Sci USA. Vol. 104. 19017-19022.

Fededa, J.P., and D.W. Gerlich. 2012. Molecular control of animal cell cytokinesis. *Nature Cell Biology.* 14:440-447.

Gascoigne, K.E., and I.M. Cheeseman. 2011. Kinetochore assembly: if you build it, they will come. *Current opinion in cell biology.* 23:102-108.

Gascoigne, K.E., K. Takeuchi, A. Suzuki, T. Hori, T. Fukagawa, and I.M. Cheeseman. 2011. Induced ectopic kinetochore assembly bypasses the requirement for CENP-A nucleosomes. *Cell.* 145:410-422.

Gordon, D.J., B. Resio, and D. Pellman. 2012. Causes and consequences of aneuploidy in cancer. *Nat Rev Genet.* 13:189-203.

Grishchuk, E.L., A.K. Efremov, V.A. Volkov, I.S. Spiridonov, N. Gudimchuk, S. Westermann, D. Drubin, G. Barnes, J.R. McIntosh, and F.I. Ataullakhanov. 2008a. The Dam1 ring binds microtubules strongly enough to be a processive as well as energy-efficient coupler for chromosome motion. *Proceedings of the National Academy of Sciences of the United States of America.* 105:15423-15428.

Grishchuk, E.L., M.I. Molodtsov, F.I. Ataullakhanov, and J.R. McIntosh. 2005a. Force production by disassembling microtubules. *Nature.* 438:384-388.

Grishchuk, E.L., M.I. Molodtsov, F.I. Ataullakhanov, and J.R. Mcintosh. 2005b. Force production by disassembling microtubules. *In* Nature. Vol. 438. 384-388.

Grishchuk, E.L., I.S. Spiridonov, V.A. Volkov, A. Efremov, S. Westermann, D. Drubin, G. Barnes, F.I. Ataullakhanov, and J.R. McIntosh. 2008b. Different assemblies of the DAM1 complex follow shortening microtubules by distinct mechanisms. *Proceedings of the National Academy of Sciences of the United States of America.* 105:6918-6923.

Gruber, J., J. Harborth, J. Schnabel, K. Weber, and M. Hatzfeld. 2002. The mitotic-spindle-associated protein astrin is essential for progression through mitosis. *In* J Cell Sci. Vol. 115. 4053-4059.

Guimaraes, G.J., Y. Dong, B.F. McEwen, and J.G. Deluca. 2008. Kinetochore-Microtubule Attachment Relies on the Disordered N-Terminal Tail Domain of Hec1. *In* Curr Biol. Vol. 18. 1778-1784.

Hanisch, A., H.H. Sillje, and E.A. Nigg. 2006a. Timely anaphase onset requires a novel spindle and kinetochore complex comprising Ska1 and Ska2. *The EMBO journal.* 25:5504-5515.

Hanisch, A., H.H.W. Silljé, and E.A. Nigg. 2006b. Timely anaphase onset requires a novel spindle and kinetochore complex comprising Ska1 and Ska2. *In* EMBO J. Vol. 25. 5504-5515.

Hill, T.L. 1985. Theoretical problems related to the attachment of microtubules to kinetochores. *In* Proc Natl Acad Sci USA. Vol. 82. 4404-4408.

Howell, B.J., B.F. McEwen, J.C. Canman, D.B. Hoffman, E.M. Farrar, C.L. Rieder, and E.D. Salmon. 2001. Cytoplasmic dynein/dynactin drives kinetochore protein transport to the spindle poles and has a role in mitotic spindle checkpoint inactivation. *In* J Cell Biol. Vol. 155. 1159-1172.

Jeyaprakash, A.A., A. Santamaria, U. Jayachandran, Y.W. Chan, C. Benda, E.A. Nigg, and E. Conti. 2012. Structural and functional organization of the Ska

complex, a key component of the kinetochore-microtubule interface. *Molecular Cell.* 46:274-286.

Kapoor, T.M., M.A. Lampson, P. Hergert, L. Cameron, D. Cimini, E.D. Salmon, B.F. McEwen, and A. Khodjakov. 2006. Chromosomes can congress to the metaphase plate before biorientation. *In* Science. Vol. 311. 388-391.

Kiyomitsu, T., C. Obuse, and M. Yanagida. 2007. Human Blinkin/AF15q14 is required for chromosome alignment and the mitotic checkpoint through direct interaction with Bub1 and BubR1. *In* Dev Cell. Vol. 13. 663-676.

Kline, S.L., I.M. Cheeseman, T. Hori, T. Fukagawa, and A. Desai. 2006. The human Mis12 complex is required for kinetochore assembly and proper chromosome segregation. *In* J Cell Biol. Vol. 173. 9-17.

Kops, G.J., A.T. Saurin, and P. Meraldi. 2010. Finding the middle ground: how kinetochores power chromosome congression. *Cell Mol Life Sci.* 67:2145-2161.

Lampson, M.A., and I.M. Cheeseman. 2011. Sensing centromere tension: Aurora B and the regulation of kinetochore function. *Trends Cell Biol.* 21:133-140.

Liu, D., M. Vleugel, C.B. Backer, T. Hori, T. Fukagawa, I.M. Cheeseman, and M.A. Lampson. 2010. Regulated targeting of protein phosphatase 1 to the outer kinetochore by KNL1 opposes Aurora B kinase. *In* J Cell Biol. Vol. 188. 809-820.

Mack, G.J., and D.A. Compton. 2001. Analysis of mitotic microtubule-associated proteins using mass spectrometry identifies astrin, a spindle-associated protein. *In* Proc Natl Acad Sci USA. Vol. 98. 14434-14439.

McEwen, B.F., A.B. Heagle, G.O. Cassels, K.F. Buttle, and C.L. Rieder. 1997. Kinetochore fiber maturation in PtK1 cells and its implications for the mechanisms of chromosome congression and anaphase onset. *In* J Cell Biol. Vol. 137. 1567-1580.

McIntosh, J.R., V. Volkov, F.I. Ataullakhanov, and E.L. Grishchuk. 2010. Tubulin depolymerization may be an ancient biological motor. *J Cell Sci.* 123:3425-3434.

Miller, S.A., M.L. Johnson, and P.T. Stukenberg. 2008. Kinetochore attachments require an interaction between unstructured tails on microtubules and Ndc80(Hec1). *Current biology : CB.* 18:1785-1791.

Musacchio, A., and E.D. Salmon. 2007. The spindle-assembly checkpoint in space and time. *Nat Rev Mol Cell Biol.* 8:379-393.

Nicklas, R.B. 1983. Measurements of the force produced by the mitotic spindle in anaphase. *In* J Cell Biol. Vol. 97. 542-548.

Nishino, T., K. Takeuchi, K.E. Gascoigne, A. Suzuki, T. Hori, T. Oyama, K. Morikawa, I.M. Cheeseman, and T. Fukagawa. 2012. CENP-T-W-S-X forms a unique centromeric chromatin structure with a histone-like fold. *Cell.* 148:487-501.

Pfarr, C.M., M. Coue, P.M. Grissom, T.S. Hays, M.E. Porter, and J.R. McIntosh. 1990. Cytoplasmic dynein is localized to kinetochores during mitosis. *In* Nature. Vol. 345. 263-265.

Powers, A.F., A.D. Franck, D.R. Gestaut, J. Cooper, B. Gracyzk, R.R. Wei, L. Wordeman, T.N. Davis, and C.L. Asbury. 2009. The Ndc80 kinetochore complex forms load-bearing attachments to dynamic microtubule tips via biased diffusion. *In* Cell. Vol. 136. 865-875.

Santaguida, S., and A. Musacchio. 2009. The life and miracles of kinetochores. *In* EMBO J. Vol. 28. 2511-2531.

Screpanti, E., A. De Antoni, G.M. Alushin, A. Petrovic, T. Melis, E. Nogales, and A. Musacchio. 2011. Direct binding of Cenp-C to the Mis12 complex joins the inner and outer kinetochore. *Current biology : CB*. 21:391-398.

Thein, K.H., J. Kleylein-Sohn, E.A. Nigg, and U. Gruneberg. 2007. Astrin is required for the maintenance of sister chromatid cohesion and centrosome integrity. *In* J Cell Biol. Vol. 178. 345-354.

Van Hooser, A.A., Ouspenski, II, H.C. Gregson, D.A. Starr, T.J. Yen, M.L. Goldberg, K. Yokomori, W.C. Earnshaw, K.F. Sullivan, and B.R. Brinkley. 2001. Specification of kinetochore-forming chromatin by the histone H3 variant CENP-A. *J Cell Sci*. 114:3529-3542.

Walczak, C.E., S. Cai, and A. Khodjakov. 2010. Mechanisms of chromosome behaviour during mitosis. *In* Nat Rev Mol Cell Biol. 1-12.

Walczak, C.E., and R. Heald. 2008. Mechanisms of mitotic spindle assembly and function. *Int Rev Cytol*. 265:111-158.

Wang, H.W., S. Long, C. Ciferri, S. Westermann, D. Drubin, G. Barnes, and E. Nogales. 2008. Architecture and flexibility of the yeast Ndc80 kinetochore complex. *J Mol Biol*. 383:894-903.

Wang, H.W., and E. Nogales. 2005. Nucleotide-dependent bending flexibility of tubulin regulates microtubule assembly. *Nature*. 435:911-915.

Welburn, J.P.I., E.L. Grishchuk, C.B. Backer, E.M. Wilson-Kubalek, J.R. Yates, and I.M. Cheeseman. 2009. The human kinetochore Ska1 complex facilitates microtubule depolymerization-coupled motility. *In* Dev Cell. Vol. 16. 374-385.

Wordeman, L., and T.J. Mitchison. 1995. Identification and partial characterization of mitotic centromere-associated kinesin, a kinesin-related protein that associates with centromeres during mitosis. *The Journal of cell biology*. 128:95-104.

Wordeman, L., M. Wagenbach, and G. von Dassow. 2007. MCAK facilitates chromosome movement by promoting kinetochore microtubule turnover. *In* J Cell Biol. Vol. 179. 869-879.

Yen, T.J., D.A. Compton, D. Wise, R.P. Zinkowski, B.R. Brinkley, W.C. Earnshaw, and D.W. Cleveland. 1991. CENP-E, a novel human centromere-associated protein required for progression from metaphase to anaphase. *The EMBO journal*. 10:1245-1254.

Zhang, G., C.D. Kelstrup, X.W. Hu, M.J. Hansen, M.R. Singleton, J.V. Olsen, and J. Nilsson. 2012. The Ndc80 internal loop is required for recruitment of the Ska complex to establish end-on microtubule attachment to kinetochores. *J Cell Sci*.

Chapter II: Aurora B kinase controls the targeting of the Astrin-SKAP complex to bioriented kinetochores

Reprinted from Rockefeller University Press:
Jens C. Schmidt, Tomomi Kiyomitsu, Tetsuya Hori, Chelsea B. Backer, Tatsuo Fukagawa, Iain M. Cheeseman. 2010. The Astrin/SKAP complex is targeted to bi-oriented kinetochores to stabilize microtubule attachments. *J Cell Biol.* 191:269-80.

Tomomi Kiyomitsu carried out characterization of dynein light chain proteins. Tetsuya Hori and Tatsuo Fukagawa carried out genetic and cell biological experiments with Chicken DT40 cells. Chelsea B. Backer generated the monoclonal GFP-SKAP expressing HeLa cell line and the antibody against SKAP.

Summary

During the mitosis, kinetochores play multiple roles to generate interactions with microtubules, and direct chromosome congression, bi-orientation, error correction, and anaphase segregation. However, it is unclear what changes at the kinetochore facilitate these distinct activities. Here, we describe a complex of the spindle and kinetochore associated proteins Astrin and SKAP, and the dynein light chain LC8. While most dynein-associated proteins localize to unaligned kinetochores in an Aurora B-dependent manner, Astrin, SKAP, and LC8 localization is antagonized by Aurora B such that they target exclusively to bi-oriented kinetochores. Astrin/SKAP depleted cells fail to maintain proper chromosome alignment resulting in a spindle assembly checkpoint-dependent mitotic delay. Consistent with a role in stabilizing bi-oriented attachments, Astrin and SKAP bind directly to microtubules and are required for CLASP localization to kinetochores. In total, our results suggest that tension-dependent Aurora B phosphorylation can act to control outer kinetochore composition to provide distinct activities to prometaphase and metaphase kinetochores.

Introduction

Proper chromosome segregation requires the macromolecular kinetochore to mediate interactions between chromosomal DNA and spindle microtubules (Cheeseman and Desai, 2008). During prometaphase, kinetochore-microtubule attachments are established allowing chromosomes to congress to the middle of the cell. In cases where erroneous interactions with the mitotic spindle occur, kinetochore-microtubule attachments must be corrected. During metaphase, bi-orientation is maintained and microtubules undergo rapid changes in dynamics resulting in kinetochore oscillations. Finally, during anaphase A, kinetochores move towards the spindle poles along depolymerizing microtubules. At present, it is unclear what alters kinetochore function to achieve these distinct activities. In principle, this could occur by regulating the activity of stably associated kinetochore proteins, or by changing kinetochore composition.

One key regulator of kinetochore function that has been implicated in both controlling kinetochore activity and assembly state is Aurora B kinase. Aurora B functions to sense and correct aberrant kinetochore-microtubule interactions (Ruchaud et al., 2007). Due to a spatial separation from its substrates (Liu et al., 2009), Aurora B phosphorylation at the outer kinetochore is high on mis-aligned kinetochores that are not under tension, but is reduced at aligned kinetochores. Aurora B can directly modulate kinetochore-microtubule attachments by altering the activity of key kinetochore proteins including the microtubule binding KNL-1/MIS-12 complex/NDC80 complex (KMN) network (Cheeseman et al., 2006; DeLuca et al., 2006; Welburn et al., 2010). Aurora B has also been suggested to play a role in kinetochore assembly. In *Xenopus* extracts, Aurora B activity is required for outer kinetochore assembly (Emanuele et al., 2008). Although a similarly strong effect is not observed in human cells (Welburn et al., 2010), Aurora B activity promotes the localization of Shugoshin/MEI-S332 (Resnick et

al., 2006), MCAK (Andrews et al., 2004; Lan et al., 2004), and Kif2b (Bakhoum et al., 2009b) to centromeres. In contrast, Aurora B phosphorylation opposes the recruitment of its counteracting protein phosphatase PP1 to kinetochores (Liu et al., 2010).

Here, we describe a complex composed of the spindle and kinetochore proteins Astrin (Chang et al., 2001; Gruber et al., 2002; Mack and Compton, 2001; Thein et al., 2007) and SKAP (Fang et al., 2009). The SKAP/Astrin complex is recruited only to kinetochores that are aligned at the metaphase plate. We demonstrate that Astrin/SKAP localization is antagonized by Aurora B phosphorylation such that they are enriched at kinetochores when Aurora B activity is inhibited and reduced when additional Aurora B kinase is recruited to the outer kinetochore. Astrin and SKAP also associate with the dynein light chain LC8 and are required for proper LC8 localization to kinetochores. Astrin/SKAP depletion results in a Mad2-dependent mitotic delay, and prevents CLASP from localizing to kinetochores. In total, our results suggest that tension-dependent Aurora B phosphorylation functions directly or indirectly to control the composition of the outer kinetochore in a chromosome-specific manner to stabilize metaphase aligned chromosomes and prepare for anaphase.

Results and Discussion

SKAP localizes to the spindle and outer kinetochore

In our ongoing proteomic analysis of the vertebrate kinetochore, we identified C15orf23 as a protein weakly associated with known kinetochore components. C15orf23 was also recently identified as Small Kinetochore Associated Protein (SKAP; Fang et al., 2009). SKAP localizes to spindle microtubules and spindle poles throughout mitosis, and to kinetochores from metaphase to telophase (Fig. 1A and B). At kinetochores, SKAP localizes peripherally to Ndc80, consistent with it functioning at the outer kinetochore (Fig. 1C). Similar to human SKAP, the *Gallus gallus* (chicken) homologue of ggSKAP localizes to the spindle throughout mitosis, and to kinetochores in metaphase and anaphase, but not during prophase or prometaphase in DT40 cells (Fig. 1D). These results demonstrate that SKAP is a conserved component of the vertebrate spindle and outer kinetochore.

SKAP and Astrin form a complex *in vivo*

To determine whether SKAP interacts with additional proteins, we conducted one step immuno-precipitations (IPs) from cells stably expressing GFP^{LAP}-SKAP or FLAG-ggSKAP. Mass spectrometry analysis of these purifications identified a complex of SKAP and the established spindle and kinetochore protein Astrin

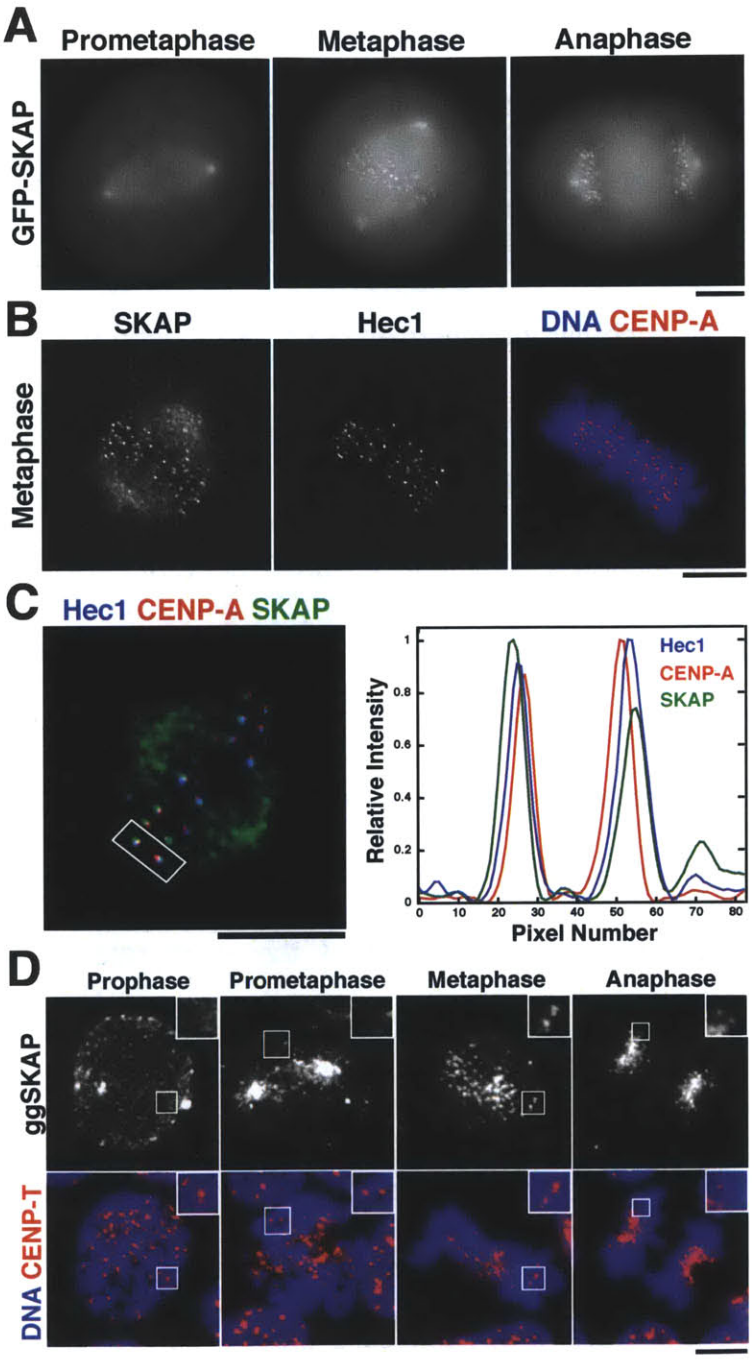

Figure 1. SKAP localizes to the outer kinetochore during metaphase and anaphase. (*A*) Images of different mitotic stages from a clonal human cell line stably expressing moderate amounts of GFP^{LAP}-SKAP. GFP-SKAP localizes to spindle microtubules throughout mitosis, and kinetochores during metaphase and anaphase. (*B*) Immunofluorescence showing the co-localization of SKAP and

Hec1/Ndc80 with DNA (blue) and CENP-A (red). (*C*) Left, immunofluorescence image showing the co-localization of SKAP (green), Hec1 (blue), and CENP-A (red). Right, graph showing a linescan from the boxed kinetochore pair showing the relative spatial distribution of SKAP, Hec1, and CENP-A. SKAP localizes slightly peripherally to Hec1 at the outer kinetochore. (*D*) Localization of chicken ggSKAP in DT40 cells. Top, co-localization of DNA (blue) and SKAP (green). Bottom, SKAP alone. Scale bars, 5 μm.

(also called SPAG5 or MAP126; Chang et al., 2001; Gruber et al., 2002; Mack and Compton, 2001; Thein et al., 2007; Fig. 2A and B). Reciprocal purifications with LAP^{GFP}-Astrin isolated SKAP, confirming this association (Fig. 2A and B). In addition to Astrin and SKAP, the only other proteins found in these purifications, but not in controls, were the dynein light chain LC8 (DYNLL1 and DYNLL2), and cytoplasmic dynein heavy chain (Fig. 2A and 2B). Importantly, reciprocal purification of LAP^{GFP}-LC8 isolated Astrin in addition to the expected components of the dynein complex (Fig. 2A). Previous studies identified Aurora A kinase and Glycogen synthase kinase 3β as Astrin interacting proteins (Cheng et al., 2008; Du et al., 2008), but we did not detect either protein in our purifications.

Consistent with a direct interaction, and with previous observations of Astrin localization (Mack and Compton, 2001; Thein et al., 2007; Duane Compton, personal communication), Astrin localized identically to SKAP throughout the cell cycle including a preference for metaphase kinetochores relative to unaligned prometaphase kinetochores (Fig. 2C; data not shown). Astrin and SKAP also displayed largely interdependent localization to spindles and kinetochores (Fig. 2C), although small amounts of Astrin remain at kinetochores in SKAP depleted cells. Both Astrin and SKAP were depleted by

>90% following 48 hr treatment with the corresponding siRNAs, while the levels of the other complex component were subtly reduced (Fig. 2D). In total, these results identified a complex of the spindle and kinetochore associated proteins Astrin and SKAP.

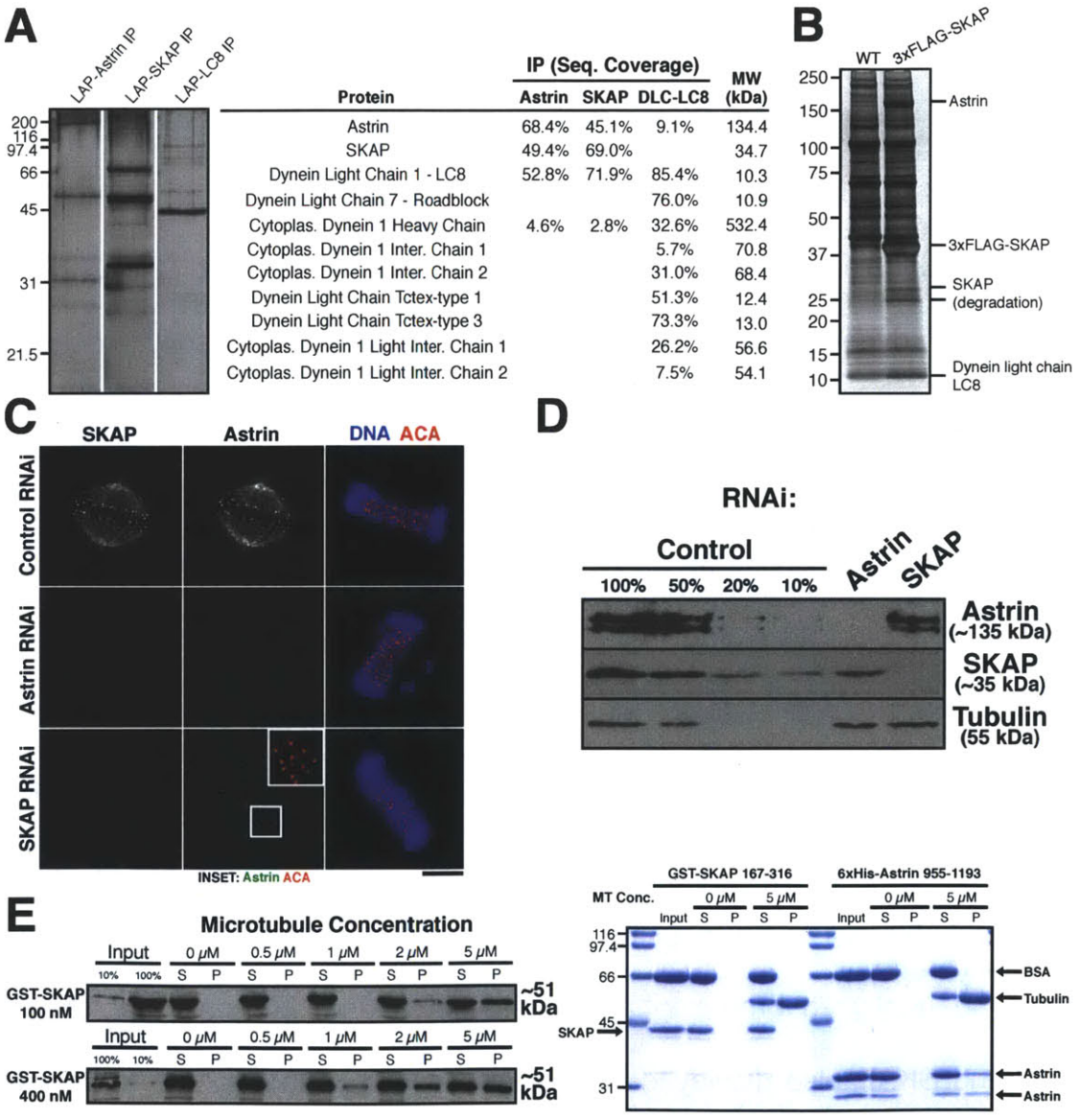

Figure 2. SKAP and Astrin form a complex. (*A*) Left, silver stained gels showing a one step immunoprecipitation (IP) of either LAP^{GFP}-Astrin, LAP^{GFP}-SKAP, or LAP^{GFP}-LC8. Right, data from the mass spectrometric analysis of the purifications indicating the percent sequence coverage from each IP. (*B*) Silver stain gel showing the purification of FLAG-SKAP from chicken DT40 cells relative to controls. The indicated proteins were identified by excising them from a gel and analyzing them by mass spectrometry. (*C*) Astrin and SKAP show interdependent localization. Immunofluorescence images showing Astrin and SKAP localization in control cells, or cells depleted for Astrin or SKAP relative to DNA (blue) and kinetochores (ACA; red). (D) Western Blot probed for anti-Astrin (top), anti-SKAP (middle) and anti-Tubulin (bottom) antibodies showing the efficiency of SKAP and Astrin depletion,. (*E*) SKAP and Astrin bind to microtubules in vitro. Top, Western blot probed with anti-SKAP antibodies showing the co-sedimentation of GST-SKAP with microtubules. Bottom, Coomassie stained gel showing the co-sedimentation of a fragment of Astrin (955-1193) with microtubules, but the inability of GST-SKAP C-terminal fragment to bind to microtubules.

SKAP and Astrin associate with microtubules directly

The localization of the SKAP/Astrin complex to spindle microtubules led us to test whether either protein associated with microtubules directly. In microtubule co-sedimentation assays, we found that both full length GST-SKAP and a C-terminal fragment of Astrin associated with microtubules (Fig. 2E). In contrast, the C-terminus of SKAP did not bind to microtubules. The dissociation constant for binding of GST-SKAP to microtubules is between 2 and 5 μM, which is slightly weaker than that of the Ndc80 complex under similar conditions (Cheeseman et al., 2006). These observations suggest that the Astrin/SKAP complex can associate with microtubules via domains in both SKAP and Astrin.

The SKAP/Astrin complex localizes preferentially to aligned chromosomes

We next sought to determine the relationship of the SKAP/Astrin complex to other established outer kinetochore components in both human and chicken cells. Depletion of KNL1 or the Ndc80 complex subunit Nuf2 prevented SKAP localization to kinetochores (Fig. 3A-C). In contrast, depletion of other established outer kinetochore components including Ska3, CENP-E, CENP-F, and CLASP1/2 co-depletion did not completely prevent SKAP/Astrin localization to kinetochores (Fig. 3A-B). However, while these depletions had no effect on SKAP localization to kinetochores aligned at the metaphase plate, SKAP failed to localize to the mis-aligned chromosomes caused by each of these perturbations (Fig. 3A, blow ups). Since similar results are observed in multiple distinct depletions, this suggests that the Astrin/SKAP complex preferentially localizes to bi-oriented kinetochores.

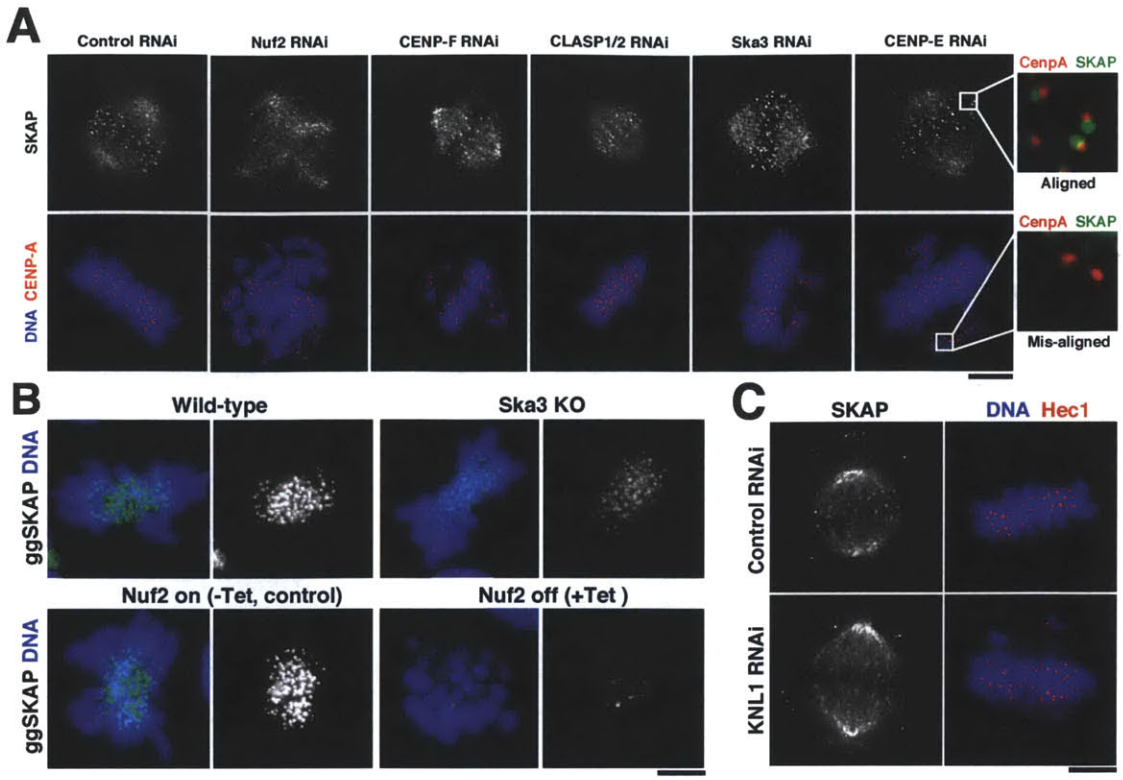

Figure 3. Requirements for Astrin/SKAP localization to kinetochores. (*A*) SKAP localizes exclusively to aligned kinetochores. Immunofluorescence images showing SKAP localization in cell treated with control siRNAs, or siRNAs against Nuf2, CENP-E, CENP-F, CLASP1 and CLASP2, or Ska3. DNA is shown in blue, and CENP-A staining is shown in red. SKAP localization requires Nuf2, but does not absolutely require the other proteins. However, in these cases, SKAP localizes only to aligned kinetochores, but not to mis-aligned kinetochores (blow ups). Scale bars, 5 μm. (*B*) Immunofluorescence showing ggSKAP localization in chicken DT40 cells in either control cells, or cells lacking Ska3 or Nuf2. Merge shows ggSKAP (green) and DNA (blue). Scale bars, 5 μm. (C) KNL1 depletion prevents SKAP localization. Immunofluorescence showing SKAP localization in human cells, and co-localization with Hec1 (red) and DNA (blue). Scale bars, 5 μm.

Aurora B activity counteracts SKAP/Astrin localization to kinetochores

As kinetochores become bi-oriented, the tension that is applied to the sister kinetochores changes substantially (Maresca and Salmon, 2009; Uchida et al., 2009). This tension decreases phosphorylation of outer kinetochore substrates for Aurora B kinase such that levels are high on misaligned chromosomes relative to aligned chromosomes (Liu et al., 2009; Welburn et al., 2010). Since SKAP and Astrin localize preferentially to kinetochores that are aligned at the metaphase plate, we sought to test the relationship between Aurora B activity and Astrin/SKAP localization.

We first analyzed the localization of the Astrin/SKAP complex relative to the level of Aurora B phosphorylation at a given kinetochore. In cells treated with low dose nocodazole (10 ng/ml) to generate cells that contain both aligned (Fig. 4A; bottom arrow) and mis-aligned (top arrow) kinetochores, Aurora B phosphorylation – detected using antibodies that recognize an Aurora B phosphorylation site in Dsn1 (Welburn et al., 2010) - was increased by 50% on the mis-aligned kinetochores (Fig. 4A). In contrast, Astrin levels were reduced by more than 85% on the same mis-aligned kinetochores (Fig. 4A). We observed microtubules apparently bound to these mis-aligned kinetochores (data not shown) suggesting that the localization of Astrin/SKAP is inversely proportional to Aurora B phosphorylation, not specifically the kinetochore attachment state.

To test the role of Aurora B phosphorylation in regulating Astrin/SKAP localization directly, we treated cells with the Aurora B inhibitor ZM447493. In

ZM447493 treated cells, SKAP localizes to kinetochores that are syntelically oriented (Fig. 4B, arrows), and thus are not under tension, suggesting that Aurora B activity normally counteracts SKAP/Astrin localization. Aurora B inhibition also promotes the localization of Astrin to mis-aligned kinetochores in U2OS cells (Duane Compton, personal communication). Next, we treated cells with the Eg5-inhibitor S-trityl-L-cysteine (STLC) which maintains kinetochore-microtubule attachments, but reduces tension. STLC treatment increases Aurora B phosphorylation (Welburn et al., 2010) and reduces SKAP localization relative to aligned kinetochores in control cells (Fig. 4B). However, cells treated with both STLC and ZM447493 showed significantly increased SKAP levels (Fig. 4B), confirming that Aurora B activity has a negative effect on SKAP localization to kinetochores. Importantly, SKAP localization depends on both Aurora B activity and the presence of microtubules since treatment with the microtubule depolymerizing drug nocodazole in either the presence or absence of ZM447493 prevented the localization of SKAP to kinetochores (Fig. 4B).

To take a reciprocal approach to analyze the effect of Aurora B on Astrin/SKAP localization, we expressed a Mis12-INCENP-mCherry fusion, which has been shown to increase the phosphorylation by recruiting additional Aurora B to the outer kinetochore (Liu et al., 2009). Expressing the Mis12-INCENP-mCherry fusion reduced the levels of GFP-SKAP at kinetochores by >2 fold (Fig. 4C), even though these kinetochores remain apparently bi-oriented. In contrast, a Mis12-INCENP(TAA)-mCherry mutant, which binds to, but does not activate

Aurora B (Sessa et al., 2005), had no effect on the levels of GFP^{LAP}-SKAP at kinetochores (Fig. 4C). To take an alternate approach to increase Aurora B phosphorylation, we eliminated the ability of KNL1 to target PP1, the counteracting phosphatase for Aurora B, to kinetochores (Liu et al., 2010). For these experiments, we depleted endogenous KNL1 and replaced this with a protein lacking the N-terminus. Cells lacking the PP1 targeting domain in KNL1 displayed greatly reduced Astrin at kinetochores (Fig. 4D), but showed normal localization of the Mis12 complex subunit Dsn1 (data not shown). However, treatment with the Aurora B inhibitor ZM447493 restored Astrin localization to kinetochores, demonstrating that Astrin is specifically sensitive to the level of Aurora B phosphorylation at kinetochores. In each case described above, inhibiting or increasing Aurora B phosphorylation produced similar results for Astrin and SKAP localization (not shown).

We conclude that local Aurora B kinase activity has a negative effect on SKAP/Astrin localization to kinetochores. The levels of both proteins are reduced when Aurora B activity at the outer kinetochore is high, and increased when Aurora B activity is reduced, causing them to localize exclusively to bi-oriented kinetochores.

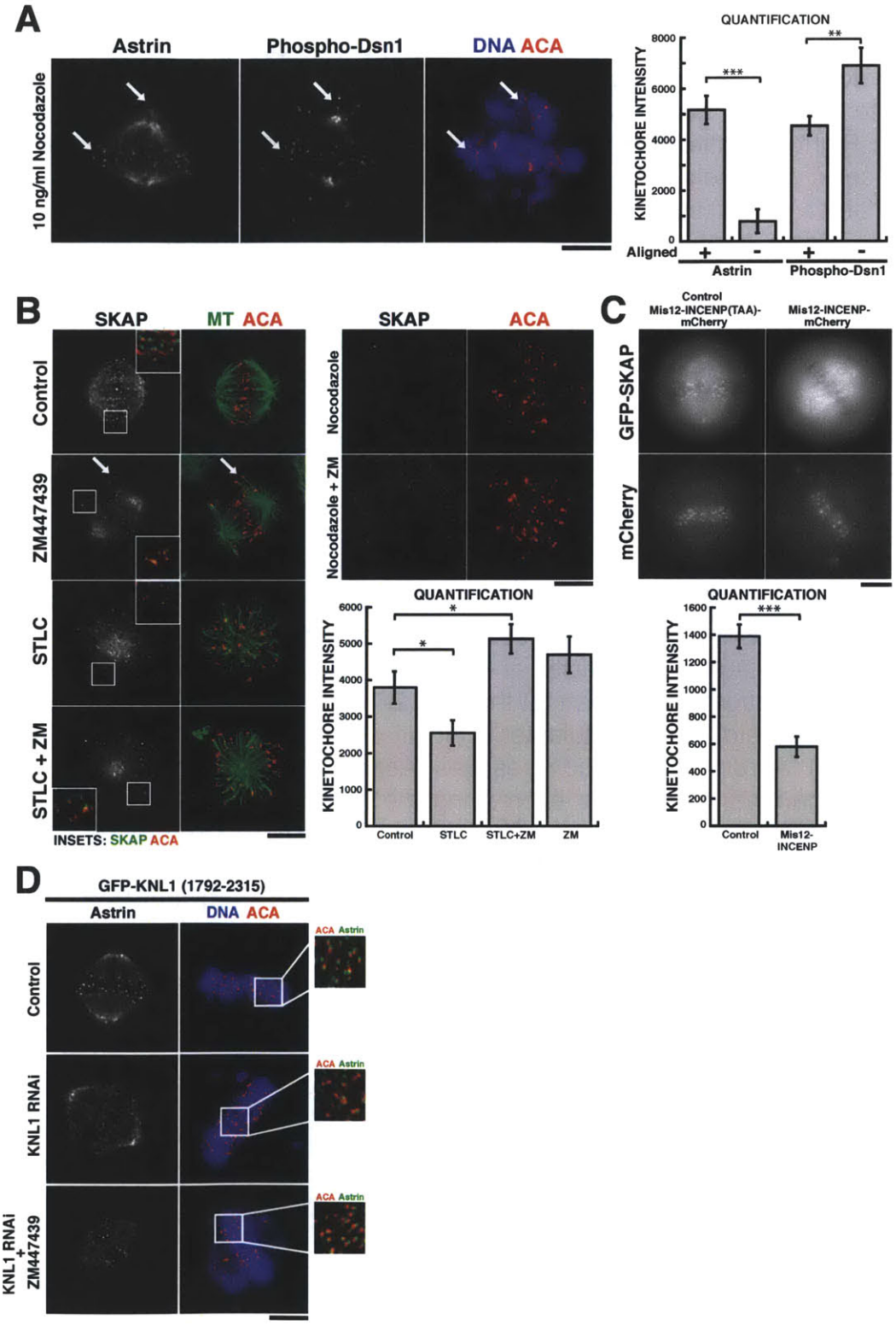
A
Astrin
Phospho-Dsn1
DNA ACA
10 ng/ml Nocodazole
QUANTIFICATION
KINETOCHORE INTENSITY
8000
6000
4000
2000
0
***
**
Aligned
+
-
+
-
Astrin
Phospho-Dsn1
B
SKAP
MT ACA
Control
ZM447439
STLC
STLC + ZM
INSETS: SKAP ACA
SKAP
ACA
Nocodazole
Nocodazole + ZM
QUANTIFICATION
KINETOCHORE INTENSITY
6000
5000
4000
3000
2000
1000
0
*
*
Control
STLC
STLC+ZM
ZM
C
Control Mis12-INCENP(TAA)-mCherry
Mis12-INCENP-mCherry
GFP-SKAP
mCherry
QUANTIFICATION
KINETOCHORE INTENSITY
1600
1400
1200
1000
800
600
400
200
0
***
Control
Mis12-INCENP
D
GFP-KNL1 (1792-2315)
Astrin
DNA ACA
Control
KNL1 RNAi
KNL1 RNAi + ZM447439
ACA Astrin
ACA Astrin
ACA Astrin

Figure 4. SKAP localization to kinetochores is counteracted by local Aurora B activity. (*A*) Astrin localization is inversely proportional to the level of Aurora B phosphorylation at a specific kinetochore. Left, immunofluorescence images showing Astrin localization relative to phospho-Dsn1, and to DNA (blue) and kinetochores (ACA; red) in a cell treated with low dose nocodazole (10 ng/ml) to generate both aligned and mis-aligned kinetochores (indicated by arrows). Right, quantification of Astrin and phospho-Dsn1 localization at aligned (n = 5 cells, 59 kinetochores) and mis-aligned (n = 5 cells, 48 kinetochores) kinetochores. ** indicates a significantly significant difference with $p < 0.01$; *** $p < 0.001$. Scale bars, 5 μm. (*B*) Immunofluorescence images showing SKAP localization relative to microtubules and CENP-A in either control cells (n = 7 cells, 108 kinetochores), cells treated individually the Aurora B inhibitor ZM447439 (n = 6 cells, 90 kinetochores), the Eg5-inhibitor STLC (n = 8 cells, 165 kinetochores), or the microtubule depolymerizing drug nocodazole, or combinations of STLC and ZM447439 (n = 10 cells, 170 kinetochores), and nocodazole and ZM447439. Quantification of the kinetochore intensity of SKAP (bottom right) indicates inhibiting Aurora B activity increases the localization of SKAP to kinetochores. * indicates statistically significant differences with $p < 0.05$. (*C*) Images from live cells showing the co-localization of GFP-SKAP with either Mis12-INCENP-mCherry (n = 7 cells, 92 kinetochores), or Mis12-INCENP-mCherry fusion in which the residues in INCENP that activate Aurora B are mutated to TAA as a control (n = 7 cells, 92 kinetochores). The Mis12-INCENP fusion increases Aurora B activity at the outer kinetochore (Liu et al., 2009). Quantification (bottom) indicates that the Mis12-INCENP fusion decreases SKAP localization to kinetochores. * indicates a significantly significant difference with $p < 0.001$. (*D*) Aurora B inhibition rescues Astrin localization to kinetochores lacking PP1gamma. HeLa cells expressing the KNL1 C-terminus (amino acids 1792-2315) were treated with control siRNAs, or KNL1 siRNAs to deplete endogenous KNL1, but not the C-terminus. Immunofluorescence showing Astrin localization in human cells, and co-localization with ACA (red) and DNA (blue). Scale bars, 5 μm.

Depletion of the SKAP/Astrin complex results in a checkpoint-dependent mitotic delay in human cells

To determine the role of the SKAP/Astrin complex in chromosome segregation, we conducted time lapse imaging of HeLa cells expressing YFP-histone H2B. Chromosome congression in SKAP or Astrin depleted cells proceeded with kinetics that were similar, but slightly slower than control cells (Fig. 5A). However, the time that chromosomes remained aligned at the metaphase plate before transitioning to anaphase was significantly increased in SKAP depleted cells (Fig. 5A-B). During this extended delay, we often observed individual chromosomes losing alignment and moving to the poles before re-aligning (Fig. 5A, arrows). In rare cases, the chromosomes would de-condense without undergoing anaphase. This phenotype is more severe than that previously reported for SKAP depletion (Fang et al., 2009), but is similar to the phenotype described for Astrin depletion (Thein et al., 2007).

To determine whether the prolonged mitotic delay observed following SKAP depletion is dependent on the spindle assembly checkpoint (SAC), we simultaneously depleted SKAP and the checkpoint component Mad2. Co-depletion of SKAP and Mad2 allowed cells to proceed quickly through mitosis indicating that the observed mitotic delay is dependent on the SAC (Fig. 5A-B). Although a subset of chromosomes align at the metaphase plate in Astrin and SKAP depleted cells, we found that BubR1 is highly enriched on the mis-aligned chromosomes generated by Astrin depletion (Fig. 5C), suggesting that the SAC

arrest is caused by the failure to maintain chromosome alignment. This contrasts with a previous study that proposed that the delay caused by SKAP depletion is downstream of the SAC (Fang et al., 2009).

To determine whether this checkpoint-dependent arrest following SKAP or Astrin depletion is caused by defective kinetochore-microtubule attachments, we measured the inter-kinetochore distances. For these experiments, we monitored chromosomes that aligned at the metaphase plate. The presence of bi-oriented attachments under tension in control cells causes the separation of sister kinetochores by ~1.2 μm relative to ~0.65 μm in nocodazole treated cells (Fig. 5D; data not shown). Depletion of proteins that compromise kinetochore-microtubule attachments, such as the Mis12 complex subunit Dsn1, results in a reduction of inter-kinetochore stretch by ~30% (Fig. 5D). In contrast, Astrin and SKAP depleted cells show a 25% increase in this stretched distance (Fig. 5D) indicating that, if anything, inter-kinetochore tension is increased. Thus, Astrin and SKAP display a checkpoint-dependent arrest despite their ability to initially bi-orient sister chromatids, align chromosomes at the metaphase plate, and develop inter-kinetochore tension.

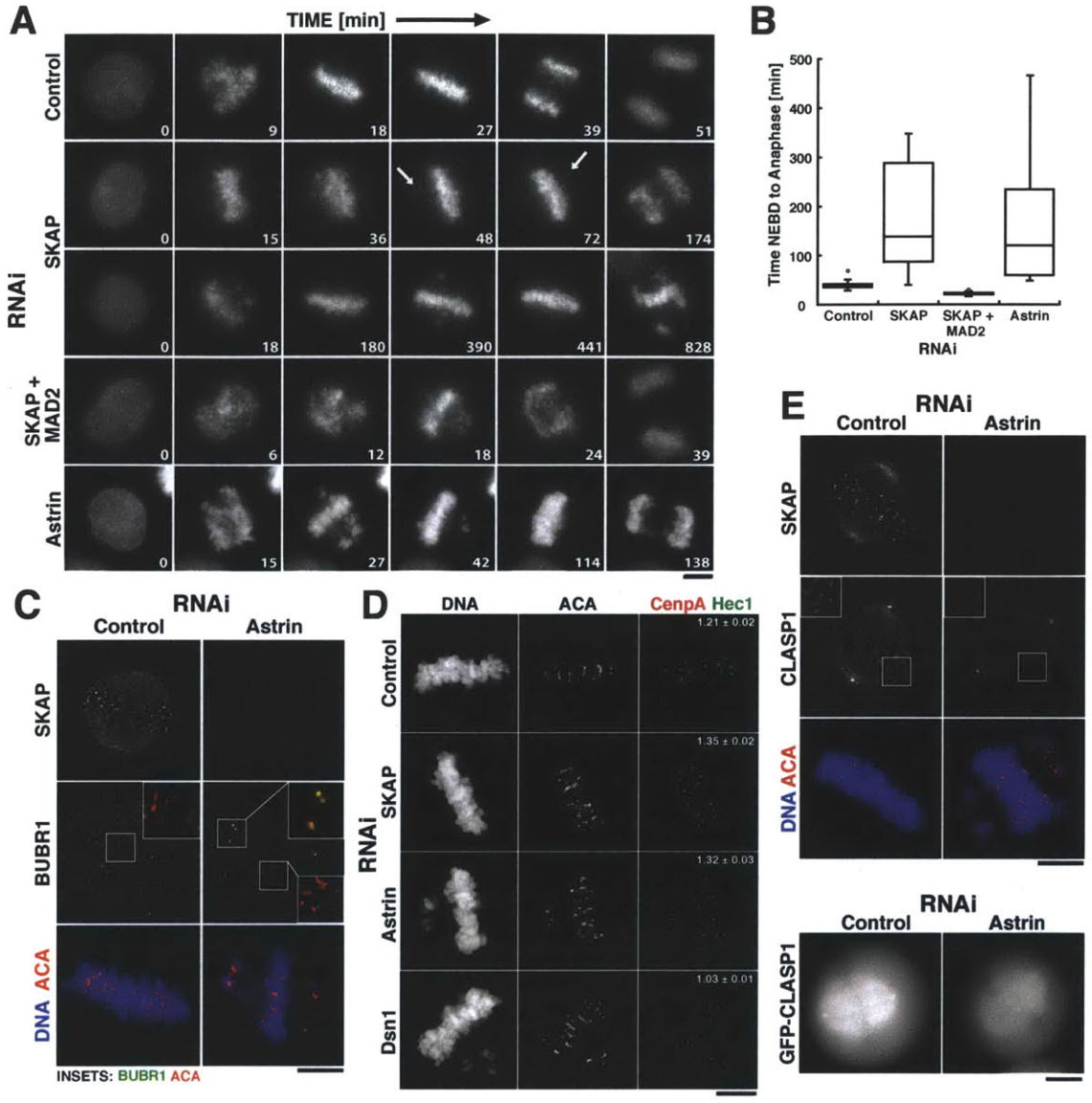

Figure 5. Astrin and SKAP depletion causes a checkpoint-dependent mitotic arrest. (*A*) Selected images from time lapse movies of HeLa cells expressing YFP-H2B in either control cells, SKAP depleted cells, Astrin depleted cells, or SKAP and Mad2 co-depleted cells. Numbers in each image indicate the relative time in minutes. Also see Supplemental movies 1-5. Scale bar, 5 μm. (*B*) Box plot showing the quantification of the time from nuclear envelope breakdown (NEBD) to anaphase onset indicating the median time, quartiles, and minimum and maximum values. (C) BubR1 is enriched on mis-aligned kinetochores in Astrin depleted cells. Immunoflourescence images showing ACA (red), BubR1 (green), DNA, and SKAP in control and Astrin depleted cells. (*D*) Astrin and SKAP depletion increase inter-kinetochore distance. Immunofluorescence images showing CENP-A (red), Hec1 (green), ACA, and DNA in either control (n = 6 cells, 151 kinetochores), Astrin (n = 3 cells, 30 kinetochores, $p < 0.01$), SKAP (n = 10 cells, 160 kinetochores, $p < 0.0001$), or

Dsn1 depleted cells (n = 6 cells, 130 kinetochores, $p < 0.0001$). Numbers indicate the average inter-kinetochore distance based on CENP-A +/- SEM. (*E*) Astrin is required for CLASP localization to kinetochores. Top, immunofluorescence images showing ACA (red), DNA (blue), CLASP1, and SKAP in either control or Astrin depleted cells. Bottom, GFP-CLASP1 localization in live control or Astrin depleted cells.

The Astrin/SKAP complex is required to target CLASP to kinetochores

Both Astrin and SKAP were recently identified in purifications with the microtubule plus end tracking protein CLASP (Maffini et al., 2009). Since we found that co-depletion of CLASP1 and CLASP2 did not affect the localization of SKAP to aligned kinetochores (Fig. 3A), we sought to determine whether the Astrin/SKAP complex affects CLASP targeting. Strikingly, we found that following depletion of Astrin, CLASP1 failed to localize to kinetochores (Fig. 5E). Astrin depletion has been shown to destabilize spindle microtubules (Bakhoum et al., 2009a; Duane Compton, personal communication), consistent with the idea that delocalization of CLASP, which affects microtubule dynamics (Maiato et al., 2003), may contribute to the defects observed in Astrin depleted cells.

SKAP deletion is viable, but displays some mitotic defects in chicken DT40 cells

To determine the role of SKAP in chicken, we generated a deletion of SKAP in DT40 cells (Fig. 6A-B). SKAP-deficient cells are viable with a growth rate similar to that of wild-type DT40 cells and display normal localization of kinetochore

proteins such as the Ndc80 complex subunit Nuf2 (Fig. 6C). SKAP knockout cells show relatively normal numbers of the different mitotic stages, but have a small increase in cells with multi-polar spindles (Fig. 6C). SKAP knockout cells also show increased mitotic defects upon removal of the microtubule depolymerizing drug nocodazole relative to control cells (data not shown). Thus, while the temporal localization and physical associations of SKAP are conserved in chicken, SKAP displays an increased functional requirement for chromosome segregation during an unperturbed cell division in human cells. A similar difference is observed for other outer kinetochore components, with Ska3 and ZW10 being essential for proper chromosome segregation in human cells, but dispensable for viability in DT40 cells (T.H. and T.F., unpublished observations).

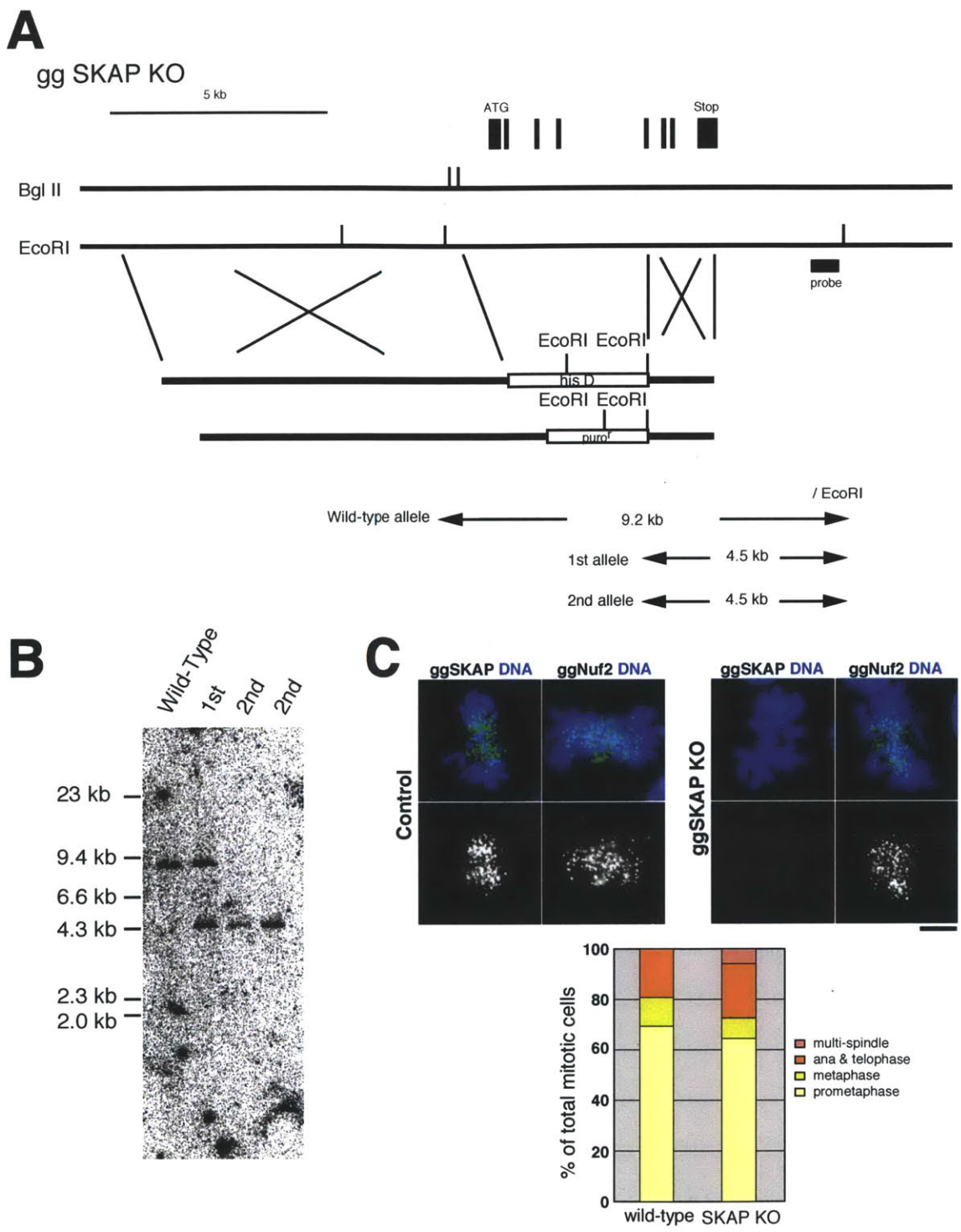

Figure 6. Generation and analysis of a SKAP knockout cell line in DT40 cells. (*A*) Restriction maps of the chicken SKAP locus, the gene disruption constructs, and the targeted loci. Black boxes indicate the positions of exons. EcoRI and BglII restriction sites are shown and the position of the probe used for

Southern hybridization is indicated. The targeted constructs are expected to disrupt four exons. Novel 4.5 kb (1st allele and 2nd allele) fragments digested with EcoRI should hybridize to the probe if the targeted integrations occur correctly. (*B*) Restriction analysis of the targeted integration for the SKAP disruption constructs. Genomic DNA from wild-type DT40 cells, a clone after first round targeting (+/-, 1st) and a clone after second round targeting (-/-, 2nd) were analyzed by Southern hybridization with the probe indicated in (A). (*C*) ggSKAP deletion in chicken DT40 cells does not alter Nuf2 localization. Immunofluorescence images showing ggSKAP or ggNuf2 localization (in green in merge) and DNA (blue) in either control DT40 cells, or SKAP knockout cells. See Supplemental Figure 2 for the generation of the SKAP knockout cell line. (*F*) Graph showing the percentage of different mitotic states in either control DT40 cells or ggSKAP knockout cells. Scale bars, 5 μm.

Aurora B differentially affects the targeting of distinct dynein subunits to kinetochores

Astrin and SKAP associate the dynein light chain LC8, as well as with small amounts of the cytoplasmic dynein heavy chain (Fig. 2A). LC8 has been implicated in the retrograde transport of dynein substrates, although it remains unclear whether LC8 mediates interactions with dynein cargo molecules or plays a different role (Puthalakath et al., 1999; Williams et al., 2007). The interaction with LC8 is surprising, as previous work on dynein suggested that it displays very different temporal localization from Astrin/SKAP to kinetochores (Pfarr et al., 1990; Steuer et al., 1990). Indeed, we found that the dynactin subunit Arp1 and the dynein light chain Tctex (DYNLT3) showed localization to kinetochores during prometaphase, but not metaphase and anaphase (Fig. 7A). In contrast, LC8 localized to metaphase and anaphase kinetochores, but not prometaphase

kinetochores (Fig. 7A). Thus, LC8 displays identical temporal localization to Astrin and SKAP during mitosis, including a preference for aligned kinetochores.

Astrin/SKAP complex localization to the outer kinetochore is strongly influenced by Aurora B activity (Fig. 4). Based on the close connection between Astrin/SKAP and the dynein-associated protein LC8, we sought to determine the dependence of other dynein interacting proteins on Aurora B phosphorylation. In contrast to Astrin/SKAP, we found that Aurora B activity is required to promote Tctex and Arp1 localization as ZM447493 treatment eliminated their localization from kinetochores in STLC treated cells (Fig. 7B). However, while expression of the Mis12-INCENP fusion prevented LC8 localization to kinetochores (Fig. 7C), this did not allow Tctex and Arp1 to localize to aligned kinetochores (Fig. 7D-E). This suggests either that both Aurora B and microtubule attachments affect Tctex and Arp1 localization, or that the additional Aurora B phosphorylation provided by the Mis12-INCENP fusion is not sufficient to target them to kinetochores. In contrast, LC8 behaves identically to Astrin and SKAP with its localization inhibited by local Aurora B activity (Fig. 7B-C). Importantly, the localization of LC8 to both the spindle and kinetochore during mitosis requires Astrin (Fig. 7F). In contrast, dynein depletion did not alter Astrin/SKAP localization to aligned kinetochores (Fig. 7G) and co-depletion of the two LC8 isoforms present in human cells does not affect SKAP localization or perturb mitotic progression (Fig. 7H-I; data not shown).

Whether the Astrin/SKAP complex recruits a sub-population of dynein to metaphase kinetochores through LC8 remains an open question. Importantly, we do find the cytoplasmic dynein motor associated with Astrin and SKAP in our purifications (Fig. 2A). However, if present, the pool of dynein at the metaphase kinetochores would only transiently interact with the Astrin/SKAP complex before moving towards the spindle pole via kinetochore microtubules. In total, this work suggests that there are two populations of dynein-interacting proteins; those whose kinetochore localization is promoted by Aurora B activity, and a second group including LC8 and Astrin/SKAP whose kinetochore localization is antagonized by Aurora B.

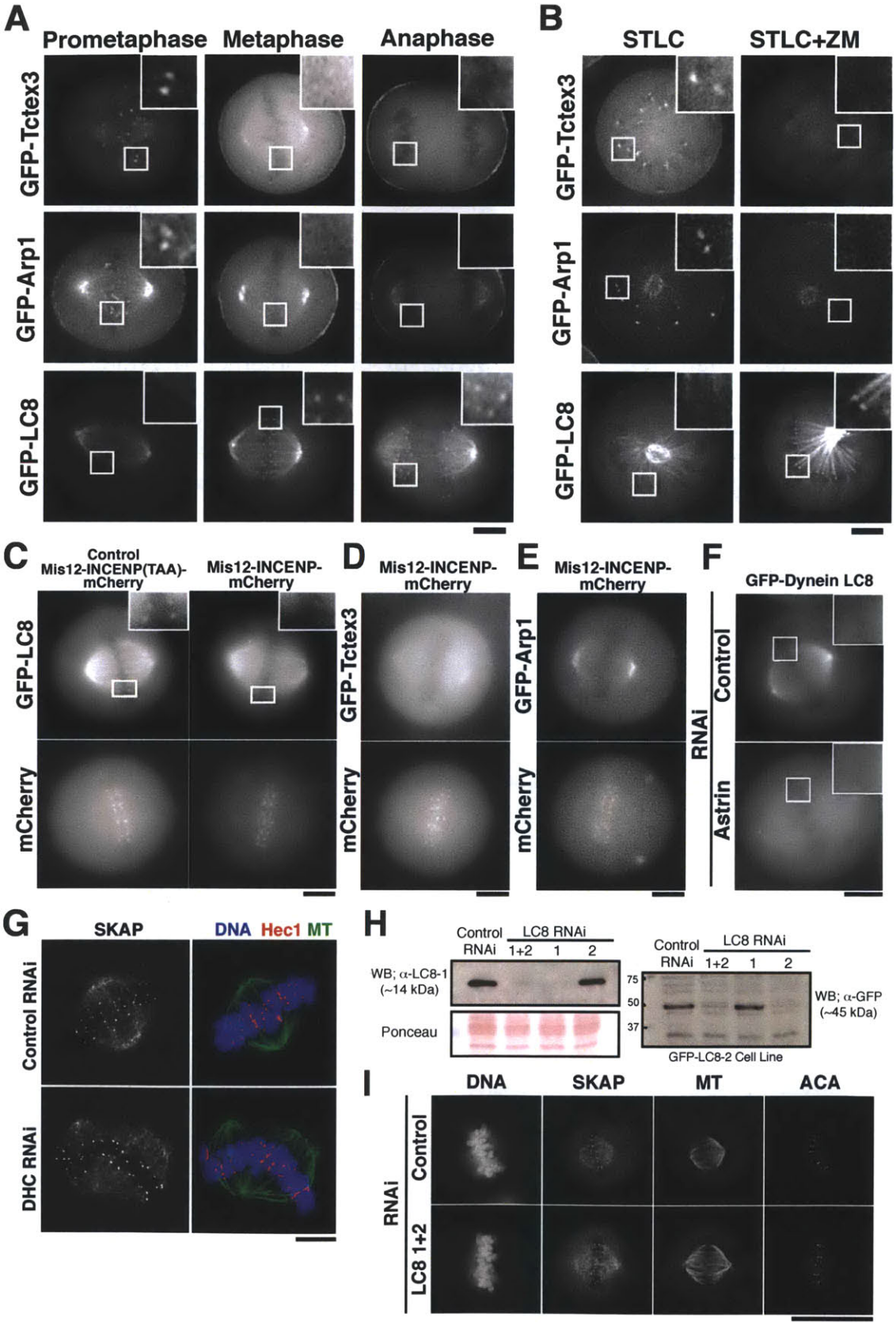
A
Prometaphase
Metaphase
Anaphase
GFP-Tctex3
GFP-Arp1
GFP-LC8
B
STLC
STLC+ZM
GFP-Tctex3
GFP-Arp1
GFP-LC8
C
Control Mis12-INCENP(TAA)-mCherry
Mis12-INCENP-mCherry
GFP-LC8
mCherry
D
Mis12-INCENP-mCherry
GFP-Tctex3
mCherry
E
Mis12-INCENP-mCherry
GFP-Arp1
mCherry
F
GFP-Dynein LC8
RNAi
Control
Astrin
G
SKAP
DNA Hec1 MT
Control RNAi
DHC RNAi
H
Control RNAi
LC8 RNAi
1+2
1
2
WB; α-LC8-1 (~14 kDa)
Ponceau
75
50
37
WB; α-GFP (~45 kDa)
GFP-LC8-2 Cell Line
I
DNA
SKAP
MT
ACA
RNAi
Control
LC8 1+2

Figure 7. Aurora B provides a switch in the targeting of different dynein subunits to kinetochores. (*A*) Images showing the localization of the dynein light chains GFP^{LAP}-Tctex3 and GFP^{LAP}-LC8, or the dynactin subunit GFP^{LAP}-Arp1 in different stages of mitosis. (*B*) Images showing the localization of GFP^{LAP}-Tctex3, GFP^{LAP}-LC8, or GFP^{LAP}-Arp1 in STLC treated cells, or STLC plus ZM447493 treated cells. (*C, D,* and *E*) Images showing the localization of GFP^{LAP}-Tctex3, GFP^{LAP}-LC8, or GFP^{LAP}-Arp1 and either Mis12-INCENP(TAA)-mCherry (control) or Mis12-INCENP-mCherry transfected cells as indicated. (F) Images showing the localization of GFP-LC8 in either control or Astrin depleted cells. Scale bar, 5 μm. (*G*) Dynein depletion does not affect Astrin localization to aligned kinetochores. Immunofluorescence showing SKAP localization in human cells, and co-localization with ACA (red), DNA (blue) and microtubules (green). Scale bars, 5 μm. (*H*) Western Blot showing depletion of LC8 isoform 1 and 2. Left, depletion of LC8 isoform 1 and 2 probed with an anti-LC8-1 antibody. Ponceau staining is shown as a loading control. Right, depletion of LC8 isoform 1 and 2 in the GFP^{LAP}-LC8-2 cell line probed with an anti-GFP antibody. (*I*) SKAP localization is unaffected by LC8 depletion. Immunofluorescence images showing ACA, SKAP, DNA, and microtubules in control and LC8 depleted cells.

Aurora B phosphorylation provides a switch for outer kinetochore composition

When sister-chromatids are correctly aligned and under tension, the reduction of Aurora B phosphorylation at the outer kinetochore (Liu et al., 2009; Welburn et al., 2010) allows the Astrin/SKAP complex to be recruited to kinetochores (Fig. 4). This may occur through the changes in the phosphorylation state of a kinetochore-bound Astrin/SKAP binding protein, or changes in the stability and number of kinetochore-bound microtubules that facilitate Astrin/SKAP recruitment. In either case, this provides a mechanism to recruit and exclude proteins from the outer kinetochore depending on the state of attachment and tension, with Aurora B phosphorylation molecularly distinguishing the two states.

Such a mechanism would allow protein activities to be specifically recruited to correctly bi-oriented kinetochores, possibly to stabilize metaphase attachments or execute anaphase. Importantly, the Astrin/SKAP complex is only present at bi-oriented kinetochores, but not kinetochores with attachment defects, suggesting that this complex does not function in the error correction process downstream of Aurora B. Instead, this raises the intriguing possibility that Aurora B phosphorylation generates a switch that molecularly distinguishes the composition prometaphase and metaphase kinetochores in a chromosome-autonomous fashion.

Materials and Methods

Cell culture and siRNA transfection

cDNAs were obtained as IMAGE clones. Stable clonal cells lines expressing GFP^{LAP} fusions were generated in HeLa cells as described previously (Cheeseman et al., 2004). We obtained HeLa cells expressing YFP-CENP-A (Kops et al., 2005) and YFP-H2B. Cells were maintained in Dulbecco's modified Eagle's medium (DMEM) supplemented with 10% fetal bovine serum (FBS), penicillin/streptomycin, and L-glutamine (Invitrogen) at 37°C in a humidified atmosphere with 5% CO_2. RNAi experiments were conducted as described previously (Kline et al., 2006). siRNAs against Astrin (UCCCGACAACUCACAGAGAAA; Thein et al., 2007), SKAP (GAAAGAGUCCGAUUCCUAG; Dharmacon), LC8-1/DYNLL1 (GUUCAAAUCUGGUUAAAAG, GAAGGACAUUGCGGCUCAU, GUACUAGUUUGUCGUGGUU, CAGCCUAAAUUCCAAAUAC; Dharmacon), LC8-2/DYNLL2 (GGAAGGCAGUGAUCAAGAA, GACAAGAAAUAUAACCCUA, CCAUGGAGAAGUACAAUAU, CAAAGCACUUCAUCUAUUU; Dharmacon), Nuf2 (AAGCAUGCCGUGAAACGUAUA; DeLuca et al., 2002), CENP-E (AAGGCUACAAUGGUACUAUA; Kapoor et al., 2006), CENP-F (GAGAAGACCCCAAGUCAUC; Johnson et al., 2004), a pool of 4 siRNAs targeting Ska3 (Welburn et al., 2009), Mad2 (UACGGACUCACCUUGCUUG; Martin-Lluesma et al., 2002), CLASP1 (GGAUGAUUUACAAGACUGG; Mimori-Kiyosue et al., 2005), CLASP2 (GACAUACAUGGGUCUUAGA; Mimori-Kiyosue et al., 2005), and a non-targeting control were obtained from Dharmacon. For co-depletions, individual siRNAs were first validated by combining these with an equal volume of non-targeting control siRNAs to ensure that they were still effective under these conditions.

Immunofluorescence and Microscopy

Immunofluorescence in human cells was conducted as described previously (Kline et al., 2006). For immunofluorescence against microtubules, DM1α (Sigma) was used at 1:500. For visualization of kinetochore proteins, we used phospho-Dsn1 (Welburn et al., 2010), mouse anti-HEC1 (9G3; Abcam, Cambridge, MA), mouse anti-Astrin (a generous gift from Mau-Sun Chang; Yang et al., 2006), mouse anti-CLASP1 (a generous gift from Helder Maiato), mouse anti-BubR1 (8G1; Abcam), rabbit anti-LC8-1 (ab51603; Abcam) and human anti-centromere antibodies (ACA; Antibodies, Inc., Davis, CA). An affinity purified rabbit polyclonal antibody was generated against full length SKAP as described previously (Desai et al., 2003). Cy2, Cy3, and Cy5-conjugated secondary antibodies (Jackson Laboratories) were used at 1:100. DNA was visualized using 10 μg/ml Hoechst.

For drug treatment, HeLa cells were incubated for 2-3 hours with drugs at the following concentrations: STLC: 10 μM, nocodazole: 0.2 μg/ml, ZM447439. Mis12-INCENP-mCherry and Mis12-INCENP(TAA)-mCherry plasmids (Liu et al., 2009) were a generous gift from Susanne Lens. To quantitate fluorescence intensity, individual kinetochores were selected from projections (chosen blindly based on co-localization with a separate stable kinetochore marker) and the integrated intensity was determined after subtracting the background fluorescence measured from adjacent regions of the cell using Metamorph. Fluorescence levels at kinetochores were normalized with respect to control cells. At least 5-10 cells were examined for each condition and antibody.

Images were acquired on a DeltaVision Core deconvolution microscope (Applied Precision) equipped with a CoolSnap HQ2 CCD camera. 30 to 40 Z-sections were acquired at 0.2-μm steps using a 100x, 1.3 NA Olympus U-

PlanApo objective with 1x1 binning. Images were deconvolved using the DeltaVision software. Images shown represent maximal intensity projections. Equivalent exposure conditions and scaling was used between controls and RNAi-depleted cells.

Analysis of SKAP in chicken DT40 cells

DT40 cells were cultured at 38°C in Dulbecco's modified medium supplemented with 10% fetal calf serum, 1% chicken serum, β-mercaptoethanol, penicillin, and streptomycin and transfected as described previously (Fukagawa et al., 2001). The SKAP targeted constructs were generated to disrupt four exons of the ggSKAP gene (Supplemental Fig. 2). After transfection, drug resistant colonies were isolated and Southern blot hybridization analysis was performed to identify clones in which the targeted integrations occurred correctly.

Immunofluorescent staining of DT40 cells was performed as described previously (Hori et al., 2008). Affinity-purified rabbit polyclonal antibodies were used against recombinant chicken Nuf2 (Hori et al., 2003) and SKAP (this study). Chromosomes and nuclei were counterstained with DAPI at 0.2 μg/ml in Vectashield Antifade (Vector Labs, Burlingame, CA). For the immunofluorescence images, 30 to 40 Z-sections were collected at 0.2 μm intervals with a cooled EM CCD camera (Quantem, Roper scientific) mounted on an Olympus IX71 inverted microscope with a 100X objective together with a filter wheel. Subsequent analysis and processing of images were performed using Metamorph software (Roper scientific).

Protein purification and biochemical assays

GFP^{LAP} tagged Astrin and SKAP were isolated from HeLa cells as described previously (Cheeseman and Desai, 2005). Purified proteins were identified by

mass spectrometry using an LTQ XL Ion trap mass spectrometer (Thermo) using MudPIT and SEQUEST software as described previously (Washburn et al., 2001).

For the expression and purification of the recombinant proteins, a GST fusion with full length SKAP was generated in pGEX-6P-1, and 6xHis-Astrin (955-1193) was generated in pRSETa. Proteins were purified using Glutathione agarose (Sigma) or Ni-NTA Agarose (Qiagen) according to the manufacturer's guidelines and then desalted into 50 mM Hepes pH 7.5, 200 mM KCl, 1 mM EDTA, 1 mM DTT (HEK200). Microtubule binding assays using the purified proteins were conducted as described previously (Cheeseman et al., 2006) using equal volumes of microtubules in BRB80 and test protein in HEK200.

References

Andrews, P.D., Y. Ovechkina, N. Morrice, M. Wagenbach, K. Duncan, L. Wordeman, and J.R. Swedlow. 2004. Aurora B regulates MCAK at the mitotic centromere. *Dev Cell.* 6:253-268.

Bakhoum, S.F., G. Genovese, and D.A. Compton. 2009a. Deviant kinetochore microtubule dynamics underlie chromosomal instability. *Curr Biol.* 19:1937-1942.

Bakhoum, S.F., S.L. Thompson, A.L. Manning, and D.A. Compton. 2009b. Genome stability is ensured by temporal control of kinetochore-microtubule dynamics. *Nat Cell Biol.* 11:27-35.

Chang, M.S., C.J. Huang, M.L. Chen, S.T. Chen, C.C. Fan, J.M. Chu, W.C. Lin, and Y.C. Yang. 2001. Cloning and characterization of hMAP126, a new member of mitotic spindle-associated proteins. *Biochem Biophys Res Commun.* 287:116-121.

Cheeseman, I.M., J.S. Chappie, E.M. Wilson-Kubalek, and A. Desai. 2006. The Conserved KMN Network Constitutes the Core Microtubule-Binding Site of the Kinetochore. *Cell.* 127:983-997.

Cheeseman, I.M., and A. Desai. 2005. A combined approach for the localization and tandem affinity purification of protein complexes from metazoans. *Sci STKE.* 2005:pl1.

Cheeseman, I.M., and A. Desai. 2008. Molecular Architecture of the Kinetochore-Microtubule Interface. *Nat Rev Mol Cell Biol.* 9:33-46.

Cheeseman, I.M., S. Niessen, S. Anderson, F. Hyndman, J.R. Yates, III, K. Oegema, and A. Desai. 2004. A conserved protein network controls assembly of the outer kinetochore and its ability to sustain tension. *Genes Dev.* 18:2255-2268.

Cheng, T.S., Y.L. Hsiao, C.C. Lin, C.T. Yu, C.M. Hsu, M.S. Chang, C.I. Lee, C.Y. Huang, S.L. Howng, and Y.R. Hong. 2008. Glycogen synthase kinase 3beta interacts with and phosphorylates the spindle-associated protein astrin. *J Biol Chem.* 283:2454-2464.

DeLuca, J.G., W.E. Gall, C. Ciferri, D. Cimini, A. Musacchio, and E.D. Salmon. 2006. Kinetochore Microtubule Dynamics and Attachment Stability Are Regulated by Hec1. *Cell.* 127:969-982.

DeLuca, J.G., B. Moree, J.M. Hickey, J.V. Kilmartin, and E.D. Salmon. 2002. hNuf2 inhibition blocks stable kinetochore-microtubule attachment and induces mitotic cell death in HeLa cells. *J Cell Biol.* 159:549-555.

Desai, A., S. Rybina, T. Muller-Reichert, A. Shevchenko, A. Shevchenko, A. Hyman, and K. Oegema. 2003. KNL-1 directs assembly of the microtubule-binding interface of the kinetochore in C. elegans. *Genes Dev.* 17:2421-2435.

Du, J., S. Jablonski, T.J. Yen, and G.J. Hannon. 2008. Astrin regulates Aurora-A localization. *Biochem Biophys Res Commun.* 370:213-219.

Emanuele, M.J., W. Lan, M. Jwa, S.A. Miller, C.S. Chan, and P.T. Stukenberg. 2008. Aurora B kinase and protein phosphatase 1 have opposing roles in modulating kinetochore assembly. *J Cell Biol.* 181:241-254.

Fang, L., A. Seki, and G. Fang. 2009. SKAP associates with kinetochores and promotes the metaphase-to-anaphase transition. *Cell Cycle*. 8:2819-2827.

Fukagawa, T., Y. Mikami, A. Nishihashi, V. Regnier, T. Haraguchi, Y. Hiraoka, N. Sugata, K. Todokoro, W. Brown, and T. Ikemura. 2001. CENP-H, a constitutive centromere component, is required for centromere targeting of CENP-C in vertebrate cells. *Embo J.* 20:4603-4617.

Gruber, J., J. Harborth, J. Schnabel, K. Weber, and M. Hatzfeld. 2002. The mitotic-spindle-associated protein astrin is essential for progression through mitosis. *J Cell Sci.* 115:4053-4059.

Hori, T., M. Amano, A. Suzuki, C.B. Backer, J.P. Welburn, Y. Dong, B.F. McEwen, W.-H. Shang, E. Suzuki, K. Okawa, I.M. Cheeseman, and T. Fukagawa. 2008. CCAN Makes Multiple Contacts with Centromeric DNA to Provide Distinct Pathways to the Outer Kinetochore. 135:1039-1052.

Hori, T., T. Haraguchi, Y. Hiraoka, H. Kimura, and T. Fukagawa. 2003. Dynamic behavior of Nuf2-Hec1 complex that localizes to the centrosome and centromere and is essential for mitotic progression in vertebrate cells. *Journal of cell science*. 116:3347-3362.

Johnson, V.L., M.I. Scott, S.V. Holt, D. Hussein, and S.S. Taylor. 2004. Bub1 is required for kinetochore localization of BubR1, Cenp-E, Cenp-F and Mad2, and chromosome congression. *J Cell Sci.* 117:1577-1589.

Kapoor, T.M., M.A. Lampson, P. Hergert, L. Cameron, D. Cimini, E.D. Salmon, B.F. McEwen, and A. Khodjakov. 2006. Chromosomes Can Congress to the Metaphase Plate Before Biorientation. *Science*. 311:388-391.

Kline, S.L., I.M. Cheeseman, T. Hori, T. Fukagawa, and A. Desai. 2006. The human Mis12 complex is required for kinetochore assembly and proper chromosome segregation. *J Cell Biol.* 173:9-17.

Kops, G.J., Y. Kim, B.A. Weaver, Y. Mao, I. McLeod, J.R. Yates, 3rd, M. Tagaya, and D.W. Cleveland. 2005. ZW10 links mitotic checkpoint signaling to the structural kinetochore. *J Cell Biol.* 169:49-60.

Lan, W., X. Zhang, S.L. Kline-Smith, S.E. Rosasco, G.A. Barrett-Wilt, J. Shabanowitz, D.F. Hunt, C.E. Walczak, and P.T. Stukenberg. 2004. Aurora B phosphorylates centromeric MCAK and regulates its localization and microtubule depolymerization activity. *Curr Biol.* 14:273-286.

Liu, D., G. Vader, M.J. Vromans, M.A. Lampson, and S.M. Lens. 2009. Sensing chromosome bi-orientation by spatial separation of aurora B kinase from kinetochore substrates. *Science*. 323:1350-1353.

Liu, D., M. Vleugel, C.B. Backer, T. Hori, T. Fukagawa, I.M. Cheeseman, and M.A. Lampson. 2010. Regulated targeting of protein phosphatase 1 to the outer kinetochore by KNL1 opposes Aurora B kinase. *J Cell Biol.* 188:809-820.

Mack, G.J., and D.A. Compton. 2001. Analysis of mitotic microtubule-associated proteins using mass spectrometry identifies astrin, a spindle-associated protein. *Proc Natl Acad Sci U S A.* 98:14434-14439.

Maffini, S., A.R. Maia, A.L. Manning, Z. Maliga, A.L. Pereira, M. Junqueira, A. Shevchenko, A. Hyman, J.R. Yates, 3rd, N. Galjart, D.A. Compton, and H. Maiato. 2009. Motor-independent targeting of CLASPs to kinetochores by

CENP-E promotes microtubule turnover and poleward flux. *Curr Biol.* 19:1566-1572.

Maiato, H., E.A. Fairley, C.L. Rieder, J.R. Swedlow, C.E. Sunkel, and W.C. Earnshaw. 2003. Human CLASP1 is an outer kinetochore component that regulates spindle microtubule dynamics. *Cell.* 113:891-904.

Maresca, T.J., and E.D. Salmon. 2009. Intrakinetochore stretch is associated with changes in kinetochore phosphorylation and spindle assembly checkpoint activity. *J Cell Biol.* 184:373-381.

Martin-Lluesma, S., V.M. Stucke, and E.A. Nigg. 2002. Role of Hec1 in spindle checkpoint signaling and kinetochore recruitment of Mad1/Mad2. *Science.* 297:2267-2270.

Mimori-Kiyosue, Y., I. Grigoriev, G. Lansbergen, H. Sasaki, C. Matsui, F. Severin, N. Galjart, F. Grosveld, I. Vorobjev, S. Tsukita, and A. Akhmanova. 2005. CLASP1 and CLASP2 bind to EB1 and regulate microtubule plus-end dynamics at the cell cortex. *J. Cell Biol.* 168:141-153.

Pfarr, C.M., M. Coue, P.M. Grissom, T.S. Hays, M.E. Porter, and J.R. McIntosh. 1990. Cytoplasmic dynein is localized to kinetochores during mitosis. *Nature.* 345:263-265.

Puthalakath, H., D.C. Huang, L.A. O'Reilly, S.M. King, and A. Strasser. 1999. The proapoptotic activity of the Bcl-2 family member Bim is regulated by interaction with the dynein motor complex. *Mol Cell.* 3:287-296.

Resnick, T.D., D.L. Satinover, F. MacIsaac, P.T. Stukenberg, W.C. Earnshaw, T.L. Orr-Weaver, and M. Carmena. 2006. INCENP and Aurora B promote meiotic sister chromatid cohesion through localization of the Shugoshin MEI-S332 in Drosophila. *Dev Cell.* 11:57-68.

Ruchaud, S., M. Carmena, and W.C. Earnshaw. 2007. Chromosomal passengers: conducting cell division. *Nat Rev Mol Cell Biol.* 8:798-812.

Sessa, F., M. Mapelli, C. Ciferri, C. Tarricone, L.B. Areces, T.R. Schneider, P.T. Stukenberg, and A. Musacchio. 2005. Mechanism of Aurora B activation by INCENP and inhibition by hesperadin. *Mol Cell.* 18:379-391.

Steuer, E.R., L. Wordeman, T.A. Schroer, and M.P. Sheetz. 1990. Localization of cytoplasmic dynein to mitotic spindles and kinetochores. *Nature.* 345:266-268.

Thein, K.H., J. Kleylein-Sohn, E.A. Nigg, and U. Gruneberg. 2007. Astrin is required for the maintenance of sister chromatid cohesion and centrosome integrity. *J Cell Biol.* 178:345-354.

Uchida, K.S., K. Takagaki, K. Kumada, Y. Hirayama, T. Noda, and T. Hirota. 2009. Kinetochore stretching inactivates the spindle assembly checkpoint. *J Cell Biol.* 184:383-390.

Washburn, M.P., D. Wolters, and J.R. Yates, 3rd. 2001. Large-scale analysis of the yeast proteome by multidimensional protein identification technology. *Nature Biotechnology.* 19:242-247.

Welburn, J.P., E.L. Grishchuk, C.B. Backer, E.M. Wilson-Kubalek, J.R. Yates, 3rd, and I.M. Cheeseman. 2009. The human kinetochore Ska1 complex facilitates microtubule depolymerization-coupled motility. *Dev Cell.* 16:374-385.

Welburn, J.P.I., M. Vleugel, D. Liu, J.R. Yates, 3rd, M.A. Lampson, T. Fukagawa, and I.M. Cheeseman. 2010. Aurora B phosphorylates spatially distinct targets to differentially regulate the kinetochore-microtubule interface. *Mol Cell.* In press.

Williams, J.C., P.L. Roulhac, A.G. Roy, R.B. Vallee, M.C. Fitzgerald, and W.A. Hendrickson. 2007. Structural and thermodynamic characterization of a cytoplasmic dynein light chain-intermediate chain complex. *Proc Natl Acad Sci U S A.* 104:10028-10033.

Yang, Y.C., Y.T. Hsu, C.C. Wu, H.T. Chen, and M.S. Chang. 2006. Silencing of astrin induces the p53-dependent apoptosis by suppression of HPV18 E6 expression and sensitizes cells to paclitaxel treatment in HeLa cells. *Biochem Biophys Res Commun.* 343:428-434.

Chapter III: The kinetochore-bound Ska1 complex tracks depolymerizing microtubule by binding curved protofilaments

Jens C. Schmidt, Haribabu Arthanari , Andras Boeszoermenyi, Elizabeth Wilson-Kubalek, Natalia M. Dashkevich, Nilah Monnier, Michelle Markus, Monika Oberer, Gerhard Wagner, Ron Milligan, Mark Bathe, Ekaterina L. Grishchuk, Iain M. Cheeseman.

Andras Boeszoermenyi, Haribabu Arthanari and Michelle Markus carried our NMR-based structure determination of the ceSKA1 MTBD. Elizabeth Wilson-Kubalek carried out electron microscopy experiments. Natalia M. Dashkevich carried out dynamic microtubule tracking assays. Nilah Monnier carried out single particle tracking of TIRFM movies.

Summary

To ensure equal chromosome segregation during mitosis, the macromolecular kinetochore must remain attached to depolymerizing microtubules, which drive poleward chromosome movement. How kinetochores associate with depolymerizing microtubules, which undergo dramatic structural changes forming curved protofilaments, has yet to be defined in vertebrates. Here, we demonstrate that the conserved kinetochore-localized Ska1 complex tracks with depolymerizing microtubule ends. Strikingly, the Ska1 complex can associate with both the microtubule lattice and curved protofilament structures. In contrast, the Ndc80 complex, a central player in the kinetochore-microtubule interface, binds only to the straight microtubule lattice and lacks tracking activity. Importantly, we demonstrate that the Ska1 complex can impart its tracking capability to the Ndc80 complex. We also present a structure of the Ska1 microtubule binding domain that defines its interaction with microtubules and its regulation by Aurora B. This work defines an integrated kinetochore-microtubule interface formed by the Ska1 and Ndc80 complexes that associates with depolymerizing microtubules by interacting with curved microtubule protofilaments.

Introduction

In eukaryotes, the physical distribution of chromosomes to the daughter cells during mitosis requires a force-generating connection between chromosomal DNA and spindle microtubules. The multi-protein kinetochore complex, comprised of more than 100 different proteins in human cells, assembles upon centromeric DNA to mediate microtubule interactions (Cheeseman and Desai, 2008). Although several molecular motors localize to kinetochores, work over the past two decades has suggested that the primary driver of chromosome movement is microtubule dynamics (McIntosh et al., 2010). During microtubule polymerization, GTP-bound tubulin dimers are incorporated into the microtubule lattice. Upon assembly, GTP is rapidly hydrolyzed to GDP (Desai and Mitchison, 1997). GDP-tubulin has a curved conformation relative to GTP-tubulin, but is forced into a straight conformation in the context of the microtubule lattice (Wang and Nogales, 2005). Thus, microtubules store potential energy that is released during microtubule depolymerization when GDP-tubulin subunits exposed at the microtubule end undergo a conformational change resulting in the peeling away of individual microtubule protofilaments. These bending protofilaments have been demonstrated to generate force with a theoretical maximum of 65 pN per microtubule (Grishchuk et al., 2005). However, to harness this force and to move processively, kinetochores must remain associated with these dramatically changing structures.

A key challenge has been to define the specific molecules that mediate kinetochore-microtubule interactions, and to determine the mechanisms by which

these proteins remain associated with depolymerizing microtubules. The central player at the kinetochore-microtubule interface is the conserved Ndc80 complex, a component of the larger KNL1/Mis12 Complex/Ndc80 Complex (KMN) network (Cheeseman et al., 2006). Loss of Ndc80 function results in catastrophic defects in kinetochore-microtubule attachments (DeLuca et al., 2002). The Ndc80 complex has been shown to track with polymerizing and depolymerizing microtubules when artificially oligomerized on the surface of a microsphere (Powers et al., 2009). However, monomeric Ndc80 complex lacks this activity. In addition to the Ndc80 complex, the fungal Dam1 complex plays a critical role in chromosome segregation in budding yeast and is capable of forming striking ring-like structures around microtubules (Miranda et al., 2005; Westermann et al., 2006), although the existence of this ring in cells has been debated. In budding yeast, the Ndc80 and Dam1 complexes work together to mediate connections to microtubules, with the Dam1 complex facilitating processive interactions of the Ndc80 complex with microtubules (Lampert et al., 2010; Tien et al., 2010). However, the Dam1 complex is absent from metazoa, including humans, and the nature of an integrated kinetochore-microtubule interface capable of processively associating with depolymerizing microtubules has yet to be defined in vertebrates.

We and others have previously implicated the human Ska1 complex as an important kinetochore component involved in the formation of kinetochore-microtubule interactions (Daum et al., 2009; Gaitanos et al., 2009; Hanisch et al., 2006; Raaijmakers et al., 2009; Theis et al., 2009; Welburn et al., 2009).

However, the mechanisms by which the Ska1 complex acts to mediate kinetochore-microtubule interactions were unclear. Here, we took combined biochemical, biophysical, structural, and cell biological approaches to analyze the functions and activities of the Ska1 complex for its interactions with microtubules. Based on our data, we propose a model in which the distinct biochemical activities of the Ska1 and Ndc80 complexes form an integrated interface to couple chromosome movement to microtubule depolymerization.

Results

The C-terminus of Ska1 contains the conserved microtubule-binding domain of the Ska1 complex

The Ska1 complex is an integral component of the kinetochore-microtubule interface in human cells, but to date the Ska1 complex has not been described outside of vertebrates. To define the conserved biochemical properties of the Ska1 complex, we sought to identify the *C. elegans* Ska1 complex. Homology-based searches identified *C. elegans* SKA-1 (Y106G6H.15; Fig. 1A). Based on RNAi experiments, SKA-1 is not essential for embryonic viability in *C. elegans* (Arshad Desai, personal communication). Similar to human Ska1 (Welburn et al., 2009), GFP-SKA-1 localized to the mitotic spindle and kinetochores from prometaphase through anaphase (Fig. 1B). One-step immunoprecipitations of GFP-SKA-1 from *C. elegans* adults identified a complex of SKA-1 and F54E7.8 (Fig. 1C), which displays limited sequence similarity to Ska3 (data not shown). We did not identify a counterpart to Ska2, suggesting that this protein may have been lost from nematodes. Sedimentation velocity analytical ultracentrifugation (SVAUC) of the reconstituted *C. elegans* Ska1 complex demonstrated that it is composed of two copies of SKA-1 and a single copy of SKA-3 (Fig. 1D-F). In contrast, our previous biochemical analysis (Welburn et al., 2009) and recent structural data (Jeyaprakash et al., 2012) suggests that the human Ska1 complex is composed of two copies each of Ska1, Ska2, and Ska3 (Fig. 1F).

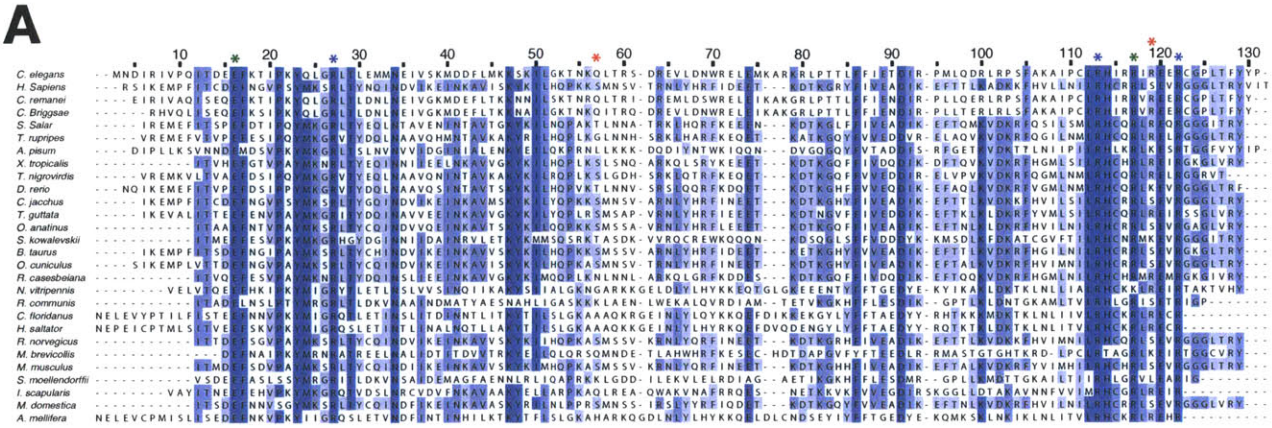

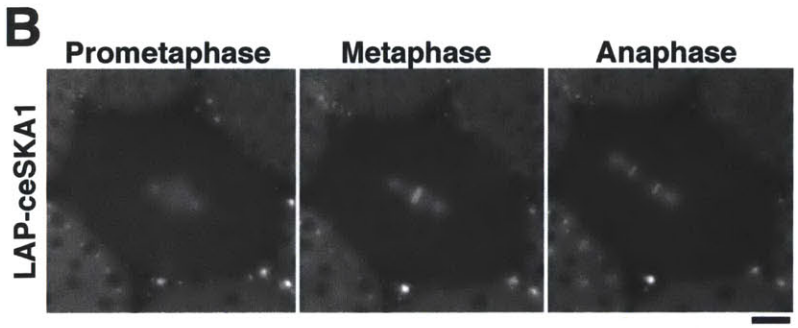

C

LAP- ceSKA1 IP

Protein	% Seq. Coverage	MW (kDa)
Y106G6H.15 (ceSKA1)	70.0	28.4
F54E7.8 (ceSKA3)	73.7	29.8

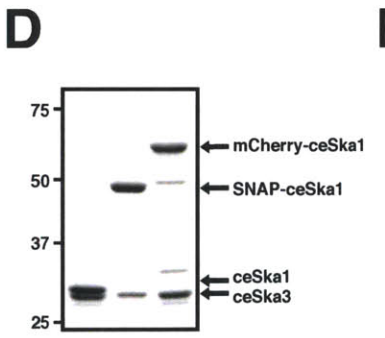

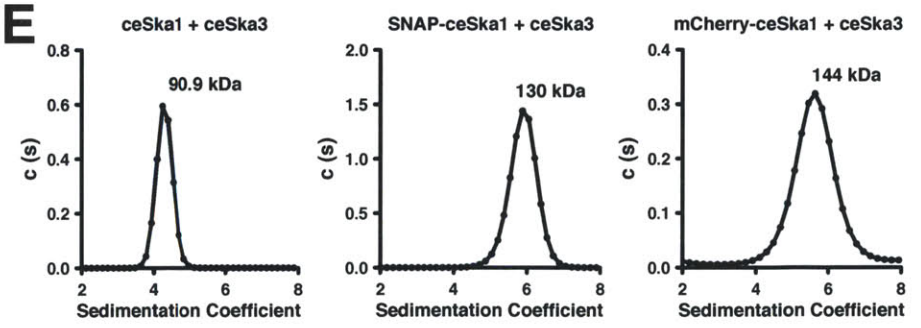

Complex	Predicted Mass (2:1)	Main Peak Mass	Frict. Coeff.	S Value	RMSD
ceSka1 + ceSka3	89.0 kDa	90.9 kDa	1.68	4.3	0.005
SNAP-ceSka1 + ceSka3	129.1 kDa	130.0 kDa	1.63	5.6	0.005
mCherry-ceSka1 + ceSka3	144.0 kDa	144.0 kDa	1.67	5.9	0.007

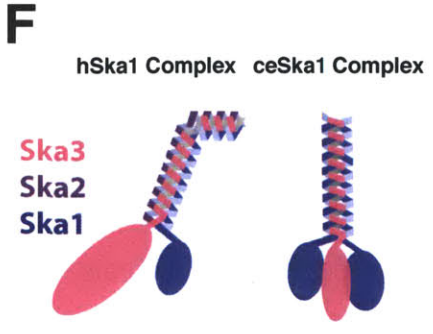

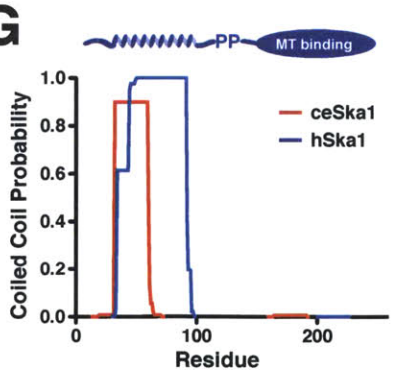

Figure 1. Identification of the *C. elegans* homologue of the Ska1 complex. (A) Multiple sequence alignment of the C-terminal half of the Ska1 protein showing the high degree of conservation of the Ska1 microtubule-binding domain. (*B*) GFP-ceSKA1 localizes to the mitotic spindle and kinetochores throughout mitosis. Fluorescence images from different mitotic stages of a one-cell *C. elegans* embryo stably expressing GFP-ceSKA-1. Scale bar, 5 μm. (C) Data from mass spectrometry analysis of LAP-ceSKA1 immunoprecipitation indicating percent sequence coverage of the listed proteins. (D) Coomassie gel of ceSKA1 complex constructs used for analytical ultracentrifugation. (E) svAUC analysis of the recombinant ceSKA1 complex (top left), SNAP-ceSKA1 complex (top middle), and mCherry-ceSKA1 complex (top right). The ceSKA1 complex, SNAP-ceSKA1 complex, and mCherry-ceSKA1 complex sediment as a single species with sedimentation coefficients of 4.3S (90.9 kDa), 5.6S (130 kDa), and 5.9S (144 kDa) respectively. (Bottom) Table summarizing the svAUC analysis of all ceSKA1 complex constructs. (*F*) Models for the molecular composition of the human and *C. elegans* Ska1 complexes based on (Jeyaprakash et al., 2012; Welburn et al., 2009) and Fig. 1E. (*G*) Graph showing the predicted probability for formation of a coiled-coil structure for hSka1 and ceSKA-1. The N-terminus of Ska1 contains a conserved coiled-coil region.

We next sought to identify the microtubule binding domain of the Ska1 complex. The C-terminal half of Ska1 is the most highly conserved (Fig. 1A), suggesting that this represents the microtubule-binding domain, whereas the N-terminus contains a conserved coiled-coil (Fig. 1F). In microtubule co-sedimentation assays, the reconstituted *C. elegans* and human Ska1 complexes both bound to taxol stabilized microtubules with apparent dissociation constants of 11.3 μM and 2.4 μM, respectively (Fig. 2A, B). In addition, the C-terminus of both human Ska1 (residues 132-255, K_D = 2.5 μM) and *C. elegans* SKA-1 (residues 118-243, K_D = 6.3 μM) bound to microtubules directly (Fig. 2A, B), whereas complexes lacking the C-terminus failed to bind to microtubules (Fig. 1D), but did not affect complex formation (Fig. 3A, B). Importantly, all antibodies used in this study have similar standard curves in western blots, allowing us to reliably determine relative affinities (Fig. 2C). These results demonstrate that the

C-terminal half of Ska1 is the conserved microtubule-binding domain of the Ska1 complex.

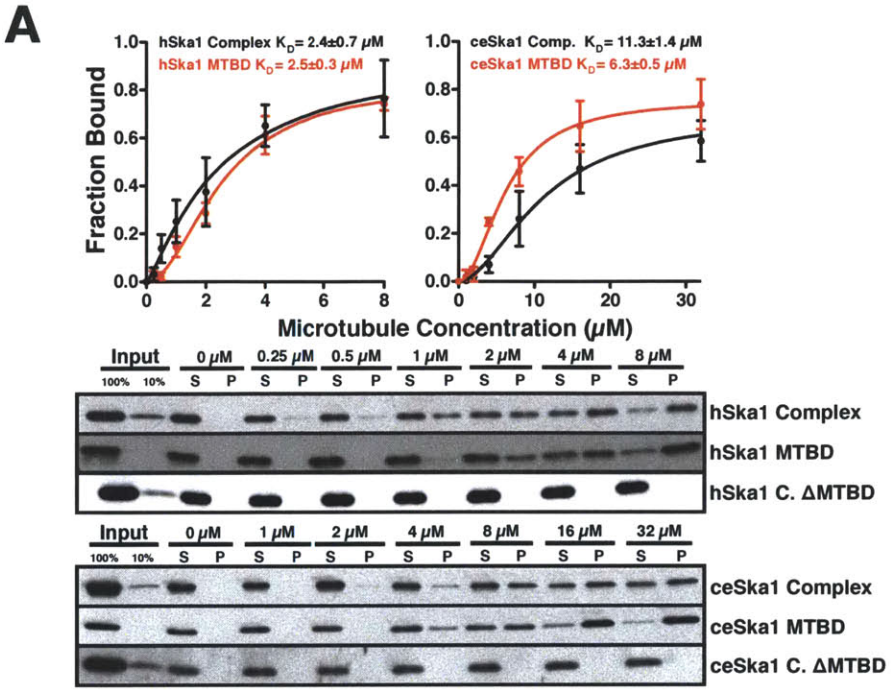

B

Protein	Kd (μM)	95% Conf. (μM)
hSka1 Complex	2.4±0.7	0.6 - 4.3
ceSka1 Complex	11.2±1.4	7.4 - 14.9
hSka1 MTBD	2.5±0.3	2.0 - 3.1
ceSka1 MTBD	6.3±0.5	4.8 - 7.8

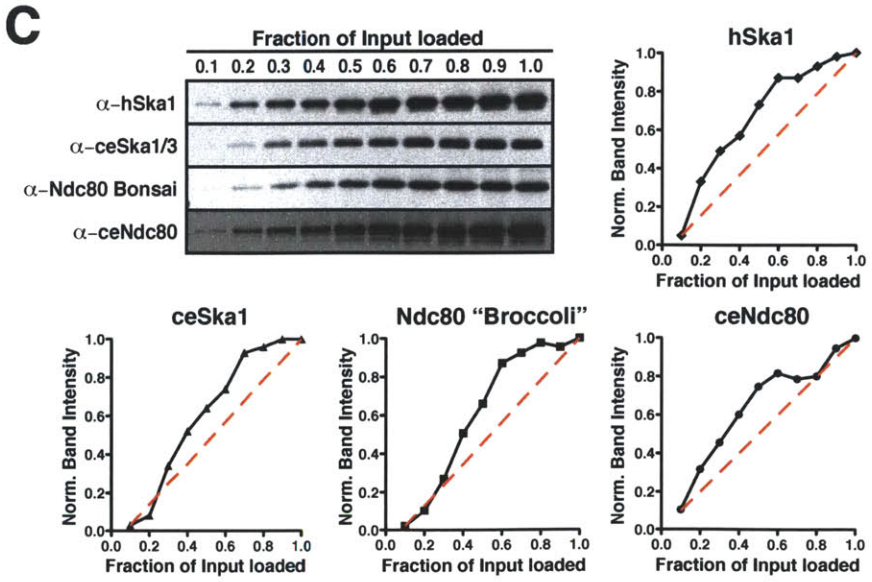

Figure 2. The C-terminus of Ska1 is the conserved microtubule-binding domain of the Ska1 complex. (*A*) Quantification (n = 3) (top) and Western blots (bottom) showing microtubule co-sedimentation for the human and *C. elegans* Ska1 complexes , the full Ska1 complexes lacking the C-terminal microtubule binding domain (MTBD) in Ska1, and the Ska1 microtubule binding domain alone (100 nM, 75 mM KCl). Western blots were probed with antibodies against hSka1 or the full ceSKA1 complex. The C-terminus of Ska1 protein is necessary and sufficient for Ska1 complex microtubule binding. (*B*) Table showing the dissociation constants and 95% confidence intervals for human and *C. elegans* Ska1 complex and Ska1 MTBD. (*C*) Western blots showing standard curves of all antibodies used in this study for the quantification of microtubule co-sedimentation assays.

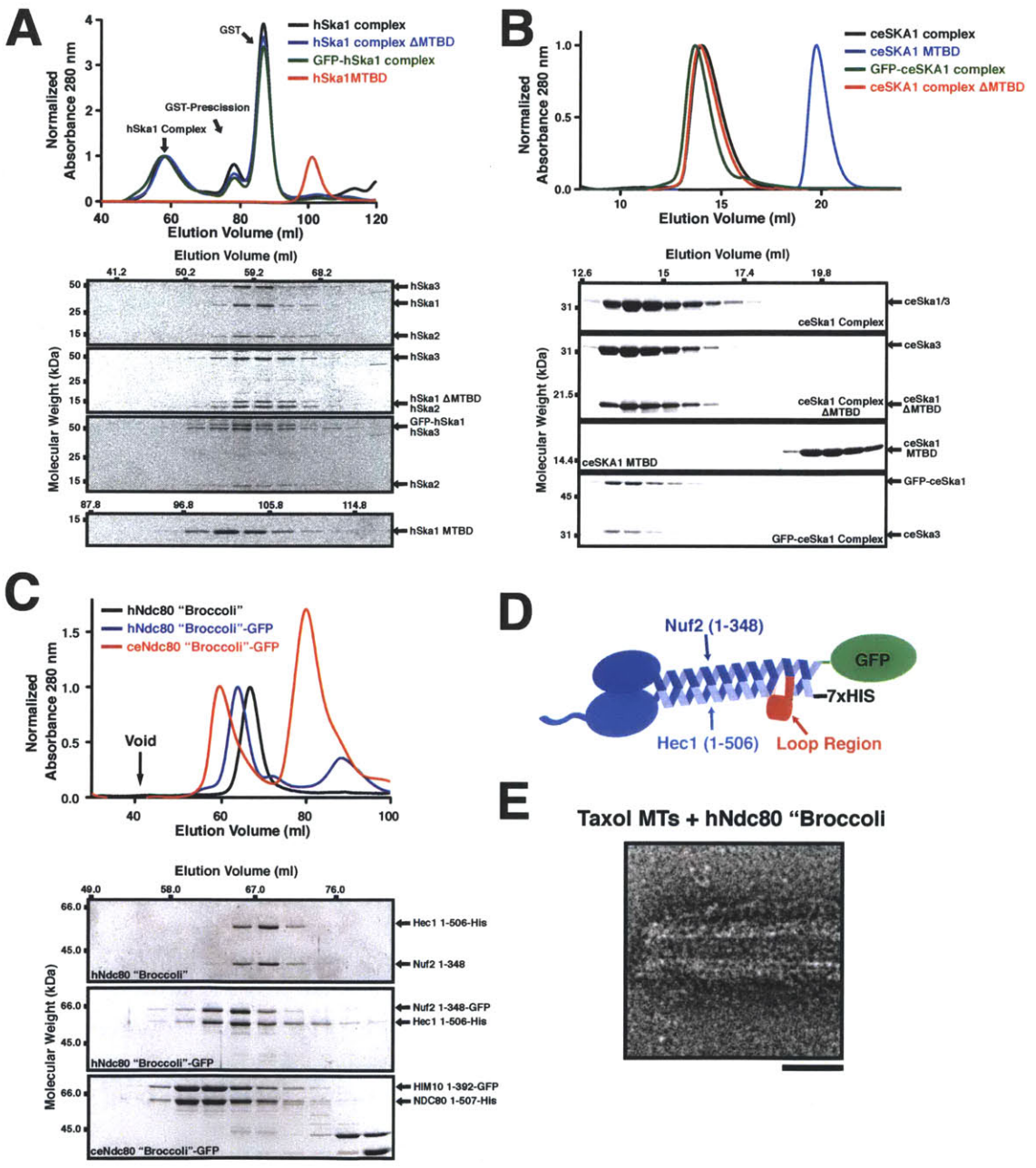

Figure 3. Purification and analysis of recombinant protein complexes used in this study. Gel filtration traces (top) and the corresponding Coomassie gels (bottom) of (A) the hSka1 complex (Superdex 200 16/60), (B) the ceSKA1 complex (Superose 6 10/300), and (C) the Ndc80 complex (Superdex 200 16/60) constructs used in this study. (D) Illustration of hNdc80 "Broccoli". (E) TEM image of hNdc80 "Broccoli" binding to microtubules (Scale Bar 40 nm).

Ska1 microtubule binding is essential for mitotic progression and the formation of robust kinetochore-microtubule attachments

We next sought to determine the contribution of the Ska1 microtubule-binding activity to chromosome segregation. Full-length GFP-Ska1 localizes to kinetochores and the mitotic spindle (Fig. 4A). In contrast, the hSka1 N-terminus lacking the microtubule binding domain (Ska1 ΔMTBD; residues 1-131) localized to kinetochores, but not spindle microtubules (Fig. 4A). GFP-Ska1 containing only the microtubule-binding domain (residues 132-255) localized to the mitotic spindle, but not kinetochores (Fig. 4A). Full length GFP-Ska1 efficiently rescued depletion of endogenous Ska1 (Fig. 4B-F). Importantly, RNAi-based replacement of endogenous Ska1 with GFP-Ska1 ΔMTBD resulted in a significant increase in the time from nuclear envelope breakdown (NEBD) to anaphase onset to 174 min (Fig. 4B) compared to 44 minutes for controls or cells in which full length GFP-Ska1 replaces the endogenous protein (Fig. 4B). Following depletion of endogenous Ska1, the majority of cells expressing GFP-Ska1 ΔMTBD contained aligned chromosomes, demonstrating that the Ska1 microtubule binding activity is not required for initial chromosome alignment (Fig. 4C). However, cells expressing GFP-Ska1 ΔMTBD displayed strongly reduced cold stable kinetochore fibers (K-fibers; Fig. 4C, D), which monitor the stability of kinetochore-microtubule interactions. In addition, based on time-lapse analysis, we found that sister chromatid oscillations were significantly impaired in cells lacking the Ska1 microtubule binding domain (Fig. 4E, F). We also observed modest defects in mitotic timing, cold stable kinetochore-fibers,

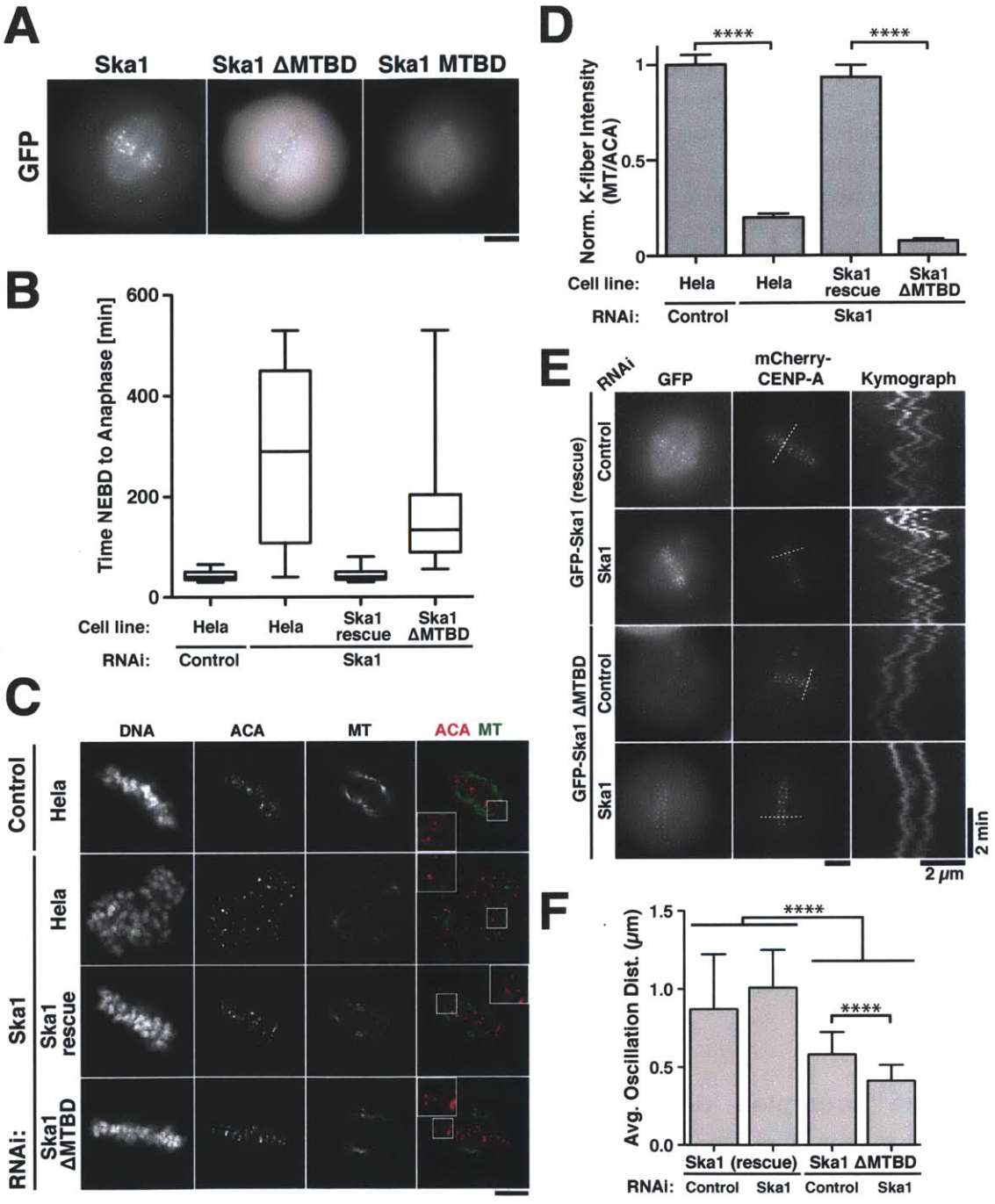

Figure 4. The microtubule-binding activity of the Ska1 complex is required for mitotic progression and kinetochore-microtubule attachments. (*A*) Fluorescent images showing the localization of GFP-tagged hSka1 constructs into HeLa cells. Full length GFP-Ska1 localizes to kinetochores and the mitotic spindle. GFP-tagged hSka1 lacking the MTBD (residues 1-131) localizes only to kinetochores, whereas the MTBD (residues 132-255) localizes exclusively to the mitotic spindle. Scale bar, 5 μm. (*B*) HeLa cell lines stably expressing GFP-tagged and RNAi resistant full-length Ska1 or Ska1 ΔMTDB were depleted for

endogenous Ska1 by RNAi. Cells were imaged by time-lapse microscopy 36 h after siRNA transfection and the time from nuclear envelope breakdown (NEBD) to anaphase was quantified (n = 42-58 cells per condition). (*C*) Immunofluorescence of HeLa cells stably expressing LAP-Ska1 or LAP-Ska1 ΔMTDB depleted for endogenous Ska1 following cold treatment for 10 min. Cells were immuno-stained against centromeres (ACA, magenta), microtubules (DM1α, green), and DNA. (*D*) Quantification of kinetochore-microtubule intensity (C) showing the mean and standard error of the mean (18-22 cells per conditions, 10 kinetochores per cell, $P < 0.0001$, t-test). Kinetochores were chosen at random and adjacent microtubule intensity was quantified and normalized using the ACA signal. (*E*) Live cell fluorescent images and kymograph showing the oscillation of sister kinetochores in HeLa cells stably expressing LAP-Ska1 or LAP-Ska1 ΔMTDB and mCherry CENP-A depleted for endogenous Ska1. (*F*) Quantification of sister chromatid oscillations from (*E*) showing the average distance and standard deviation that a kinetochore pair moved prior to reversing direction (LAP-Ska1 Control n = 7 cells, 129 oscillations, Ska1 RNAi n = 6 cells, 119 Oscillations; LAP-Ska1 ΔMTDB Control n = 11 cells, 178 oscillations, Ska1 RNAi n = 7 cells, 199 Oscillations; $P < 0.0001$, t-test).

and sister chromatid oscillations for GFP-Ska1 ΔMTBD in the presence of the endogenous proteins (Fig. 4, data not shown) consistent with dominant negative effects due to the dimerization of the Ska1 complex. These results demonstrate that the microtubule binding activity of Ska1 is necessary for the formation of robustkinetochore-microtubule interactions and proper kinetochore movement, which in turn are required for timely mitotic progression.

The Ska1 complex diffuses on microtubules as complex containing multiple microtubule binding sites

To analyze the microtubule-binding activity of individual molecules of the human and *C. elegans* Ska1 complexes, we next visualized the Ska1 complex containing GFP-Ska1 using total internal reflection fluorescence microscopy (TIR-FM; Fig. 5A). Human GFP-Ska1 complex readily diffused on microtubules

(Fig. 5B), similar to the human Ndc80-GFP complex (Fig. 5B). We note that for the biochemical experiments in this paper, we used well-behaved truncated versions of Ndc80 and Nuf2 that include all microtubule-binding and adjacent regions and behaves identically to full-length Ndc80 complex (termed Ndc80 "Broccoli"; see Fig. 3C - E). Based on the intensity distributions and the lack of bleaching events in our TIRF analysis, hNdc80 "Broccoli"-GFP is mostly monomeric on microtubules (Fig. 5C; also see (Powers et al., 2009)). In contrast, the GFP-hSka1 complex intensity distribution displayed two distinct peaks; particles with a mean brightness similar to the Ndc80-GFP complex, and particles that have a two-fold increased intensity (Fig. 5C), suggesting that GFP-hSka1 complex is present on microtubules as monomers and dimers. Importantly, time-lapse analysis of GFP-hSka1 complex binding events revealed bleaching steps with the intensity value of a single GFP fluorophore (Fig. 5D), confirming the presence of two GFP-Ska1 molecules. This is consistent with our previous biochemical analysis (Welburn et al., 2009) and recent structural work (Jeyaprakash et al., 2012) indicating that the hSka1 complex dimerizes to generate a complex with two microtubule binding sites. In contrast, in the absence of Ska3, which is required to dimerize the Ska1 complex (Welburn et al., 2009), the GFP-hSka1/2 complex behaved as a monomer (Fig. 5E, F). GFP-hSka1 complex, GFP-hSka1/2, and Ndc80 "Broccoli"-GFP diffused on microtubule with diffusion coefficients of 0.09 $\mu m^2/s$, 0.18 $\mu m^2/s$, and 0.03 $\mu m^2/s$ respectively (Fig. 5G), consistent with previous observations made for the Ndc80 complex (Powers et al., 2009).

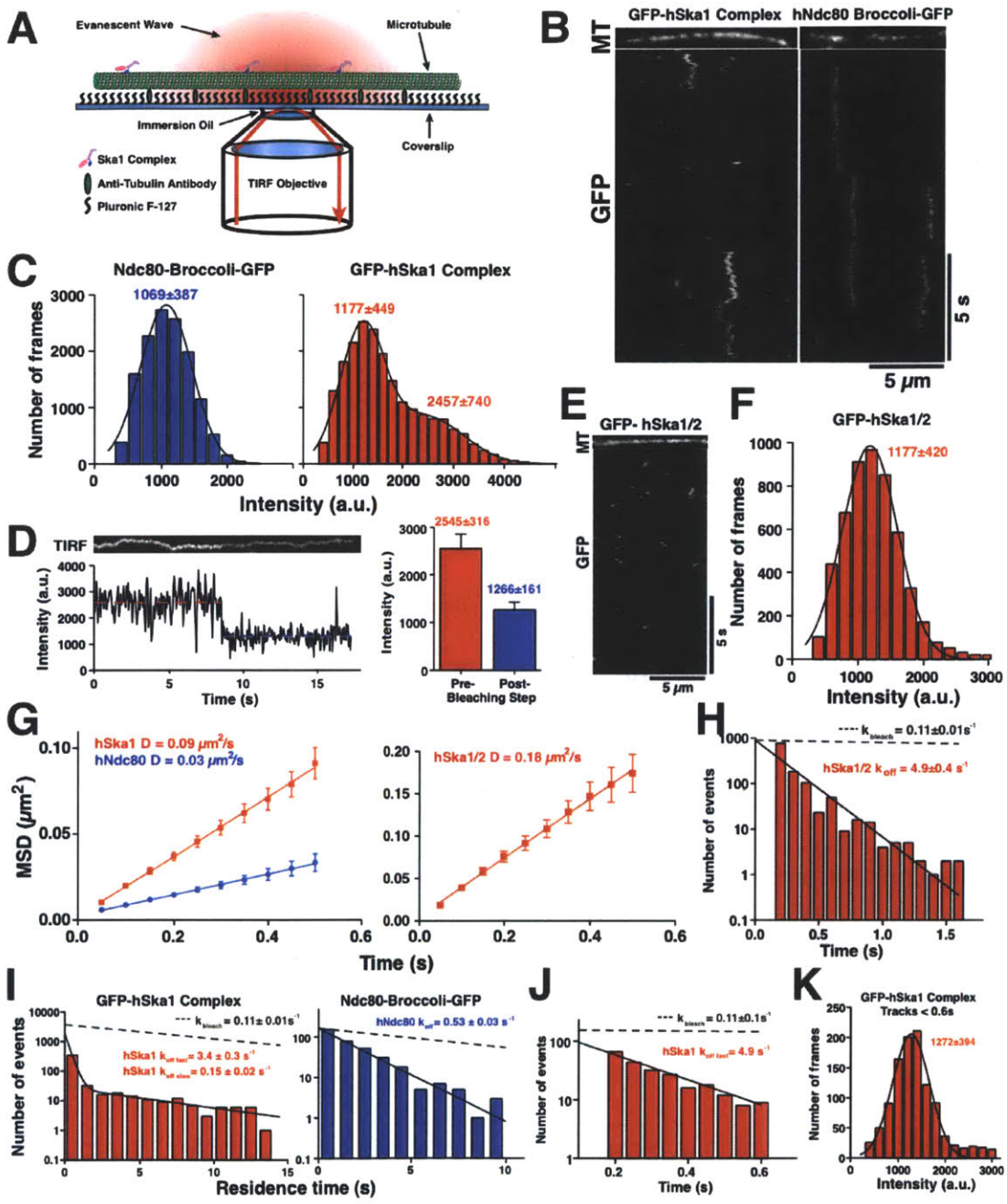

Figure 5. The human Ska1 complex diffuses on microtubules. (*A*) Schematic of the TIRF setup used to visualize microtubules and individual microtubule binding proteins. (*B*) Representative kymographs with microtubule position along the horizontal axis and time along vertical axis showing one-dimensional diffusion of GFP-hSka1 complex (left, 100 pM) and Ndc80 "Broccoli"- GFP (right, 50 pM) on taxol-stabilized microtubules labeled with HiLyte 647. (*C*) Intensity distribution of the binding events for 100 pM GFP-hSka1 complex (red, n = 20676) and 50 pM Ndc80 "Broccoli"-GFP (blue, n = 13411). Intensities were determined by fitting a 2D Gaussian distribution to each identified spot, ignoring first and last

frames of tracks. (*D*) Photo-bleaching analysis of Ska1 complex particles. Left, kymograph and corresponding fluorescent intensity for one photobleaching event. Right, graph showing the average intensity before and after photobleaching events (n = 32). (*E*) Representative kymographs with microtubule position along the horizontal axis and time along vertical axis showing one-dimensional diffusion of 200 pM GFP-hSka1/2. (*F*) Intensity distribution of the binding events for 200 pM GFP-hSka1/2 (n = 5281). (*G*) Mean square displacement (MSD, mean and SEM) plotted against time for 100 pM GFP-hSka1 complex (red, left, n = 187) and 50 pM Ndc80 "Broccoli"-GFP (blue, left, n = 258) and 200 pM GFP-hSka1/2 (red, right, n = 120). Diffusion coefficients were calculated from the slope of the linear fit of the MSD. (*H*) Distribution of the residence times of GFP-hSka1/2 binding to taxol stabilized microtubules (n = 1196). (*I*) Distribution of the residence times of GFP-hSka1 complex (100 pM, n = 502) and hNdc80 "Broccoli"-GFP (50 pM, n = 359) binding events to taxol stabilized microtubules. (*J*) Distribution of the residence times of GFP-hSka1 complex (100 pM, n = 232), showing only tracks with residence times smaller or equal to 0.6 s. Fit assuming the dissociation constant for GFP-hSka1/2 monomers. (*K*) Intensity distribution of the binding events for 100 pM GFP-hSka1 complex (n = 1107), showing only tracks with residence times smaller or equal to 0.6 s.

Under the conditions tested, the residence time distribution of GFP-hSka1 complex displays bi-phasic dissociation kinetics (Fig. 5I) - a rapid phase with a rate constant of k_{fast} = 3.4 ± 0.3 s^{-1} and a slow phase with a rate constant of k_{slow} = 0.15 ± 0.02 s^{-1}. Importantly, the disassociation rate of the rapid phase is similar to the behavior of monomeric GFP-hSka1/2 (k_{off} = 4.9 ± 0.4 s^{-1}) (Fig. 5J), suggesting that the rapid phase represents hSka1 complex monomers. Indeed, analysis of short-lived (<0.6 s) hSka1 complex binding events indicated that these were primarily monomeric based on their intensity distribution (Fig. 5K). Ndc80 "Brocolli"-GFP has a dissociation constant of k_{off} = 0.53 ± 0.03 s^{-1} (Fig. 5I). Importantly, all measured dissociation rate constants were faster than the bleaching rate constant determined for immobilized Ndc80-GFP under identical imaging conditions (k_{bleach} = 0.11 ± 0.01 s^{-1}; data not shown).

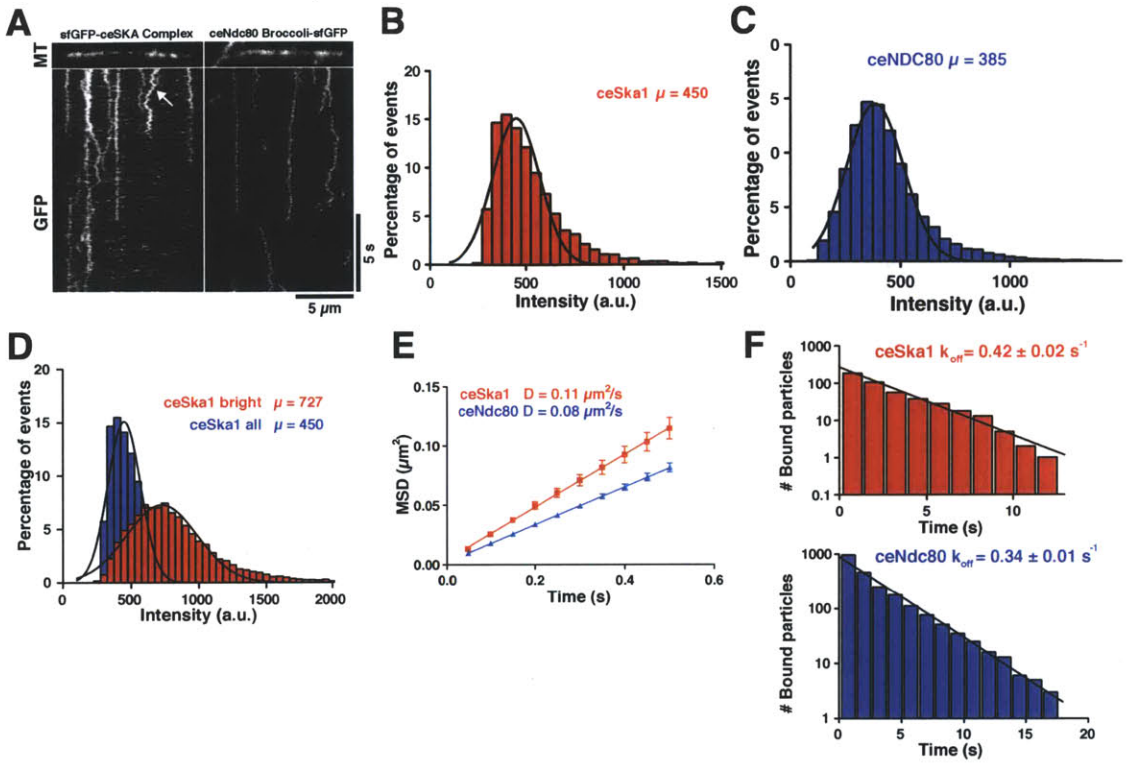

Figure 6. The *C. elegans* Ska1 complex diffuses on microtubules. (A) Representative kymographs with microtubule position along the horizontal axis and time along vertical axis showing one-dimensional diffusion of sfGFP-ceSka1 complex (left, 4 nM) and ceNdc80 "Broccoli"- sfGFP (right, 1 nM) on taxol-stabilized microtubules labeled with HiLyte 647. (B) Distribution of the initial intensity (second frame) of all sfGFP-ceSKA1 complex tracks binding to taxol stabilized microtubules (n = 6487). (C) Intensity distribution of all frames of ceNdc80 "Broccoli"-sfGFP tracks binding to taxol-stabilized microtubules (964 tracks, 35714 frames). (D) Comparison of the initial intensity of all sfGFP-ceSKA1 complex tracks (n = 6487, blue) and all frames of manually selected bright, long-lived sfGFP-ceSKA1 complex tracks (186 tracks, 12107 frames, red) binding to taxol-stabilize microtubules. The intensity of the bright sfGFP-ceSKA1 tracks is approximately 2-fold the intensity of ceNdc80 "Broccoli"-sfGFP tracks. (E) Mean square displacement (MSD, mean and SEM) plotted against time for 4 nM sfGFP-ceSka1 complex (red, n=209) and 1 nM ceNdc80 "Broccoli"-sfGFP (blue, n = 50). Diffusion coefficients were calculated from the slope of the linear fit of the MSD. (F) Graphs showing the number of particles that remain bound to taxol-stabilized microtubules after the indicated time of bright, long-lived sfGFP-ceSKA1 complex (top, 4 nM, n = 186) and ceNdc80 "Broccoli"-sfGFP tracks (bottom, 1 nM, n = 964).

Similar to the hSka1 complex, the *C. elegans* GFP-ceSKA1 complex also associates with microtubules as a mixture of dimers and monomers. However, in contrast to hSka1 complex, the sfGFP-ceSKA1 complex was primarily monomeric under the tested conditions (Fig. 6A-D). Manual inspection of the less abundant long-lived binding events (white arrow, Fig. 6A) revealed that their intensity was approximately 2-fold higher compared to monomeric ceNdc80-sfGFP (Fig. 6C, D), consistent with the presence of two ceSKA1 subunits. We note that sfGFP-ceSKA1 was used in these assays at 40-fold higher concentrations (4 nM) relative to GFP-hSka1 complex (100 pM). We conclude that even at concentrations of 4 nM, the ceSKA1 complex primarily contains one ceSKA1 subunit, indicating that it dissociates under these conditions.

The human (D = 0.09 $\mu m^2/s$) and *C. elegans* (D = 0.11 $\mu m^2/s$) Ska1 complex both diffused on microtubules with similar diffusion coefficients (Fig. 5G, 6E), whereas the *C. elegans* Ndc80 complex (D = 0.08 $\mu m^2/s$) diffuses more rapidly than its human counterpart (D = 0.03 $\mu m^2/s$) (Fig. 5G, 6E). Importantly, dimeric sfGFP-ceSKA1 binding events dissociate more rapidly (k_{off} = 0.42 s^{-1}) from microtubules than GFP-hSka1 complex dimers (k_{slow} = 0.15 s^{-1}) (Fig. 5I, 6F), consistent with the lower affinity of the ceSKA1 complex in microtubule pelleting assays. In contrast the ceNdc80 "Broccoli" has a lower dissociating constant (k_{off} = 0.34 s^{-1}) than hNdc80 "Broccoli" (koff = 0.53 s^{-1}; Fig. 5I, 6F).

Thus, even at low concentrations (100 pM) the human Ska1 complex can bind to microtubules as a dimer containing two Ska1 subunits. These observations do not exclude the formation of higher order oligomers at higher

protein concentrations as we have previously reported (Welburn et al., 2009). In total, these results demonstrate that diffusion on the microtubule lattice is a conserved property of the Ska1 complex.

The Ska1 complex tracks with depolymerizing microtubule ends

Previous work demonstrated that the Ska1 complex can couple movement of 0.5 μm microspheres to microtubule depolymerization (Welburn et al., 2009), but the mechanism by which this occurs was unknown. To test whether the Ska1 complex itself can remain associated with depolymerizing microtubule ends, we visualized GFP-hSka1 complex bound to microtubules that were induced to depolymerize by ablation of a stabilizing GMPCPP-cap (Fig. 7A). We found that GFP-hSka1 complex accumulated at microtubule ends during the majority of depolymerization events observed (70%; n = 79). In most cases, the hSka1 complex tracked processively with the depolymerizing end until it reached the microtubule seed (Fig. 7B). Interestingly, the hSka1 complex present at the microtubule end consistently increased intensity throughout the time course of microtubule depolymerization (Fig. 7C) suggesting that an accumulation of GFP-Ska1 complexes from the microtubule lattice is occurring at the depolymerizing end. In contrast, hNdc80 "Broccoli"-GFP diffusely decorated microtubules and failed to track with depolymerizing microtubule ends (Fig. 7B). We also did not observe binding of the ceSKA1 complex to microtubules under these experimental conditions, most likely due to dissociation

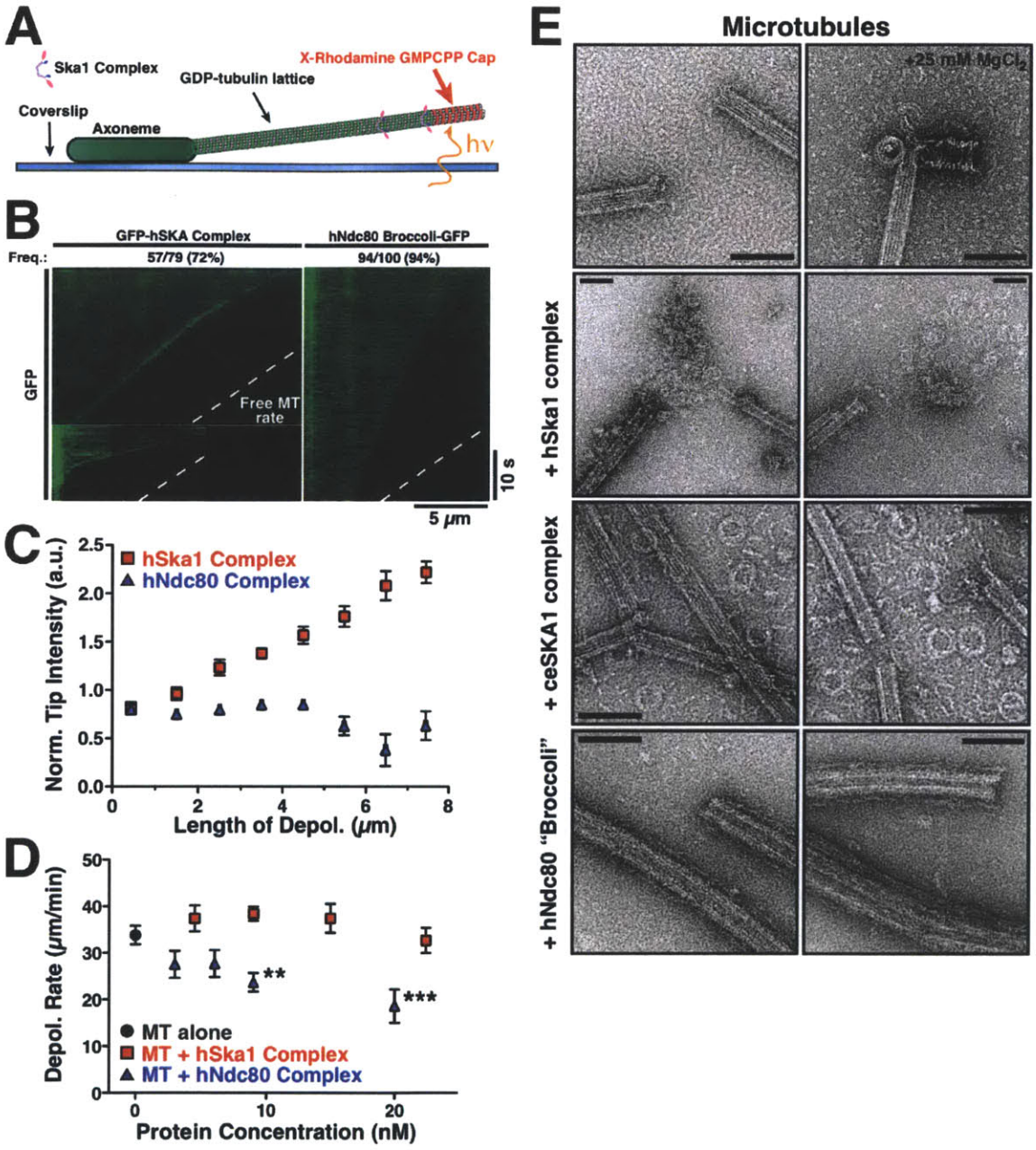

Figure 7. The Ska1 complex tracks with depolymerizing microtubule ends and induces the formation of curved microtubule structures. (*A*) Schematic of the experimental setup used to visualize the GFP-hSka1 complex binding to depolymerizing microtubules. Microtubules were induced to depolymerize by ablating a stabilizing GMPCPP cap with excitation light. (*B*) Representative kymographs showing the binding of GFP-hSka1 complex (left, 9 nM) and Ndc80 "Broccoli"-GFP (right, 9 nM) to depolymerizing microtubules (Dashed line indicates median protein-free microtubule depolymerization rate). Tracking events were identified as kymographs with substantial periods of an increased fluorescence signal at the microtubule end relative to the lattice. (*C*) Graph

showing the normalized intensity of the GFP-hSka1 (n = 47-108) complex or GFP-Ndc80 complex (n = 4-72) at the depolymerizing microtubule end over time. The Ska1 complex accumulates constantly at the depolymerizing end. (*D*) Depolymerization rates of microtubules in the presence and absence of a range of GFP-hSka1 complex and Ndc80 "Broccoli"-GFP concentrations (n = 18-87, Mean and SEM). The presence of of 9 nM ($P < 0.01$) and 20 nM ($P < 0.001$) Ndc80 "Broccoli"-GFP significantly reduces the rate of microtubule depolymerization (Kruskal-Wallis test with Dunn's post test), which is unaffected by similar concentrations of the Ska1 complex. Depolymerization rates were determined from the slopes of the corresponding kymographs. (*E*) TEM images of the dynamic microtubules in the absence and presence of 25 $MgCl_2$, or the Ska1 and Ndc80 complexes (Scale bars, 100 nm). The Ska1, but not the Ndc80 complex, induces the formation of protofilament rings.

of the ceSKA1 complex at the low (nM) protein concentrations required for this experiment (see above).

Intriguingly, we found that addition of ≥9 nM Ndc80 "Broccoli"-GFP significantly reduced the depolymerization rate of microtubules from 33.8 µm/min to 23.7 µm/min (Fig. 7D), whereas addition of the Ska1 complex did not retard microtubule depolymerization. Together with the lack of tracking activity for the Ndc80 complex, this suggests that the interactions of the Ska1 and Ndc80 complexes with depolymerizing microtubules are fundamentally different. In total, these results demonstrate that the hSka1 complex can processively track with depolymerizing microtubules.

The Ska1 induces the formation of curved microtubule structures

The experiments described above demonstrate that the Ska1 complex can robustly track with depolymerizing microtubules (Fig. 7B). To structurally define the interaction between the Ska1 complex and depolymerizing microtubules, we incubated dynamic microtubules in the presence of Ska1 complex. Strikingly,

transmission electron microscopy (TEM) analysis demonstrated that addition of equimolar amounts of either the human or *C. elegans* Ska1 complex to microtubules resulted in the formation of numerous protofilament rings or spiral structures, often in direct proximity to microtubule ends (Fig. 7E). Spiral-like structures can be induced by addition of 25 mM $MgCl_2$, although in this case the spirals are typically directly connected to the microtubule end (Fig. 7E; also see (Mandelkow et al., 1991)). In contrast, such structures were rarely observed for microtubules alone or microtubules incubated in the presence of the Ndc80 complex (Fig. 7E). These results demonstrate that the Ska1 complex has the conserved ability to induce and stabilize the formation of protofilament rings or spiral-like tubulin structures.

The Ska1 complex directly associates with curved microtubule structures

The Ska1 complex induces the formation of ring-like protofilament structures when incubated with dynamic microtubules (Fig. 7E). Previous work on microtubule tracking proteins has focused on their association with the straight microtubule lattice proximal to the depolymerizing microtubule end. However, the depolymerizing end, which consists of bent microtubule protofilaments (Mandelkow et al., 1991), also represents a potential site of interaction to remain associated with depolymerizing microtubules. To assess the relative affinities of the Ska1 complex binding to straight and curved microtubule structures, we compared the binding of the human and *C. elegans* Ska1 complexes to straight taxol-stabilized microtubules and dolastatin-10-induced tubulin rings, which

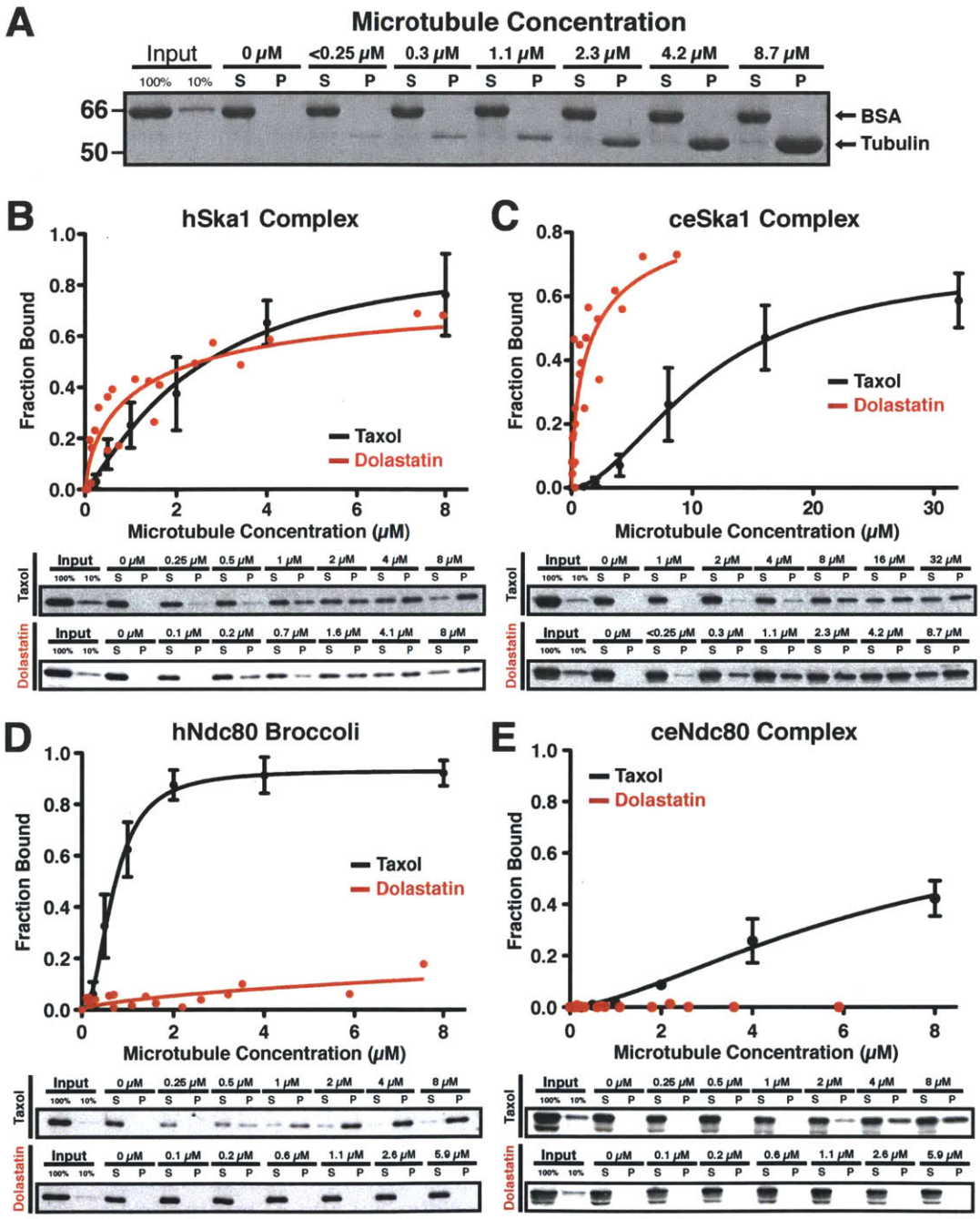

Figure 8. The Ska1 complex, but not the Ndc80 complex, associates with depolymerizing microtubule end mimics. (*A*) Commassie gel, showing the quantitative pelleting of dolastatin-10 induced protofilament rings in co-sedimentation assays. (*B-E*) (Top) Quantification of microtubule co-sedimentation assays (n = 3) and (Bottom) representative Western blots of microtubule co-sedimentation assays of (A) hSka1 complex (100 nM, 75 mM KCl), (B) ceSKA1 complex (100 nM, 75 mM KCl), (C) hNdc80 "Broccoli" (100 nM, 75 mM KCl), and (D) ceNdc80 complex (100 nM, 75 mM KCl) binding to taxol stabilized microtubules (black) and dolestatin-10 induced protofilament rings (red).

mimic curved protofilament structures (Bai et al., 1999; Boukari et al., 2007). Under equivalent conditions, the hSka1 complex bound with similar affinities to both taxol-stabilized microtubules and dolastatin rings (Fig. 8B), whereas the ceSka1 complex bound significantly better to dolastatin-10 induced microtubule rings (Fig. 8C). In contrast, both the human and *C. elegans* Ndc80 complexes bound preferentially to straight microtubules (Fig. 8D, 8E; also see (Alushin et al., 2010)).

We next imaged the Ska1 complex bound to dolastatin-induced rings by TEM. In the presence of the Ska1 complex, we observed binding to the inner face of the dolastatin rings (Fig. 9A), which corresponds to the outer surface of a microtubule protofilament. Similarly, in the presence of GFP-hSka1 MTBD, the outer diameter of the dolastatin-10 induced rings is unchanged, but thickness the rings increased by 5 nm (Fig. 9B) consistent with GFP-hSka1 MTBD binding to the inner surface. In contrast, the dolastatin rings remained largely undecorated in the presence of the Ndc80 complex (Fig. 9A). In total, these results demonstrate that the Ska1 complex, but not the Ndc80 complex, directly associates with curved microtubule structures.

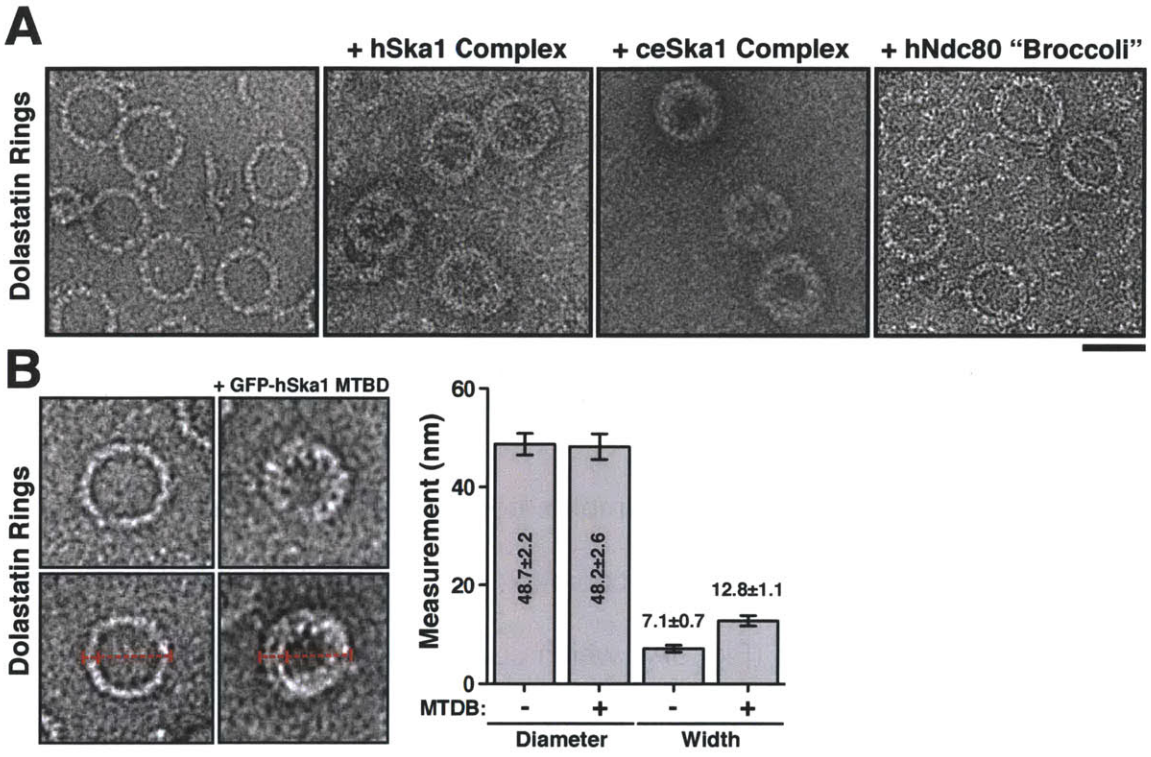

Figure 9. Structural analysis of the Ska1 complex binding to dolastatin-10 induced protofilament rings. (*A*) Transmission electron microscopy (TEM) images of dolestatin-10 induced protofilament rings alone or decorated with the ceSKA1 complex or hSka1 complex, and in the presence of hNdc80 "Broccoli" (Scale bars, 40 nm). (*B*) Left, TEM images showing individual dolestatin-10 rings in the presence or absence of the GFP-hSka1 microtubule binding domain (MTBD). Right, graph showing the outer diameter and width of the dolestatin-10 rings in each condition. In the presence of Ska1 MTBD, the width of the ring is increased, but not the outer diameter indicating that Ska1 binds to the inner surface.

The Ska1 Complex and Ndc80 complex bind to microtubules synergistically

Previous work demonstrated that the Ndc80 complex is required for Ska1 complex localization to kinetochores (Chan et al., 2012; Raaijmakers et al., 2009; Welburn et al., 2009; Zhang et al., 2012). As the Ndc80 and Ska1 complexes are both implicated in the formation of stable kinetochore-microtubule interactions, we next sought to define how these activities are coordinated. To test the

relationship between the Ndc80 and Ska1 complexes for microtubule binding, we conducted microtubule co-sedimentation assays using both the hSka1 complex and hNdc80 "Broccoli". These experiments demonstrated that the hNdc80 complex increases the affinity of the hSka1 complex for microtubules by up to 8-fold in a dose-dependent manner (Fig. 10A, B), suggesting that there is a direct interaction between the hNdc80 and hSka1 complexes in the context of microtubules. Similarly, the *C. elegans* Ndc80 complex increased the affinity of the *C. elegans* Ska1 complex for microtubules and vice versa (Fig. 10C-E). In contrast, we were unable to detect a direct interaction between the Ndc80 and Ska1 complexes in solution (data not shown), suggesting that the synergy requires the microtubule lattice. The affinity of the human Ska1 MTBD for taxol stabilized microtubules was unaffected by the presence of Ndc80 complex, indicating that the interaction is mediated by the non-microtubule binding portion of the Ska1 complex (Fig. 10F). These results demonstrate that there is an evolutionarily conserved interaction between the Ska1 complex and the Ndc80 complex in the context of microtubules.

The Ska1 complex promotes the association of the Ndc80 complex with depolymerizing microtubule ends

To test the synergy between the Ska1 and Ndc80 complexes in the context of dynamic microtubules, we visualized hNdc80 "Broccoli"-GFP on depolymerizing microtubules in the presence and absence of unlabeled hSka1 complex. The presence of the hSka1 complex increased the overall signal intensity of the

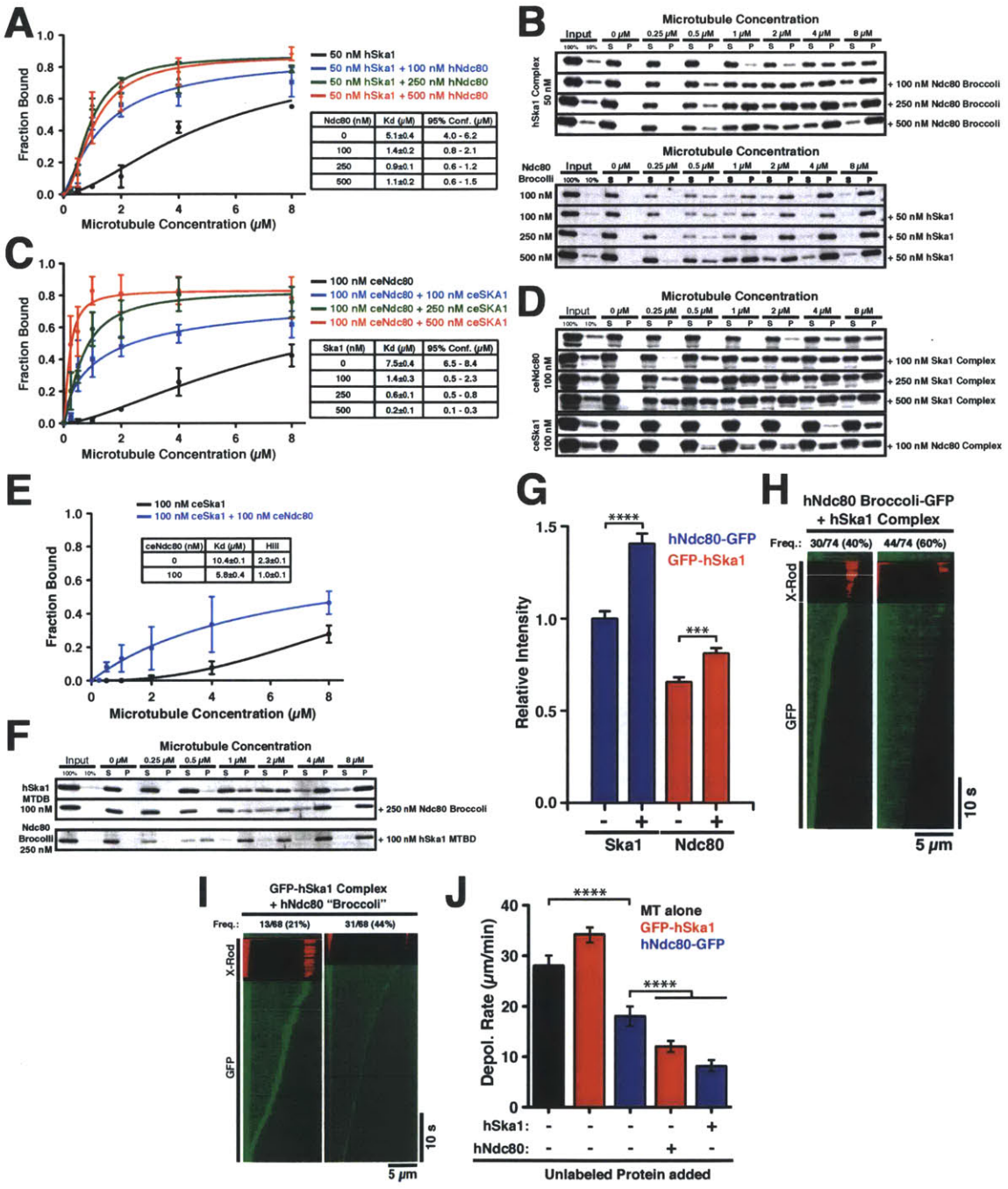

Figure 10. The Ska1 complex confers microtubule tracking activity to the Ndc80 complex. (*A*) The Ska1 complex and Ndc80 complex bind to microtubules synergistically. Quantification of microtubule co-sedimentation assays for hSka1 complex binding to taxol-stabilized microtubules alone and in the presence of a range of concentration of hNdc80 "Broccoli" (n = 3). (*B*) (Top) Representative Western blots of microtubule pelleting assays for the hSka1 complex in the presence of a range of hNdc80 "Broccoli" concentrations. (Bottom) Representative Western blots of microtubule pelleting assays for a

range of hNdc80 "Broccoli" concentrations in the presence and absence of hSka1 complex. (*C*) Quantification of microtubule pelleting assays of *C. elegans* Ndc80 complex binding to taxol-stabilized microtubules alone and in the presence of a range of ceSKA1 complex (n = 3). (D) (Top) Representative Western blots of microtubule co-sedimentation assays for ceNDC80 complex in the presence of a range of ceSKA1 complex concentrations. (Bottom) Representative Western blots of microtubule pelleting assays of ceSKA1 complex in the presence and absence of ceNDC80 complex. (*E*) Quantification of microtubule pelleting assays of ceSKA1 complex binding to taxol-stabilized microtubules alone and in the presence of ceNDC80 complex (n = 3). (*F*) (Top) Representative Western blots of microtubule pelleting assays of hSka1 MTBD in the absence and presence of hNdc80 "Broccoli". (Bottom) Representative Western blots of microtubule pelleting assays of hNdc80 "Broccoli" in the presence hSka1 MTBD. (*G*) Quantification of the fluorescence intensity on microtubules of hNdc80 "Broccoli"-GFP (blue) in the absence (n = 95) and presence of hSka1 (n = 136; $P < 0.0001$, t-test), and GFP-hSka1 (red) in the absence (n = 73) and presence of hNdc80 "Broccoli" (n = 81; $P < 0.001$, t-test). (*H*) Representative kymographs (microtubule position along horizontal axis, time along vertical axis) of time-lapse movies showing hNdc80 "Broccoli"-GFP (9 nM) binding to depolymerizing microtubules in the presence of unlabeled hSka1 complex (9 nM, n = 74). Tracking events were identified as kymographs with substantial periods of an increased fluorescence signal at the microtubule end relative to the remaining lattice. When both Ndc80 and Ska1 are present, the GMPCPP-caps are often converted into cargo and become transported by the shortening microtubules. (*I*) Representative kymographs (microtubule position along horizontal axis, time along vertical axis) of time-lapse movies showing GFP-hSka1 complex binding to depolymerizing microtubules in the presence of hNdc80-Broccoli (n = 68). Tracking events were identified as kymographs with substantial periods of an increased fluorescence signal at the microtubule end relative to the remaining lattice. (*J*) Depolymerization rates of microtubules alone, in the presence of GFP-hSka1 complex, with and without unlabeled hNdc80 "Broccoli", and hNdc80 "Broccoli"-GFP, with and without unlabeled hSka1 complex (n = 65-87; **** = $P < 0.0001$, Mann Whitney test).

hNdc80 complex on microtubules and vice versa, further indicating that the Ska1 and Ndc80 complexes bind microtubules synergistically (Fig. 10G). Although hNdc80 "Broccoli"-GFP does not track with depolymerizing microtubule ends on its own (Fig. 7B), in 40% of the depolymerization events observed in the presence of unlabeled hSka1 complex, hNdc80 "Broccoli"-GFP formed bright complexes that tracked the depolymerizing microtubule (Fig. 10H). In the

remaining 60% of events, no tracking was observed (Fig. 10H). The tracking assemblies of Ndc80 complex in the presence of the Ska1 complex are substantially brighter than those observed for the Ska1 complex alone. These bright assemblies most likely represent remnants of the stabilizing GMPCPP-cap, decorated with hNdc80 "Broccoli"-GFP, that are transported along the depolymerizing microtubule in a Ska1-dependent manner. In contrast, if only the Ska1 or Ndc80 complex was present, the GMPCPP-caps dissociated from the depolymerizing microtubule. Importantly, GFP-hSka1 complex also forms bright tracking assemblies in the presence of unlabeled hNdc80 "Broccoli" (Fig. 10I), indicating that the identity of the GFP-labeled protein does not influence the formation of these assemblies, but that the presence of both complexes is necessary. The presence of both hSka1 complex and hNdc80 "Broccoli" significantly reduced the rate of microtubule depolymerization regardless of which complex is labeled with GFP, demonstrating that the integrated assembly resists microtubule depolymerization (Fig. 10J). These results demonstrate that the Ndc80 and Ska1 complexes display a synergistic interaction at the depolymerizing microtubule end and their combined action can sustain movement of cargo along the depolymerizing microtubule.

The Ska1 microtubule binding domain contains conserved basic surfaces that are regulated by Aurora B phosphorylation

To define the mechanism by which Ska1 binds to microtubules, we next determined the high resolution structure of the *C. elegans* Ska1 microtubule binding domain using Nuclear Magnetic Resonance (NMR, Table 1). Our structural analysis demonstrates that the Ska1 microtubule binding domain is a variation of the winged helix domain (Fig. 11A - D). The winged helix domain is a ~100 amino acid domain that has previously been implicated primarily as a DNA binding motif, but which can also function as a protein-protein interaction domain (Gajiwala and Burley, 2000; Haering et al., 2004). In addition to the three helix-bundle and anti-parallel beta-sheets found in canonical winged-helix domains, the Ska1 microtubule binding domain contains an extended helix (αB) as part of three helix bundle and an additional helix (αC) inserted between alphaB and βA. Furthemore, αB is preceded by a loop (loopA) and a short helix (αA) (Fig. 11B). E130 in αA and R229 form a highly conserved salt bridge positioning αA and loopA relative to the three-helix bundle (Fig. 11E, 1A green stars).

Importantly, three highly conserved arginine residues (R141, R225, R234, Fig. 1A blue stars) located in loopA, αE, and βB are part of a conserved basic patch on the surface on the Ska1 microtubule binding domain (Fig. 11F - H). As binding of the Ska1 complex to microtubules requires the acidic C-terminal tails of tubulin (Welburn et al., 2009), we reasoned that this basic patch might represent the microtubule binding surface. Consistent with this, mutation of the

Number of NOE constraints	
Total	**2069**
Intra-residue	**559**
Short and Medium (|i-j| = 1 ~ 4)	**1210**
Long (|i-j| > 4)	**331**
Backbone angular restraints (Φ and Ψ)	**182**
Violations (mean and SD)	
Distance constraints (Å)	**0.0431±0.0008**
Dihedral angle constraints (°)	**0.8619±0.0866**
Max. dihedral angle violation (°)	**1.0507**
Max. distance constraints violations (Å)	**0.0488**
Ramachandran Plot (20 structures)	
Residues in most favored regions (%)	**83.0**
Residues in additionally allowed regions (%)	**15.4**
Residues in generously allowed regions (%)	**0.8**
Residues in disallowed regions (%)	**0.8**
Average RMSD	
Backbone (Å)	**0.51±0.16**
All heavy atoms (Å)	**1.15±0.18**

Table 1. Summary summarizing the NMR structure determination of the *C. elegans* SKA1 MTBD. None of the 20 structures exhibited distance violations > 0.6 Å or dihedral angle violations > 5 °. There are no bad contacts in the structure. The RMSD for covalent bonds and angles relative to the standard dictionary are 0.005 Å and 0.7 °, with all covalent bonds and angles within 6*RMSD for the structures.

homologous arginine residues in human Ska1 (R155, R236, R245) to alanine eliminated microtubule binding activity in vitro (Fig. 12A), and resulted in a mitotic delay and a reduction of kinetochore-fibers in human cells, similar to cells expressing hSka1 ΔMTBD (Fig. 12C - F).

Recent work has identified multiple phosphorylation sites in the Ska1 complex that are regulated by Aurora B (Chan et al., 2012). These sites were proposed to regulate the recruitment of the Ska1 complex to kinetochores, but not its microtubule binding activity. Importantly, all four Aurora B phosphorylation sites identified in human Ska1 (Chan et al., 2012) are located in the region that

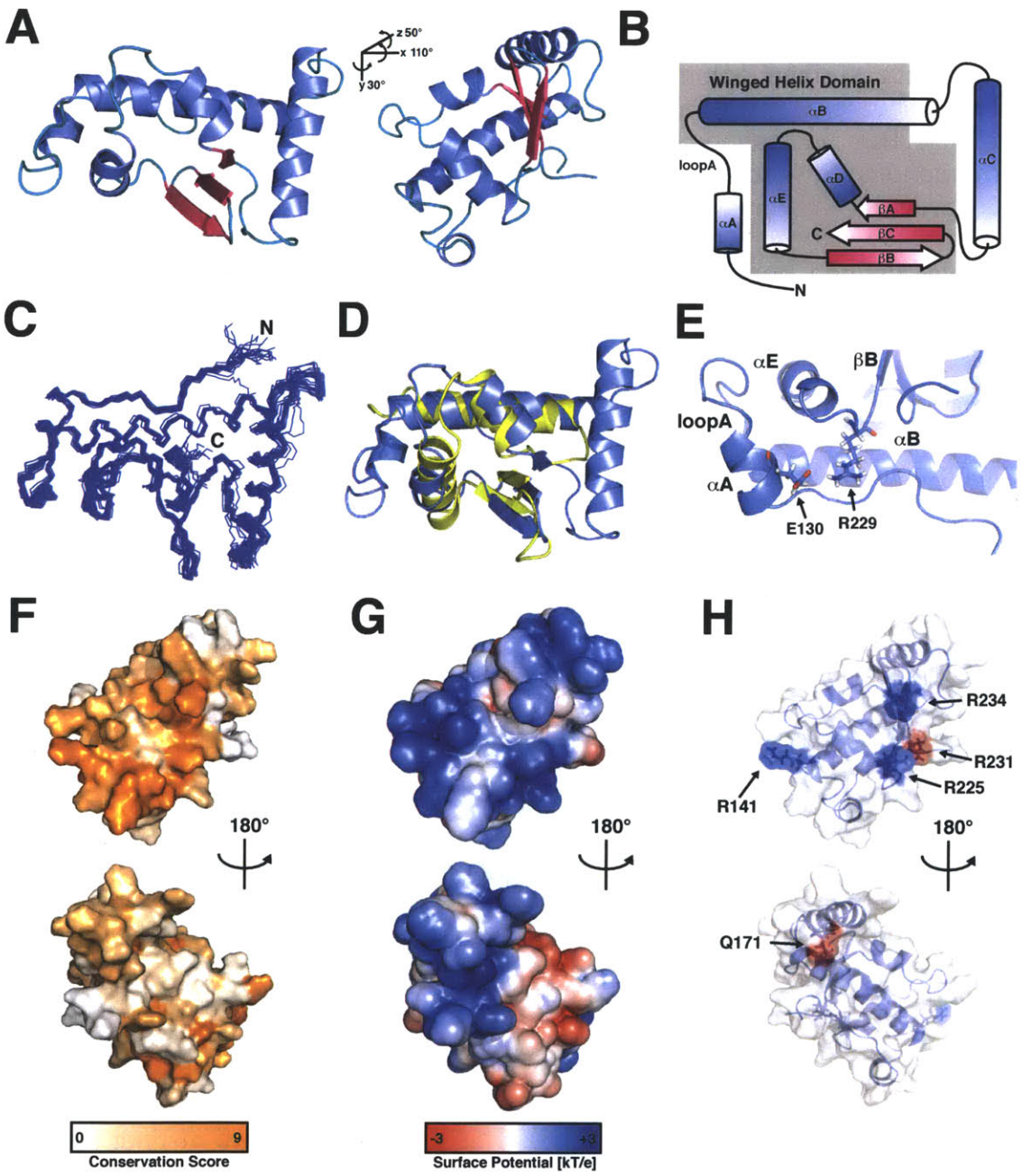

Figure 11. The Ska1 microtubule binding domain is a winged-helix domain. (*A*) Cartoon representation of an ensemble of NMR-structures of the *C. elegans* Ska1 MTBD. (*B*) Topology diagram of the *C. elegans* Ska1 MTBD, showing the elements of the canonical winged-helix domain (grey). (*C*) Cα traces superimposing all 20 NMR-structures calculated. *(D)* Superimposition of the *C. elegans* Ska1 MTBD with the bacterial winged-helix transcription factor PefI (PDB = 2JT1, Dali Z score = 5.5, RMSD 2.3 Å, (Holm et al., 2008)). (*E*) Details on the conserved salt bridge formed between E130 and R229 in the *C. elegans* Ska1 MTBD. (*F*) Surface representation of the *C. elegans* Ska1 MTBD, showing

conservation scores calculated using the Consurf Server (Ashkenazy et al., 2010). (*G*) Surface representation of the *C. elegans* Ska1 MTBD, showing electrostatic surface potential calculated using the Adaptive Poisson-Boltzman Solver software (Baker et al., 2001). (*H*) Surface representation of the *C. elegans* Ska1 MTBD, indicating conserved arginine residues (blue) and residues corresponding to Aurora B consensus sites in hSka1 (red).

we have defined here as the microtubule binding domain. Mutation of two of these Aurora B phosphorylation sites (S185, S242 in hSka1 MTDB) to aspartate to mimic constitutive phosphorylation dramatically reduced the microtubule binding activity of the Ska1 complex *in vitro* (Fig. 11H) and resulted in a mitotic delay and reduced kinetochore-fibers *in vivo* (Fig. 12C - F). However, these defects were slightly less severe than the arginine mutant or the deletion of the MTBD. Interestingly, S185 and S242 are located in distinct regions within the microtubule binding domain. The residue corresponding to S242 (R231 in *C. elegans* MTBD) resides in the direct vicinity of the basic patch identified above, suggesting that the introduction of negative charge by S242 phosphorylation might disrupt the interaction of the positively charged patch with microtubules (Fig. 11H). In contrast, the residue corresponding to S185 (Q171 in *C. elegans* MTBD) is located in a loop between αB and αC on the opposite face of the microtubule binding domain (Fig. 11H). This suggests that two distinct surfaces play a role in microtubule binding, potentially binding to adjacent tubulin monomers. Individual mutation of S185 or S242 also reduced microtubule binding activity, although to a lesser extent than the double mutant (data not shown). Importantly, mutation of the conserved arginine residues or Aurora B phosphorylation sites did not affect the folding of the microtubule binding domain

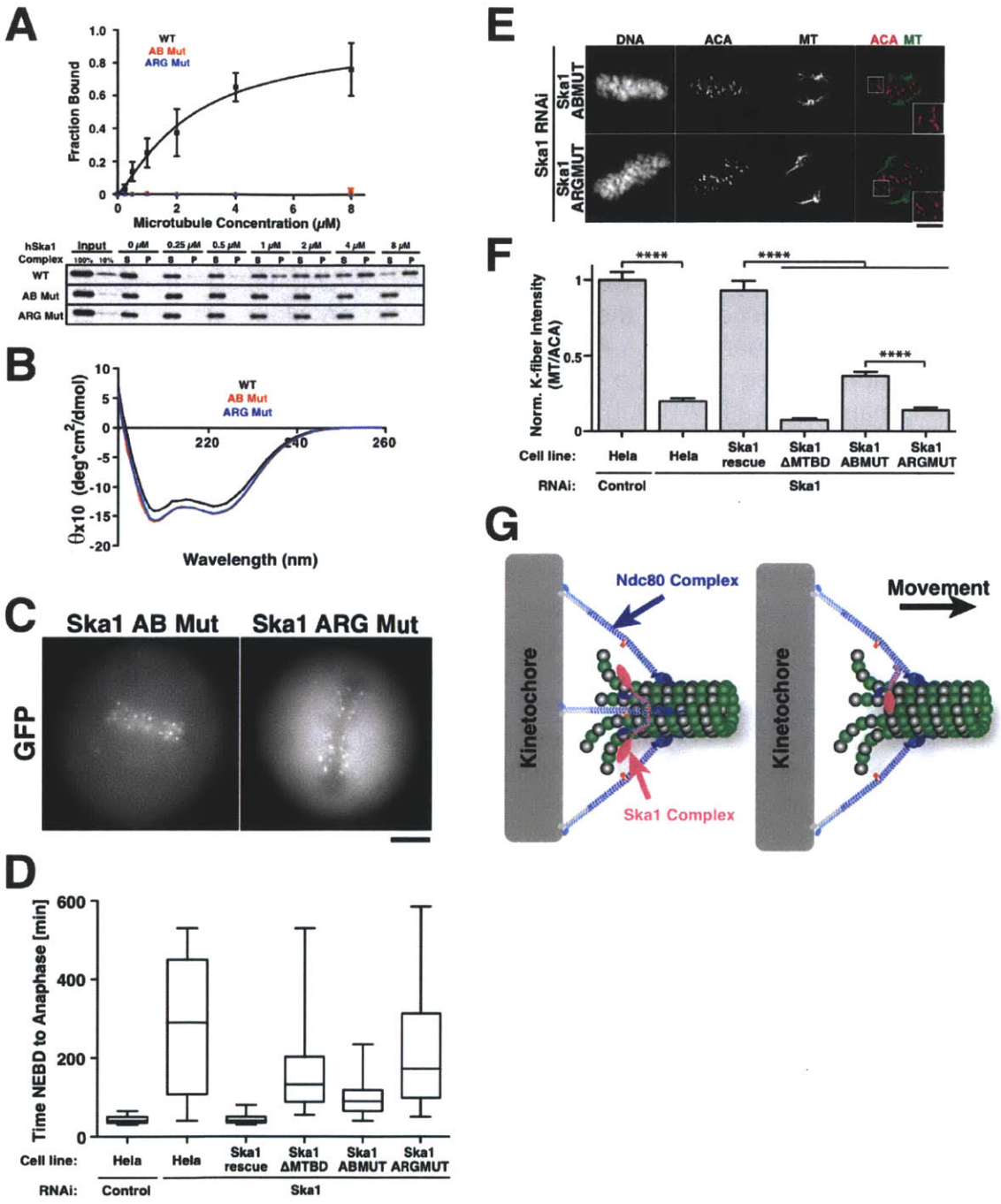

Figure 12. Structure based mutational analysis of the Ska1 MTBD. (*A*) (Top) Quantification of microtubule co-sedimentation assays (n = 3, 100 nM Ska1 complex, 75 mM KCl) and (Bottom) representative Western blots of microtubule co-sedimentation assays of hSka1 complex (black), hSka1 complex R155A, R236A, R245A (blue), and hSka1 complex S185D, S242D (red). Mutation of conserved arginine residues to alanine or Aurora B consensus sites is aspartate abolishes microtubule binding of the Ska1 complex. (*B*) Circular dichroism

measurements of wild type hSka1 MTBD, Aurora B phosphomimetic (S185D, S242D; AB Mut) hSka1 MTBD (red), and hSka1 MTBD with three conserved arginine residues mutated to alanine (R155A, R236A, R245A; ARG Mut; blue). Mutation of the hSka1 MTDB does not affect its folding. (*C*) Fluorescent images showing the localization of GFP-tagged hSka1 constructs into HeLa cells. Both Aurora B phosphomimetic Ska1 and Arginine mutant Ska1 localize only to kinetochores. Scale bar, 5 μm. (*D*) HeLa cell lines stably expressing GFP-tagged and RNAi resistant full-length Ska1, Ska1 ΔMTDB, Aurora B phosphomimetic Ska1 (AB Mut), or arginine mutant Ska1 (ARG Mut) were depleted for endogenous Ska1 by RNAi. Cells were imaged by time-lapse microscopy 36 h after siRNA transfection and the time from nuclear envelope breakdown (NEBD) to anaphase was quantified (n = 42-112 cells per condition). Scale bar, 5 μm. (*E*) Immunofluorescence of HeLa cells stably expressing GFP-tagged Aurora B phosphomimetic Ska1 (ABMut), or arginine mutant Ska1 (ArgMut) depleted for endogenous Ska1 following cold treatment for 10 min. Cells were immuno-stained against centromeres (ACA, magenta), microtubules (DM1α, green), and DNA. (*F*) Quantification of kinetochore-microtubule intensity from (*E*) showing the mean and standard error of the mean (18-22 cells per conditions, 10 kinetochores per cell, $P < 0.0001$, t-test). Kinetochores were chosen at random and adjacent microtubule intensity was quantified and normalized using the ACA signal. Data from Figure 2 are included as references. (*G*) Model showing the coordination of Ska1 and Ndc80 microtubule binding. The Ndc80 complex senses the polarity of the microtubule and integrates the Ska1 complex into the kinetochore. The Ska1 complex binds to the curved microtubule protofilaments at the depolymerizing microtubule ends, facilitating processive attachment to depolymerizing microtubules.

(Fig. 12B). In total, these results demonstrate that the Ska1 complex uses a winged helix domain to bind to microtubules and that point mutations that disrupt microtubule binding phenocopy deletion of the Ska1 MTBD. Thus, microtubule binding is a crucial mitotic function of the Ska1 complex.

Discussion

Chromosome movement driven by microtubule dynamics is essential for proper cell division. Here, we defined conserved biochemical activities of the Ska1 complex, a key player in coupling chromosome movement to microtubule dynamics. Our work provides mechanistic and structural insights into the interaction of the Ska1 complex with depolymerizing microtubules and demonstrates that its activity is integrated with the Ndc80 complex to generate an assembly that can remain processively associated with depolymerizing microtubules.

The Ska1 complex tracks depolymerizing microtubules using a unique mechanism

Since it was first demonstrated that microtubule depolymerization is sufficient to move chromosomes (Coue et al., 1991), a key goal has been to identify the molecular players involved in this process. The Dam1 complex was the first kinetochore component that was shown to track with depolymerizing microtubules (Westermann et al., 2006), but the Dam1 complex is only present in fungi and is not essential for chromosome segregation in fission yeast (Sanchez-Perez et al., 2005). The striking formation of ring-like Dam1 structures around microtubules has led to forced walk or ring-coupler models to explain how the kinetochore maintains attachment to depolymerizing microtubules (Efremov et al., 2007; Miranda et al., 2005; Westermann et al., 2006). The Ndc80 complex is conserved throughout eukaryotes and is essential for chromosome segregation

in all organisms where it has been studied (Cheeseman and Desai, 2008). Recently, Powers and colleagues proposed that the Ndc80 complex remains attached to depolymerizing microtubules by biased diffusion (Powers et al., 2009). However, the Ndc80 complex can only track with depolymerizing microtubules when it is artificially induced to oligomerize (Powers et al., 2009). The Dam1 and Ndc80 complexes from budding yeast have also been shown to synergize in forming load-bearing attachments to depolymerizing microtubules (Lampert et al., 2010; Tien et al., 2010).

The models previously described for the Ndc80 and Dam1 complexes were all under the implicit assumption that each complex interacts with the straight microtubule lattice (Efremov et al., 2007; Hill, 1985). Here, we demonstrated that the human Ska1 complex autonomously tracks with depolymerizing microtubules - to our knowledge the first human kinetochore protein with this capability. We propose that the Ska1 complex remains associated with depolymerizing microtubules by not only associating with and diffusing along the straight microtubule lattice, but also by interacting with the curved microtubule structures at depolymerizing microtubule ends. Importantly, the human and *C. elegans* Ska1 complexes both associate with dolastatin-10-induced rings, which mimic the curved structures formed at depolymerizing microtubule ends, indicating that binding of curved microtubule structures is a key conserved property of the Ska1 complex. We note that the Dam1 complex has been shown to form rings *around* microtubules, but this behavior is fundamentally distinct from the Ska1 complex in which dolastatin induces the

formation of a protofilament ring to which the Ska1 complex binds. Interestingly, the Ndc80 complex neither associates with dolastatin-10-induced rings nor tracks with depolymerizing microtubules under the conditions tested, indicating that its association with microtubules is inherently different from the Ska1 complex. This is further supported by the observation that the presence of the Ska1 complex induces the formation of protofilament rings when added to dynamic microtubule polymers, whereas the Ndc80 complex does not.

Importantly, the Ska1 complex associates with microtubules using a variation of a winged-helix domain, while the Ndc80 complex utilizes a calponin-homology domain (Ciferri et al., 2008). Previous work has demonstrated that the "toe-print" of the Ndc80 calponin homology domain contains residues from two consecutive tubulin monomers (Alushin et al., 2010). Thus, protofilament bending could distort this binding site and thereby reduce the affinity of the Ndc80 complex for curved microtubules. In contrast, the Ska1 complex maintains or, in case of the *C. elegans* homologue, even increases its binding affinity when associating with curved protofilaments. The long-axis of the Ska1 MTBD is approximately the same length as the longest axis of the tubulin monomer (~5 nm). Thus, the Ska1 MTBD domain could interact with consecutive tubulin monomers and the binding surfaces, such as the C-terminal charged tail, could be ideally positioned when the protofilaments assume a curved conformation. Alternatively, the Ska1 MTBD could have a binding site on the tubulin monomer that is unaffected by the conformation of the protofilament. In case of the *C.*

elegans homologue, additional interactions may be formed with dolastatin-10 induced protofilament rings.

Interestingly, the winged-helix domain is predominantly present in DNA-binding proteins, but is also present as a protein-protein interaction domain, for example in the kleisin subunit of the cohesion complex (Gajiwala and Burley, 2000; Haering et al., 2004). Utilizing a common DNA binding motif for microtubule binding suggests that the Ska1 complex may have evolved from a DNA binding protein. Duplication and divergence of a dimeric DNA binding protein could lead to a complex that harbors both DNA binding and microtubule binding activities, providing a simple chromosome segregation machine comparable to bacterial plasmid segregation systems (Gerdes et al., 2010).

In total, we propose that the Ska1 complex can associate with the bending protofilaments of depolymerizing microtubules, thereby assuring that the kinetochore remains attached to the microtubule when it encounters a depolymerizing microtubule end. The Ndc80 complex preferentially binds to the straight microtubule lattice, thus stabilizing it relative to the bent conformation and counteracting microtubule depolymerization (Fig. 12G). Importantly, these distinct microtubule-binding activities must be coordinated to facilitate robust kinetochore-microtubule attachments.

The Ska1 and Ndc80 complexes form an integrated microtubule binding assembly

We demonstrated that the Ska1 and Ndc80 complexes bind to microtubules synergistically, a property that is conserved from humans to nematodes, indicating that the Ska1 complex and Ndc80 complexes interact directly in the context of microtubules. Our analysis indicates that this is a specific effect, as we were unable to detect a synergy between the Ska1 microtubule-binding domain and the Ndc80 complex (Fig. S4D), or between the human Ska1 complex and the *C. elegans* Ndc80 complex (data not shown). Furthermore, under the conditions tested, the Ndc80 complex alone does not have the capacity to remain associated with depolymerizing microtubules. In contrast, in the presence of the Ska1 complex, large Ndc80 assemblies are processively transported along depolymerizing microtubule. Importantly, the rate of microtubule depolymerization in the presence of these assemblies is strongly reduced relative to free microtubules, indicating that these assemblies resist microtubule depolymerization. Therefore, we propose that Ska1 and Ndc80 complexes interact to form a unique coupler that can remain associated with depolymerizing microtubules and harness their energy to drive chromosome movement (Fig. 12G). The Ndc80 complex can sense microtubule orientation and integrates the Ska1 complex into the macromolecular kinetochore, whereas the activity of the Ska1 complex is necessary to remain attached to depolymerizing microtubules by associating with both curved protofilaments and the straight microtubule wall. Although the Ndc80 and Ska1 complexes can coordinate to track microtubules, future studies will be required to study this behavior in the presence of a load, such as would be present at kinetochores in cells.

Our cell biological analysis suggests that the Ska1 and Ndc80 complexes make distinct contributions to kinetochore microtubule attachments *in vivo*. In the absence of Ska1 complex microtubule binding activity, the Ska1 complex localizes to kinetochores and together with the Ndc80 complex is sufficient to direct chromosome alignment and end-on kinetochore microtubule attachments (Fig. 4). Indeed, when Ska1 complex function is eliminated entirely, cells are unable to form kinetochore-microtubule attachments (Gaitanos et al., 2009; Raaijmakers et al., 2009; Welburn et al., 2009). Importantly, in the absence of Ska1 microtubule binding activity kinetochore fibres are strongly reduced and kinetochore oscillations are absent, suggesting that the Ndc80 complex microtubule binding activity is insufficient to carry out these functions. Instead, the unique microtubule binding activity of the Ska1 complex is required to maintain kinetochore fibres and to power kinetochore oscillations, indicating that is required to allow the kinetochore to remain associated with depolymerizing microtubules.

Experimental Procedures

Protein purification and cloning

For purifications from worms, *C. elegans* SKA-1 was amplified from N2 genomic DNA and cloned into pIC26 (*unc*-119; pie1 promotor driving N-terminal GFP-TEV-S fusion). For purifications from *E. coli*, SKA-1 was amplified from N2 cDNA including a C-terminal 7XHis-tag and cloned into pET3aTr. *C. elegans* SKA-3 gene was synthesized (Mr. Gene) and cloned into pET3aTr. Both genes were cloned into the polycistronic expression vector pST39 for co-expression. The *C. elegans* SKA-1 complex truncations ceSKA1 MTDB-7XHis (residues 118-243) and ceSKA1 ΔMTBD-7XHis (residues 1-117) were generated by inverse PCR (iPCR). 7XHis-sfGFP-ceSKA1 was generated by cloning ceSKA1 into a modified version of pET3aTr containing a sequence encoding the N-terminal 7XHIS-sfGFP-tag (Pedelacq et al., 2006). 7XHis-sfGFP-ceSKA1 was transferred into pST39 along with ceSKA3 for co-expression.

His-GFP-hSka1 was generated by cloning hSka1 into a modified version of the transfer vector pST50Tr-HISNDHFR containing a His-GFP-tag. His-GFP-hSka1 was transferred along with hSka2 into pST39 for co-expression. hSka1 MTBD was generated by cloning hSka1 (residues 132-255) into a modified version of the pET3aTr transfer vector containing sequence encoding for a N-terminal His-tag followed by a PreScission protease cleavage site. hSka1 ΔMTBD-7XHis (residues 1-131) was generated by iPCR. GFP-tagged hSka1, hSka1 ΔMTBD, and hSka1 MTDB for expression in human tissue culture cells

and the generation of stable cell lines were generated by cloning the corresponding fragments into pBABEblast-GFP (Shah et al., 2004).

hNdc80 "Broccoli" was generated by cloning Nuf2 (residues 1-348) and Hec1 (residues 1-506-7xHis) into pET3aTr and then into pST39 for co-expression. To generate hNdc80 "Broccoli", Nuf2 (residues 1-348) was cloned into a modified pET3aTr containing sequence encoding a C-terminal GFP-tag. ceNDC80 "Broccoli"-sfGFP was generated by cloning HIM-10 (residues 1-392) into a modified version of pET3aTr containing sequence encoding a C-terminal sfGFP-tag and NDC-80 (residues 1-507-7xHis) into pET3aTr and then into pST39 for co-expression.

Trimeric hSka1 complex variants were purified as described previously (Welburn et al., 2009) with the following modifications. To purify untagged hSka1 complex, GST-hSka3 was bound to glutathione agarose and incubated with lysate from bacteria expressing untagged hSka1 and hSka2 for 1 hr at 4°C. All variants were removed from the glutathione agarose by elution with 50 mM Tris (pH 8.1), 75 mM KCl, 10 mM glutathione. The eluates were supplemented with PreScission protease and dialyzed against 20 mM Hepes (pH 7.0), 150 mM KCl, 1 mM DTT overnight at 4°C, followed by gel filtration on a Superdex 200 column into 20 mM Hepes (pH 7.0), 150 mM KCl, 1 mM DTT. Peak fractions were pooled, concentrated using Vivaspin 20 concentrators with a 30 kDa molecular weight cutoff (GE Healthcare), and snap frozen in liquid nitrogen at a concentration of 0.5-1 mg/ml. All remaining proteins were purified by Ni-NTA affinity purification. Bacterial lysates were prepared in 50 mM potassium

phosphate buffer (KPi) pH 8.0, 300 mM NaCl, 10 mM imidazole, 5 mM beta-mercaptoethanol (bME) incubated with Ni-NTA agarose for 1 hr at 4°C, washed three times with 50 mM KPi (pH 8.0), 500 mM NaCl, 40 mM imidazole, 5 mM βME, followed by elution with 50 mM KPi (pH 7.0), 500 mM NaCl, 250 mM imidazole, 5 mM βME. Proteins were further purified by gel filtration on a Superdex 200 column into 20 mM Hepes (pH 7.0), 150 mM KCl, 1 mM DTT. Peak fractions were pooled, concentrated using Vivaspin 20 concentrators with an appropriate molecular weight cutoff (GE Healthcare) and snap frozen in liquid nitrogen at a concentration of 0.5-1 mg/ml. The His-tag was removed from hSka1 MTBD by PreScission cleavage as described above, prior to gel filtration. Protein concentrations were determined by measuring the absorbance at 280 nm using extinction coefficients derived from the primary protein sequence using the online tool ProtParam.

Point mutations to confer resistance against RNAi knockdown were generated by Quickchange mutagenesis (Agilent) introducing the maximal number of basepair mismatches retaining the same amino acid sequence.

Immunoprecipitations and mass spectrometry

Transgenic worm strains were generated as previously described using ballastic particle bombardment (Cheeseman et al., 2004). Immunoprecipitations from *C. elegans* worms were carried out as previously described (Cheeseman et al., 2004). Purified proteins were identified by mass spectrometry using an LTQ XL

Ion trap mass spectrometer (Thermo) with MudPIT and SEQUEST software described previously (Welburn et al., 2009).

Analytical ultracentrifugation

Sedimentation-velocity experiments for ceSKA1 complex constructs were carried out in 20 mM Hepes (pH 7.0), 150 mM KCl, 1 mM TCEP, using a Beckman Optima XL-I analytical ultracentrifuge in absorbance mode (Biophysical Instrumentation Facility, MIT). Data was collected at 20°C, 30000 rpm, and protein concentrations ranging from 0.5-1 mg/ml. The data was fit using SEDFIT to a model for continuous sedimentation coefficient distribution, assuming a single frictional coefficient for each sample. The molecular weights were estimated using the best-fit frictional coefficients.

Cell culture and RNAi

Stable cell lines derived from HeLa cells were generated as previously described (Shah et al., 2004). Cells were cultured in Dulbecco's modified Eagle's medium supplemented with 10% fetal bovine serum, penicillin/streptomycin, and L-glutamine at 37°C in a humidified atmosphere with 5% CO_2. RNAi experiments were conducted using Lipofectamine RNAiMAX (Invitrogen) using the manufacturers instructions. siRNAs against Ska1 were described previously (Welburn et al., 2009).

Immunofluorescence and Microscopy

Immunofluorescence in human cells was conducted as described previously (Welburn et al., 2009). Microtubules were visualized using the DM1α (Sigma) at 1:2000. To detect kinetochores, anti-centromere antibodies (Antibodies, Inc., Davis, CA) were used at 1:100. To visualize GFP-tagged Ska1, the intrinsic GFP fluorescence was used. Cy2-, Cy3-, and Cy5-conjugated secondary antibodies (Jackson Laboratories) were used at 1:100. DNA was visualized using 10 μg/ml Hoechst. Images were acquired on a DeltaVision Core deconvolution microscope (Applied Precision) equipped with a CoolSnap HQ2 CCD camera. For cold stable microtubule assays, 20 Z-sections were acquired with 0.2 μm spacing, using a 100x 1.4 NA Olympus U-PlanApo objective with 1x1 binning. All images were taken with identical exposure conditions and scaled equally. Images were deconvolved using the DeltaVision software. To quantify kinetochore-microtubule intensity 10 kinetochores pre cell were randomly chosen and the associated microtubule intensity was quantified and normalized by the intensity of the respective ACA signal. To determine the localization of GFP-tagged hSka1 constructs, live cells were imaged by acquiring 8 Z-sections with 1 μm spacing at 100x magnification. Images presented are single Z-sections. To determine the time from nuclear envelope breakdown (NEBD) to anaphase onset, time-lapse movies of live cells were generated using differential interference contrast microscopy at 5 min time intervals. For each time point, 4 Z-sections at 2 μM intervals were acquired by DIC using a 40x objective. A reference image of the respective GFP-tagged hSka1 was taken at each time point using the central Z-

position. The time from the frame in which NEBD was apparent until the first frame in which chromosome segregation or sister kinetochore separation was visible was quantified. Kinetochore oscillations were filmed in 6 s time intervals using mCherry-CENP-A. The oscillation distance was determined from kymographs, measuring the distance along the pole-to-pole axis that the kinetochore moved prior to change of direction.

Total internal reflection fluorescence microscopy

TIR-FM movies were acquired with a Nikon Ti-E inverted microscope with perfect focus, equipped with an Andor Revolution 500 XD laser system (488 nm 50 mW, 640 nm 100 mW), a Ti-TIRF-E motorized illumination unit (Nikon), an Apo 100x/1.49 TIRF objective (Nikon), 1.5x auxiliary magnification, and an Andor iXon3 897 EMCCD-camera using the Andor iQ2 software. 600 images were acquired under continuous illumination with 45 ms exposure times (20 fps). A single image of the microtubules was taken before and after each movie. All imaging was carried out at 30°C. The movies were analyzed with a custom algorithm and manually screened for false. Flow chambers for total internal reflection fluorescence microscopy (TIR-FM) were assembled by taping a 18x18 mm No. 1 coverslip onto a 22x22 mm No. 1.5 coverslip using double-sided tape (Scotch permanent), yielding a channel volume of 5-10 µl. Prior to usage, coverslips were cleaned and silanized essentially as described by Gell *et al.* (Gell et al., 2010). To prepare the coverslips for the microscopy-based analysis of microtubule binding, coverslips were washed in double distilled water (ddH_20)

supplemented with dishwashing detergent while sonicating. Coverslips were then bathed, sequentially, in acetone, ethanol, and ddH_20, before treating with piranha solution (1 part 30% H_2O_2, 2 parts concentrated H_2SO_4) at 60°C for 1 hr. Following three short incubations in ddH_2O, the coverslips were treated with fresh 0.1 M KOH solution for 15 min. After washing with ddH_20 twice, the coverslips were dried with compressed air and transferred into PlusOne Repel Silane ES (GE Healthcare) for 1 hr. Following silanization, the coverslips were sonicated three times in methanol for 5 min, 15 min, and 30 min. After drying with compressed air, the coverslips were stored in a dust free container for up to 1 month before use.

To immobilize microtubules, anti-β-tubulin antibodies (SAP4G5, Sigma, Munich, Germany, T7816) were perfused into the flow chamber at a 1:100 dilution in BRB80 and incubated for 5 min, followed by a wash with 40 µl BRB80. To passivate the surface, 40 µl of a 1% Pluronic F-127 was perfused into the chamber and incubated for 5 min. The channel was prepared for microtubule binding by washing with 40 µl BRB80 containing 15 µM taxol. Taxol-stabilized microtubules containing 5% HiLyte 647 labeled tubulin were bound to the coverslip for 5 min before washing with TIRF buffer: BRB80 supplemented with 7.5 µM taxol, 1 mg/ml BSA, 0.4 mg/ml Casein, and oxygen scavenger (0.2 mg/ml Glucose Oxidase, 0.035 mg/ml Catalase, 4.5 mg/ml glucose, 10 mM DTT). GFP-tagged kinetochore proteins were perfused in TIRF Buffer.

Single particle detection and quantification

A background fluorescence image was calculated for each 2D TIRF image using morphological opening with a 6-um radius disk as the structuring element to remove bright objects smaller than this radius, including the labeled Ska complex particles. The resulting background image, corresponding to the background fluorescence and any non-uniform illumination, was then subtracted from the raw intensity image. Spots corresponding to labeled proteins were segmented from Gaussian-filtered and background-subtracted 2D images at each time point by automatic thresholding as described previously (Mori et al., 2011), followed by watershedding and fitting a 2D Gaussian peak to each detected spot. Only spots in the neighborhood of microtubules (within ~0.5 um) were considered. Spots were linked into tracks based on the distance between each spot and both the expected position and last position of each track. The resulting tracks for each movie were manually screened for accuracy before being included in subsequent analysis. The intensity of each spot was defined as either the total photon counts over all pixels making up the spot, or as the amplitude of the Gaussian peak fit to each spot. The initial intensity of each track was defined as the spot intensity in the second frame of the track. The mean-square displacement (MSD) was computed for a single-particle trajectory with N particle positions $\{\mathbf{r}_i\}_{i=1}^{N} = \{x_i, y_i, z_i\}_{i=1}^{N}$ observed at specific times $\{t_i\}_{i=1}^{N}$ (separated by a time step dt) at different time lags τ (in units of time steps) according to $MSD(\tau) \equiv \langle \Delta\mathbf{r}(\tau)^2 \rangle = \frac{1}{N-\tau}\sum_{i=1}^{N-\tau}|\mathbf{r}_{i+\tau} - \mathbf{r}_i|^2$. Diffusion coefficients for the proteins along the microtubules were then calculated by fitting

the mean-squared displacement of each trajectory with a model of 1D diffusion: $MSD = 2D\tau$.

Microtubule co-sedimentation assays

Microtubule pelleting assays were conducted as described previously (Cheeseman et al., 2006) using taxol stabilized microtubules or dolastatin-10 induced rings. Dolastatin-10 induced rings were generated by incubating 17.3 μM tubulin-dimer in BRB80 with 6% DMSO and 40 μM dolastatin-10 (provided by the Drug Synthesis and Chemistry Branch, Developmental Therapeutics Program, Division of Cancer Treatment and Diagnosis, National Cancer Institute) for 1 hr at room temperature. Rings were purified by pelleting through a cushion of BRB80 with 40% glycerol for 10 min at 300000xg at room temperature. Rings were resuspended in BRB80 with 6% DMSO and 40 μM dolastatin-10. The amount of rings in pellet fractions was quantified by Coommassie staining relative to a standard curve of tubulin on the same gel. Antibodies to detect the Ndc80 complex and the ceSKA1 complex were raised against Ndc80 "Bonsai" and full ceSKA1 complex and affinity purified, as described previously (Desai et al., 2003). The hSka1 antibody was described previously (Welburn et al., 2009). Integrated band intensities of scanned western blots were quantified using Photoshop software and corrected for the local background, by subtracting the integrated intensity of a nearby area of the same size. To determine the signal intensity as a fraction of the protein input, the signal was compared to the intensity of the 10% input sample. If the intensity was lower than the 10% input

band, the fraction was determined by dividing the band intensity by the 10% input intensity. If the band intensity was higher than the 10% input band, the fraction was determined by using a standard curve assuming a linear signal increase from 10% to 100%. All western blots included 100% and 10% input samples for reliable quantification. To determine the fraction bound, the pellet sample fraction was divided by the sum of the pellet and supernatant fractions. The data was fit with Prism using specific binding with a Hill slope.

Dynamic microtubule tracking assays

Tracking assays were conducted as described previously (Grishchuk and Ataullakhanov, 2010; Grishchuk et al., 2005). Briefly, microtubules were grown from coverslip-attached *Chlamydomonas* axonemes in the presence to bovine tubulin and GTP. Stabilizing caps where then assembled by elongating microtubules in the presence GMPCPP, and with Rhodamine-labeled tubulin. After washing chambers with these coverslip-anchored segmented microtubules, GFP-labeled proteins were perfused in motility buffer (BRB80, 4 mM $MgCl_2$, 5 mg/ml BSA, 0.4 mg/ml Casein, 10 mM DTT). Microtubule depolymerization was induced by a brief exposure to a bright green light. Images were acquired and processed using Metamorph, using a Zeiss Axiophot 2, with a 100x 1.4NA objectice, and a Andor iXon3 camera, under continuous illumination at 32°C. Tip intensity was determined with line scans along kymographs, which were background corrected and normalized by the lattice intensity.

Electron Microscopy

Dynamic microtubules were assembled by incubating 45 μM tubulin (Cytoskeleton, Inc.) in 50 mM PIPES pH 6.8, 4 mM $MgCl_2$, 12% (V/V) DMSO, and 2 mM GTP at 34 C for 1 hour. Microtubules were diluted in BRB80 to 4.5 μM in the presence of 2 μM hSka1 complex, ceSKA1 complex, or hNdc80 "Broccoli", immediately added to glow discharged electron microscopy grids and stained with 1% uranyl acetate. Dolastatin-10 induced rings were assembled as described above and incubated at 1 μM with a 1.5-fold excess of hSka1 complex, ceSKA1 complex, or hNdc80 "Broccoli". Images were acquired using FEI Tecnai and FEI Spirit transmission electron microscopes equipped with Teitz (2k x 2k) and Gatan (4k x 4k) CCD cameras.

NMR Spectroscopy

The plasmid containing ceSKA1 MTDB-7XHis was transformed into BL21 (DE3) cells. Cells were grown to an OD600 of 0.6 and induced for 12-16 h at 25 °C with 1 mM isopropyl β-D-1-thiogalactopyranoside (IPTG). ^{15}N and ^{13}C isotope labeled proteins were grown in M9 media containing 1 g ^{15}N-NH_4Cl and 2 g ^{13}C glucose per liter. FILV labeled proteins for time-shared NOESY and 4D NOESY experiments were grown in perdeuterated M9 media with 1 g ^{15}N-NH_4Cl and 2 g ^{2}H-^{13}C-glucose in $^{2}H_2O$. One hour before induction with IPTG the following precursors were added: 0.1 g 15N-l-phenylalanine (Sigma, 490105), 75 mg ketobutyrate sodium $^{13}C/^{1}H$ methyl, deuterated (FBreagents.com; Ile methyl precursor), 300 mg ethyl 2-hydroxy-2-^{13}C methyl 3-oxobutanoate (stereo specific

Leu and Val methyl precursor). The proton at position 4 was hydrolyzed and deuterated according to Gans *et al.* The methyl precursors were stereospecific ^{13}C labeled and protonated resulting in stereospecific labeling of only one of the Leu-λ2 and Val-γ2 methyl groups as previously described (Gans et al., 2010). Cells were harvested by centrifugation and sonicated in 35 ml buffer-1 (50 mM Tris-HCl pH 8.0, 350 mM NaCl, 10 mM imidazole), 3.5 mM β-mercaptoethanol, benzonase, 1 mg ml^{-1} lysozyme and 1 tablet of protease inhibitor cocktail (Complete, Roche). Lysate was cleared by centrifugation at 30000 g for 40 min, applied to Ni-NTA resin (Qiagen) washed with 10 column volumes of Buffer-1 supplemented with 1 M NaCl and 10 column volumes of Buffer-1 supplemented with 40 mM imidazole. ceSKA1 MTBD was eluted in 35 ml buffer-2 (50mM Tris-HCl pH 8.0, 1 M NaCl, 250 mM imidazole) and dialyzed in two steps against 4 l of buffer-3 (20 mM potassium phosphate pH 6.5, 150 mM NaCl, 1 mM DTT). Before concentration of the sample, DTT was added to a final concentration of 1.5 mM. Dialyzed protein was concentrated using Amicon Ultra concentrators with a 10 kDa molecular weight cutoff (Millipore). Samples were prepared for NMR spectroscopy by adding 0.01% NaN_3 and 5% D_2O. For samples for ^{13}C NOESY and HMQC-NOESY-HMQC experiments, which were recorded in D_2O, ceSKA1 MTDB-7XHis was lyophilized and re-suspended in 99.9% ^2H_2O.

All NMR samples were prepared in 20 mM potassium phosphate pH 6.5, 150 mM NaCl, 1.5 mM DTT. Spectra were recorded on Varian/Agilent Inova 600 MHz and 500 MHz and Bruker 700 and 900 MHz spectrometers at 298 K. All spectrometers (with the exception of Varian/Agilent Inova 500 MHz

spectrometer) were equipped with cryogenically cooled probes. Backbone resonance assignments were made by standard triple resonance backbone NMR experiments (HNCA/HNCOCA, HNCO/HNCACO, HNCACB). The side chain residues were assigned using HCCONH, CCONH and HCCH-TOCSY experiments in H_2O. Aromatic side chains were assigned using 2D HBCBCGCDHD and HBCBCGCDCEHE experiments (Yamazaki et al., 1993). NOE constrains were derived from nitrogen dispersed 3D ^{15}N-NOESY-HSQC, carbon dispersed 3D ^{13}C-NOESY-HSQC, ^{13}C and ^{15}N dispersed 3D time-shared HSQC-NOESY (Frueh et al., 2009) and 4D HMQC-NOESY-HMQC experiments (Hiller et al., 2009). A mixing time of 90 ms was used for the ^{15}N-disperesed NOESY-HSQC and the ^{13}C-dispersed NOESY-HSQC. 200 ms mixing time was used for the ^{13}C/^{15}N time-shared HSQC-NOESY and 4D HMQC-NOESY-HMQC experiments. The time-shared NOESY and the 4D-NOESY were recorded with the ^{1}H-^{13}C methyl-Ile-, Leu (λ2)-, Val (γ2)-labeled and Phe protonated sample (Gardner and Kay, 1997) (Gans et al., 2010) in an otherwise deuterated background. The 4D HMQC-NOESY-HMQC was recorded using non-uniform sampling in the three indirect dimensions. 5% of the 3D grid (3 indirect dimensions) was sampled using Poisson-Gap sampling (Hyberts et al., 2010) and the spectrum was reconstructed using iterative soft thresholding approach (Hyberts et al., 2012). All other the other spectra were processed with NMRpipe (Delaglio et al., 1995). All NMR spectra were visualized and analyzed with the programs CcpNmr (Vranken et al., 2005) and CARA (Keller, 2004).

Backbone and side chain resonances were picked and assigned manually in CARA (Keller, 2004), NOEs were picked and assigned manually in CcpNmr (Vranken et al., 2005). Torsion angle constraints were derived from chemical shifts using the program TALOS+ (Shen et al., 2009). NOE intensities were integrated and converted into distance constraints using CcpNmr (Vranken et al., 2005). Hydrogen bond restraints for beta-sheets and helices were assigned when supported by NOEs and secondary structure prediction. 20 structures were created in a simulated annealing protocol using CYANA (Guntert et al., 1997). Structures were visualized with PyMOL and MOLMOL (Koradi et al., 1996). PROCHECK-NMR was used to assess the stereochemical quality of the structure (Laskowski et al., 1996Laskowski et al., 1996).

References

Alushin, G.M., Ramey, V.H., Pasqualato, S., Ball, D.A., Grigorieff, N., Musacchio, A., and Nogales, E. (2010). The Ndc80 kinetochore complex forms oligomeric arrays along microtubules. Nature 467, 805-810.

Ashkenazy, H., Erez, E., Martz, E., Pupko, T., and Ben-Tal, N. (2010). ConSurf 2010: calculating evolutionary conservation in sequence and structure of proteins and nucleic acids. Nucleic Acids Res 38, W529-533.

Bai, R., Durso, N.A., Sackett, D.L., and Hamel, E. (1999). Interactions of the sponge-derived antimitotic tripeptide hemiasterlin with tubulin: comparison with dolastatin 10 and cryptophycin 1. Biochemistry 38, 14302-14310.

Baker, N.A., Sept, D., Joseph, S., Holst, M.J., and McCammon, J.A. (2001). Electrostatics of nanosystems: application to microtubules and the ribosome. Proceedings of the National Academy of Sciences of the United States of America 98, 10037-10041.

Boukari, H., Sackett, D.L., Schuck, P., and Nossal, R.J. (2007). Single-walled tubulin ring polymers. Biopolymers 86, 424-436.

Chan, Y.W., Jeyaprakash, A.A., Nigg, E.A., and Santamaria, A. (2012). Aurora B controls kinetochore-microtubule attachments by inhibiting Ska complex-KMN network interaction. The Journal of cell biology 196, 563-571.

Cheeseman, I.M., Chappie, J.S., Wilson-Kubalek, E.M., and Desai, A. (2006). The conserved KMN network constitutes the core microtubule-binding site of the kinetochore. In Cell, pp. 983-997.

Cheeseman, I.M., and Desai, A. (2008). Molecular architecture of the kinetochore-microtubule interface. In Nat Rev Mol Cell Biol, pp. 33-46.

Cheeseman, I.M., Niessen, S., Anderson, S., Hyndman, F., Yates, J.R., Oegema, K., and Desai, A. (2004). A conserved protein network controls assembly of the outer kinetochore and its ability to sustain tension. In Genes Dev, pp. 2255-2268.

Ciferri, C., Pasqualato, S., Screpanti, E., Varetti, G., Santaguida, S., Dos Reis, G., Maiolica, A., Polka, J., De Luca, J.G., De Wulf, P., et al. (2008). Implications for kinetochore-microtubule attachment from the structure of an engineered Ndc80 complex. In Cell, pp. 427-439.

Coue, M., Lombillo, V.A., and McIntosh, J.R. (1991). Microtubule depolymerization promotes particle and chromosome movement in vitro. The Journal of cell biology 112, 1165-1175.

Daum, J., Wren, J., Daniel, J., Sivakumar, S., McAvoy, J., Potapova, T., and Gorbsky, G. (2009). Ska3 Is Required for Spindle Checkpoint Silencing and the Maintenance of Chromosome Cohesion in Mitosis. In Curr Biol.

Delaglio, F., Grzesiek, S., Vuister, G.W., Zhu, G., Pfeifer, J., and Bax, A. (1995). NMRPipe: a multidimensional spectral processing system based on UNIX pipes. J Biomol NMR 6, 277-293.

DeLuca, J.G., Moree, B., Hickey, J.M., Kilmartin, J.V., and Salmon, E.D. (2002). hNuf2 inhibition blocks stable kinetochore-microtubule attachment and induces mitotic cell death in HeLa cells. The Journal of cell biology 159, 549-555.

Desai, A., and Mitchison, T.J. (1997). Microtubule polymerization dynamics. In Annu Rev Cell Dev Biol, pp. 83-117.

Desai, A., Rybina, S., Muller-Reichert, T., Shevchenko, A., Hyman, A., and Oegema, K. (2003). KNL-1 directs assembly of the microtubule-binding interface of the kinetochore in C. elegans. Genes & development 17, 2421-2435.

Efremov, A., Grishchuk, E.L., McIntosh, J.R., and Ataullakhanov, F.I. (2007). In search of an optimal ring to couple microtubule depolymerization to processive chromosome motions. In Proc Natl Acad Sci USA, pp. 19017-19022.

Frueh, D.P., Leed, A., Arthanari, H., Koglin, A., Walsh, C.T., and Wagner, G. (2009). Time-shared HSQC-NOESY for accurate distance constraints measured at high-field in (15)N-(13)C-ILV methyl labeled proteins. J Biomol NMR 45, 311-318.

Gaitanos, T.N., Santamaria, A., Jeyaprakash, A.A., Wang, B., Conti, E., and Nigg, E.A. (2009). Stable kinetochore-microtubule interactions depend on the Ska complex and its new component Ska3/C13Orf3. The EMBO journal 28, 1442-1452.

Gajiwala, K.S., and Burley, S.K. (2000). Winged helix proteins. Curr Opin Struct Biol 10, 110-116.

Gans, P., Hamelin, O., Sounier, R., Ayala, I., Dura, M.A., Amero, C.D., Noirclerc-Savoye, M., Franzetti, B., Plevin, M.J., and Boisbouvier, J. (2010). Stereospecific isotopic labeling of methyl groups for NMR spectroscopic studies of high-molecular-weight proteins. Angew Chem Int Ed Engl 49, 1958-1962.

Gardner, K.H., and Kay, L.E. (1997). Production and Incorporation of 15N, 13C, 2H (1H-Œ¥1 Methyl) Isoleucine into Proteins for Multidimensional NMR Studies. Journal of the American Chemical Society 119, 7599-7600.

Gell, C., Bormuth, V., Brouhard, G.J., Cohen, D.N., Diez, S., Friel, C.T., Helenius, J., Nitzsche, B., Petzold, H., Ribbe, J., et al. (2010). Microtubule dynamics reconstituted in vitro and imaged by single-molecule fluorescence microscopy. Methods in cell biology 95, 221-245.

Gerdes, K., Howard, M., and Szardenings, F. (2010). Pushing and pulling in prokaryotic DNA segregation. Cell 141, 927-942.

Grishchuk, E.L., and Ataullakhanov, F.I. (2010). In Vitro Assays to Study the Tracking of Shortening Microtubule Ends and to Measure Associated Forces. Method Cell Biol 95, 657-676.

Grishchuk, E.L., Molodtsov, M.I., Ataullakhanov, F.I., and Mcintosh, J.R. (2005). Force production by disassembling microtubules. In Nature, pp. 384-388.

Guntert, P., Mumenthaler, C., and Wuthrich, K. (1997). Torsion angle dynamics for NMR structure calculation with the new program DYANA. Journal of molecular biology 273, 283-298.

Haering, C.H., Schoffnegger, D., Nishino, T., Helmhart, W., Nasmyth, K., and Lowe, J. (2004). Structure and stability of cohesin's Smc1-kleisin interaction. Molecular Cell 15, 951-964.

Hanisch, A., Silljé, H.H.W., and Nigg, E.A. (2006). Timely anaphase onset requires a novel spindle and kinetochore complex comprising Ska1 and Ska2. In EMBO J, pp. 5504-5515.
Hill, T.L. (1985). Theoretical problems related to the attachment of microtubules to kinetochores. In Proc Natl Acad Sci USA, pp. 4404-4408.
Hiller, S., Ibraghimov, I., Wagner, G., and Orekhov, V.Y. (2009). Coupled decomposition of four-dimensional NOESY spectra. Journal of the American Chemical Society 131, 12970-12978.
Holm, L., Kaariainen, S., Rosenstrom, P., and Schenkel, A. (2008). Searching protein structure databases with DaliLite v.3. Bioinformatics 24, 2780-2781.
Hyberts, S.G., Milbradt, A.G., Wagner, A.B., Arthanari, H., and Wagner, G. (2012). Application of iterative soft thresholding for fast reconstruction of NMR data non-uniformly sampled with multidimensional Poisson Gap scheduling. J Biomol NMR 52, 315-327.
Hyberts, S.G., Takeuchi, K., and Wagner, G. (2010). Poisson-gap sampling and forward maximum entropy reconstruction for enhancing the resolution and sensitivity of protein NMR data. Journal of the American Chemical Society 132, 2145-2147.
Jeyaprakash, A.A., Santamaria, A., Jayachandran, U., Chan, Y.W., Benda, C., Nigg, E.A., and Conti, E. (2012). Structural and functional organization of the Ska complex, a key component of the kinetochore-microtubule interface. Molecular Cell 46, 274-286.
Keller, R. (2004). The Computer Aided Resonance Assignment Tutorial (Goldau, CANTINA Verlag).
Koradi, R., Billeter, M., and Wuthrich, K. (1996). MOLMOL: a program for display and analysis of macromolecular structures. J Mol Graph 14, 51-55, 29-32.
Lampert, F., Hornung, P., and Westermann, S. (2010). The Dam1 complex confers microtubule plus end-tracking activity to the Ndc80 kinetochore complex. In J Cell Biol, pp. 641-649.
Laskowski, R.A., Rullmannn, J.A., MacArthur, M.W., Kaptein, R., and Thornton, J.M. (1996). AQUA and PROCHECK-NMR: programs for checking the quality of protein structures solved by NMR. J Biomol NMR 8, 477-486.
Mandelkow, E.M., Mandelkow, E., and Milligan, R.A. (1991). Microtubule dynamics and microtubule caps: a time-resolved cryo-electron microscopy study. In J Cell Biol, pp. 977-991.
McIntosh, J.R., Volkov, V., Ataullakhanov, F.I., and Grishchuk, E.L. (2010). Tubulin depolymerization may be an ancient biological motor. J Cell Sci 123, 3425-3434.
Miranda, J.J.L., De Wulf, P., Sorger, P.K., and Harrison, S.C. (2005). The yeast DASH complex forms closed rings on microtubules. In Nat Struct Mol Biol, pp. 138-143.
Mori, M., Monnier, N., Daigle, N., Bathe, M., Ellenberg, J., and Lenart, P. (2011). Intracellular transport by an anchored homogeneously contracting F-actin meshwork. Current biology : CB 21, 606-611.

Pedelacq, J.D., Cabantous, S., Tran, T., Terwilliger, T.C., and Waldo, G.S. (2006). Engineering and characterization of a superfolder green fluorescent protein. Nat Biotechnol 24, 79-88.

Powers, A.F., Franck, A.D., Gestaut, D.R., Cooper, J., Gracyzk, B., Wei, R.R., Wordeman, L., Davis, T.N., and Asbury, C.L. (2009). The Ndc80 kinetochore complex forms load-bearing attachments to dynamic microtubule tips via biased diffusion. In Cell, pp. 865-875.

Raaijmakers, J.A., Tanenbaum, M.E., Maia, A.F., and Medema, R.H. (2009). RAMA1 is a novel kinetochore protein involved in kinetochore-microtubule attachment. J Cell Sci 122, 2436-2445.

Sanchez-Perez, I., Renwick, S.J., Crawley, K., Karig, I., Buck, V., Meadows, J.C., Franco-Sanchez, A., Fleig, U., Toda, T., and Millar, J.B. (2005). The DASH complex and Klp5/Klp6 kinesin coordinate bipolar chromosome attachment in fission yeast. The EMBO journal 24, 2931-2943.

Shah, J.V., Botvinick, E., Bonday, Z., Furnari, F., Berns, M., and Cleveland, D.W. (2004). Dynamics of centromere and kinetochore proteins; implications for checkpoint signaling and silencing. Current biology : CB 14, 942-952.

Shen, Y., Delaglio, F., Cornilescu, G., and Bax, A. (2009). TALOS+: a hybrid method for predicting protein backbone torsion angles from NMR chemical shifts. J Biomol NMR 44, 213-223.

Theis, M., Slabicki, M., Junqueira, M., Paszkowski-Rogacz, M., Sontheimer, J., Kittler, R., Heninger, A., Glatter, T., Kruusmaa, K., Poser, I., et al. (2009). Comparative profiling identifies C13orf3 as a component of the Ska complex required for mammalian cell division. In EMBO J.

Tien, J.F., Umbreit, N.T., Gestaut, D.R., Franck, A.D., Cooper, J., Wordeman, L., Gonen, T., Asbury, C.L., and Davis, T.N. (2010). Cooperation of the Dam1 and Ndc80 kinetochore complexes enhances microtubule coupling and is regulated by aurora B. In J Cell Biol, pp. 713-723.

Vranken, W.F., Boucher, W., Stevens, T.J., Fogh, R.H., Pajon, A., Llinas, M., Ulrich, E.L., Markley, J.L., Ionides, J., and Laue, E.D. (2005). The CCPN data model for NMR spectroscopy: development of a software pipeline. Proteins 59, 687-696.

Wang, H.W., and Nogales, E. (2005). Nucleotide-dependent bending flexibility of tubulin regulates microtubule assembly. Nature 435, 911-915.

Welburn, J.P.I., Grishchuk, E.L., Backer, C.B., Wilson-Kubalek, E.M., Yates, J.R., and Cheeseman, I.M. (2009). The human kinetochore Ska1 complex facilitates microtubule depolymerization-coupled motility. In Dev Cell, pp. 374-385.

Westermann, S., Wang, H.-W., Avila-Sakar, A., Drubin, D.G., Nogales, E., and Barnes, G. (2006). The Dam1 kinetochore ring complex moves processively on depolymerizing microtubule ends. In Nature, pp. 565-569.

Yamazaki, T., Forman-Kay, J.D., and Kay, L.E. (1993). Two-dimensional NMR experiments for correlating carbon-13.beta. and proton.delta./epsioln. chemical shifts of aromatic residues in 13C-labeled proteins via scalar couplings. J Am Chem Soc 115, 11054-11055.

Zhang, G., Kelstrup, C.D., Hu, X.W., Hansen, M.J., Singleton, M.R., Olsen, J.V., and Nilsson, J. (2012). The Ndc80 internal loop is required for recruitment of the Ska complex to establish end-on microtubule attachment to kinetochores. J Cell Sci.

Chapter IV: Discussion

Key conclusions of this thesis

Aurora B regulates the recruitment of the Astrin-SKAP-LC8 complex to kinetochores

The results presented in this thesis demonstrate that Astrin forms a complex with the previously unidentified kinetochore protein SKAP and the dynein light chain LC8. The Astrin/SKAP/LC8 complex preferentially localizes to bi-oriented kinetochores, directly associates with microtubules, and is essential for mitotic progression. Furthermore, Aurora B kinase, a key regulator of kinetochore-microtubule attachments, has a negative effect on Astrin/SKAP/LC8 recruitment to the kinetochore. Previous studies have shown that Aurora B phosphorylation of its substrates can modulate their biochemical activities. The results presented in this study demonstrate that Aurora B can furthermore regulate the recruitment of factors that stabilize kinetochore microtubule attachments, thereby preferentially excluding these stabilizing factors from improperly attached kinetochores.

The Ska1 complex tracks depolymerizing microtubules by associating with curved protofilaments

The molecular machinery that couples microtubule depolymerization to chromosome movements in human cells was largely unknown. The results presented in this thesis demonstrate that the Ska1 complex possesses many of

the biochemical and biophysical activities required to couple chromosome movement to microtubule depolymerization. The Ska1 complex diffuses on microtubules as a dimer of Ska1/2/3 trimers and has the capacity to autonomously track with depolymerizing microtubules. Importantly, the Ska1 complex can confer this activity to the Ndc80 complex, a key component of the kinetochore microtubule interface. Strikingly, we found that the Ska1 complex, but not the Ndc80 complex, directly associates with the curved protofilament structures present at depolymerizing microtubule ends, leading us to propose a model in which the Ska1 complex tracks with depolymerizing microtubules in part by directly associating with the curved microtubule protofilaments. In addition, we identified the microtubule-binding domain of the Ska1 complex. Preliminary structural analysis of the Ska1 microtubule binding domain revealed two conserved positively charged regions, both of which are necessary for microtubule binding and contain Aurora B phosphorylation sites that reduce the Ska1 microtubule binding affinity when mutated to mimic phosphorylation by Aurora B.

Unanswered questions and future directions

The results presented in this thesis shed light on the cellular functions and molecular mechanisms of the Astrin/SKAP/LC8 and the Ska1 complex. Many open questions, discussed below, remain to be addressed to fully understand their roles in chromosome segregation.

Defining the molecular function of the Astrin/SKAP/LC8 complex

We demonstrated that the Astrin/SKAP/LC8 complex is necessary for mitotic progression. Furthermore, the Astrin/SKAP/LC8 complex is required to recruit CLASP to kinetochores, which stabilizes microtubules. Thus, the Astrin/SKAP/LC8 complex could be required to selectively recruit CLASP to bi-oriented kinetochores to stabilize microtubules. It is not clear whether, in the absence of Astrin/SKAP/LC8 complex activity, the lack of microtubule stabilization at bi-oriented kinetochores is responsible for the mitotic delay in Astrin or SKAP depleted cells. Therefore, it is important to identify the regions the of Astrin/SKAP/LC8 complex that are responsible for recruiting CLASP to the kinetochore, and to determine whether this indeed is the crucial function of the Astrin/SKAP/LC8 complex. Additionally, defining the microtubule-binding region of SKAP could lead to important insight into the direct contribution of the Astrin/SKAP/LC8 complex to kinetochore-microtubule attachment.

Can the Ska1 complex form load-bearing attachments with microtubules?

The results presented in this thesis demonstrate that the Ska1 complex can autonomously track with depolymerizing microtubules and confer this activity to the Ndc80 complex. Importantly, under physiological conditions, these interactions are under load. Bi-oriented sister-chromatids experience pulling forces generated by microtubules emanating from the opposite spindle poles.

These pulling forces are required to generate tension across sister-kinetochores. During anaphase the cytosol through which the chromosomes move generates viscous drag. Therefore, the kinetochore-microtubule attachment site is always under load. To test, whether the Ska1 complex can remain attached to depolymerizing microtubules under load, experiments using a force clamp will need to be carried out. The Ndc80 and Dam1 complexes, which have been implicated in coupling chromosome movement to microtubule depolymerization, both support microsphere movement under load (Asbury et al., 2006; Powers et al., 2009).

Defining the interaction surface between the Ska1 and Ndc80 complexes

The Ska1 complex interacts with the Ndc80 complex in the context of microtubules. Importantly, the microtubule binding domain of the Ska1 complex is unaffected by the presence of the Ndc80 complex on microtubules in pelleting assays, indicating that this domain of the Ska1 complex is not sufficient to interact with the Ndc80 complex. To test whether the interaction between the Ndc80 and Ska1 complexes detected in microtubule pelleting assays is relevant for cell division *in vivo,* it is crucial to identify the region of both complexes responsible for the interaction. Preliminary experiments testing whether the loop region in Ndc80, which has been implicated in recruiting the Ska1 complex to kinetochores *in vivo* (Zhang et al., 2012), were inconclusive (data not shown). Importantly, the Ndc80 loop region has also been shown to recruit Cdt1 to

kinetochores, a protein known for its role in DNA replication (Varma et al., 2012). Recruitment of Cdt1 is required for stable kinetochore-microtubule attachment, and neither Cdt1 nor the Ndc80 loop region, are required for Ska1 complex recruitment in that study. Thus, based on conflicting results in the literature and preliminary experimental results, the involvement of the Ndc80 loop region for Ska1 kinetochore recruitment is poorly defined. Additionally, my preliminary experimental results indicate that Ska3 is not required for the Ska1 complex to interact with Ndc80 as the Ska1/2 complex and the Ndc80 complex bind to microtubules synergistically (data not shown). Thus, the region of the Ska1 complex required to bind to the Ndc80 complex can be narrowed down to the C-terminal half of Ska1 and Ska2.

How do chromosomes congress and remain aligned in the absence of Ska1 microtubule binding activity?

The Ska1 complex is essential for the formation of kinetochore-microtubule interactions (Raaijmakers et al., 2009; Welburn et al., 2009). Depletion of the Ska1 complex results in complete failure of chromosome alignment as well as absence of kinetochore-microtubule interactions. Importantly, cells lacking only the Ska1 microtubule binding domain, or are expressing point mutations in Ska1 that impair microtubule binding, align their chromosomes, but arrest in mitosis with strongly reduced kinetochore fibers and lack chromosome oscillations. Thus, chromosome alignment does not require the Ska1 microtubule binding activity,

but depends on the presence of the remainder of the Ska1 complex. We conclude that the Ska1 complex plays a role in the formation of end-on kinetochore-microtubule attachment, potentially by interacting with and facilitating or organizing Ndc80 microtubule interactions. In addition, Ska1 microtubule binding is required to maintain attachment to depolymerizing microtubules and utilize the force generated to drive chromosome oscillations. This raises the question of how chromosomes remain aligned at the metaphase plate in the absence of Ska1 microtubule binding activity, since Ska1 microtubule binding is required to maintain kinetochore-fibers. Importantly, we propose that the Ska1 complex is necessary to transmit poleward forces derived from microtubule depolymerization to the chromosomes. Therefore, in the absence of Ska1 complex microtubule binding, such forces cannot displace chromosomes from the metaphase plate. As a consequence, the chromosomes would be subject only to polar ejection forces mediated by the chromosome-associated chromokinesins. Polar ejection forces would drive the chromosomes towards the metaphase plate from both poles, thereby causing them to remain positioned in the middle of the spindle.

Microtubule depolymerization derived chromosome motion has also been implicated in chromosome congression. However, the directionality of chromosome congression does not correlate with the number of kinetochore microtubules attached to a congressing chromosome (McEwen et al., 1997), indicating that chromosome congression cannot simply be driven by microtubule

depolymerization. Additional mechanisms must act to transport chromosomes to the metaphase plate, such as plus-end directed movement driven by the kinetochore associated kinesin CENP-E (Kapoor et al., 2006). It is therefore possible that chromosomes are capable of aligning at the metaphase plate without the capacity to utilize the forces derived from microtubule depolymerization, as we propose is the case in the absence of Ska1 microtubule binding activity.

What are the contributions of the C-terminal half of Ska3?

The results presented in this thesis and other studies have assigned functions to Ska1, Ska2 and the first 100 amino acids of Ska3 including complex formation, complex dimerization, and microtubule binding. In human cells, Ska3 is 412 amino acids. It is not known whether the region of Ska3 that is not required for the formation of the trimeric coiled-coil with Ska1 and Ska2 is necessary for cell division. The C-terminal half of Ska3 has a predicted GLEBS motif, a short amino acid sequence that is present in the checkpoint protein Bub1 and binds to Bub3 (Larsen et al., 2007; Theis et al., 2009). Thus, it is possible that the Ska1 complex could interact with checkpoint proteins. Indeed, immune-precipitations of Ska1 followed by mass-spectrometry identified Bub1 and Bub3 as binding partners of Ska1 (Welburn et al., 2009). Furthermore, experiments in chicken DT40 cells demonstrated that chromosomes isolated from cells lacking the Ska1 complex associate with significantly smaller amounts of components the

Anaphase Promoting Complex (Ohta et al., 2010). In addition to interacting with other protein components of the kinetochore, the Ska1 complex has also been proposed to form oligomeric structures on microtubules (Welburn et al., 2009), which could require the C-terminus of Ska3.

Aurora B phosphorylation of the Ska1 complex has recently been shown to regulate the recruitment of the Ska1 complex to kinetochores (Chan et al., 2012). In this thesis, I demonstrated that the phosphorylation sites present on Ska1 do not influence kinetochore localization, but instead control the microtubule binding affinity of the Ska1 complex. Additional Aurora B sites are present in the C-terminal half of Ska3 (S87, S110, S159), which could regulate the kinetochore recruitment of the Ska1 complex. Importantly, residual phosphorylation by Aurora B kinase remains when these residues are mutated to alanine (Chan et al., 2012). Previous work in the lab have identified additional Aurora B phosphorylation sites in Ska3 (S196, S302, S329), which when combined with the sites mentioned above completely eliminate Aurora B phosphorylation of Ska3 (data not shown). Importantly, mutation of these sites to phosphomimetic aspartic acid does not influence the interaction with the Ndc80 complex in the context of microtubules (data not shown). Therefore, phosphorylation of these residues could disrupt the interaction of the Ska1 complex with another kinetochore protein.

Aurora B regulation: Relative contributions of Ska1 complex and Ndc80 complex phosphorylation sites

The Ndc80 complex is a key regulatory target of Aurora B kinase (Cheeseman et al., 2006; DeLuca et al., 2011; Welburn et al., 2010). To destabilize incorrect kinetochore microtubule attachments, the N-terminal tail of Ndc80 is phosphorylated at multiple sites to reduce its microtubule binding affinity. Previous studies and the results presented in this thesis have demonstrated that the localization of the Ska1 complex as well as it microtubule binding affinity is inhibited by Aurora B kinase phosphorylation (Chan et al., 2012). Furthermore, chromosome alignment after washout of the Eg5-inhbitor monastrol is impaired when the Ska1 complex cannot be phosphorylated by Aurora B, suggesting that phosphorylation of the Ska1 complex is necessary for the correction of erroneous kinetochore-microtubule attachments (Chan et al., 2012). Interestingly, both microtubule binding and kinetochore localization of the Ska1 complex are regulated by Aurora B phosphorylation. Ska1 microtubule binding is required to maintain kinetochore-fibers, while the localization of the Ska1 complex to the kinetochore, even when it lacks microtubule binding activity, is required for the formation of kinetochore-microtubule attachments. Thus, Aurora B phosphorylation of the Ska1 complex would strongly destabilize kinetochore-microtubule attachments, since the Ska1 complex, when fully phosphorylated, neither associates with microtubules nor localizes to the kinetochore.

Regulation of the kinetochore-microtubule attachment through Aurora B phosphorylation of the Ndc80 complex and the Ska1 complex are mechanistically different. The Ndc80 complex localizes to the kinetochore throughout mitosis and its levels at the kinetochore are unaffected by Aurora B activity (Welburn et al., 2010). Therefore, the Ndc80 complex starts out in a low affinity state, before the kinetochore associates with microtubules, since the tension required to spatially separate it from Aurora B kinase is not yet established. Thus, while kinetochore-microtubule attachment matures, the Ndc80 complex increases its affinity for microtubules, selectively stabilizing correct kinetochore-microtubule attachments. The Ska1 complex on the other hand, accumulates at the kinetochore throughout prometaphase. Additional Ska1 complex therefore is recruited to bi-oriented kinetochores, stabilizing these attachments. Importantly, if due to an error bi-orientation is lost, phosphorylation of the Ska1 complex would allow the kinetochore to dissociate from the microtubules, by reducing its microtubule binding affinity and displacing it from kinetochores. However, although this model explains many features observed for error correction, a key question remains how initial microtubule attachments are established if the Ndc80 complex is in a low affinity state for microtubules and the Ska1 complex only weakly localizes to kinetochores.

Concluding remarks

The work presented in this thesis expands our understanding of the molecular mechanisms underlying kinetochore microtubule attachment. Establishing and maintaining sister-chromatid bi-orientation is the crucial step to ensure equal chromosome segregation. Thus, tension across sister-kinetochores derived from microtubule depolymerization ultimately ensures equal chromosome segregation. The Ska1 complex is essential for this process, but more work is required to fully understand the molecular details of how the Ska1 complex can harness the energy from depolymerizing microtubules to assure equal segregation of the genomic material during cell division.

References

Asbury, C.L., D.R. Gestaut, A.F. Powers, A.D. Franck, and T.N. Davis. 2006. The Dam1 kinetochore complex harnesses microtubule dynamics to produce force and movement. *In* Proc Natl Acad Sci USA. Vol. 103. 9873-9878.

Chan, Y.W., A.A. Jeyaprakash, E.A. Nigg, and A. Santamaria. 2012. Aurora B controls kinetochore-microtubule attachments by inhibiting Ska complex-KMN network interaction. *The Journal of cell biology.* 196:563-571.

Cheeseman, I.M., J.S. Chappie, E.M. Wilson-Kubalek, and A. Desai. 2006. The conserved KMN network constitutes the core microtubule-binding site of the kinetochore. *In* Cell. Vol. 127. 983-997.

DeLuca, K.F., S.M. Lens, and J.G. DeLuca. 2011. Temporal changes in Hec1 phosphorylation control kinetochore-microtubule attachment stability during mitosis. *J Cell Sci.* 124:622-634.

Kapoor, T.M., M.A. Lampson, P. Hergert, L. Cameron, D. Cimini, E.D. Salmon, B.F. McEwen, and A. Khodjakov. 2006. Chromosomes can congress to the metaphase plate before biorientation. *In* Science. Vol. 311. 388-391.

Larsen, N.A., J. Al-Bassam, R.R. Wei, and S.C. Harrison. 2007. Structural analysis of Bub3 interactions in the mitotic spindle checkpoint. *In* Proc Natl Acad Sci USA. Vol. 104. 1201-1206.

McEwen, B.F., A.B. Heagle, G.O. Cassels, K.F. Buttle, and C.L. Rieder. 1997. Kinetochore fiber maturation in PtK1 cells and its implications for the mechanisms of chromosome congression and anaphase onset. *In* J Cell Biol. Vol. 137. 1567-1580.

Ohta, S., J.C. Bukowski-Wills, L. Sanchez-Pulido, L. Alves Fde, L. Wood, Z.A. Chen, M. Platani, L. Fischer, D.F. Hudson, C.P. Ponting, T. Fukagawa, W.C. Earnshaw, and J. Rappsilber. 2010. The protein composition of mitotic chromosomes determined using multiclassifier combinatorial proteomics. *Cell.* 142:810-821.

Powers, A.F., A.D. Franck, D.R. Gestaut, J. Cooper, B. Gracyzk, R.R. Wei, L. Wordeman, T.N. Davis, and C.L. Asbury. 2009. The Ndc80 kinetochore complex forms load-bearing attachments to dynamic microtubule tips via biased diffusion. *In* Cell. Vol. 136. 865-875.

Raaijmakers, J.A., M.E. Tanenbaum, A.F. Maia, and R.H. Medema. 2009. RAMA1 is a novel kinetochore protein involved in kinetochore-microtubule attachment. *J Cell Sci.* 122:2436-2445.

Theis, M., M. Slabicki, M. Junqueira, M. Paszkowski-Rogacz, J. Sontheimer, R. Kittler, A.K. Heninger, T. Glatter, K. Kruusmaa, I. Poser, A.A. Hyman, M.T. Pisabarro, M. Gstaiger, R. Aebersold, A. Shevchenko, and F. Buchholz. 2009. Comparative profiling identifies C13orf3 as a component of the Ska complex required for mammalian cell division. *The EMBO journal.* 28:1453-1465.

Varma, D., S. Chandrasekaran, L.J. Sundin, K.T. Reidy, X. Wan, D.A. Chasse, K.R. Nevis, J.G. Deluca, E.D. Salmon, and J.G. Cook. 2012. Recruitment of the human Cdt1 replication licensing protein by the loop domain of Hec1 is required for stable kinetochore-microtubule attachment. *Nature Cell Biology*. 14:593-603.

Welburn, J.P., M. Vleugel, D. Liu, J.R. Yates, 3rd, M.A. Lampson, T. Fukagawa, and I.M. Cheeseman. 2010. Aurora B phosphorylates spatially distinct targets to differentially regulate the kinetochore-microtubule interface. *Molecular Cell*. 38:383-392.

Welburn, J.P.I., E.L. Grishchuk, C.B. Backer, E.M. Wilson-Kubalek, J.R. Yates, and I.M. Cheeseman. 2009. The Human Kinetochore Ska1 Complex Facilitates Microtubule Depolymerization-Coupled Motility. *Dev Cell*. 16:374-385.

Zhang, G., C.D. Kelstrup, X.W. Hu, M.J. Hansen, M.R. Singleton, J.V. Olsen, and J. Nilsson. 2012. The Ndc80 internal loop is required for recruitment of the Ska complex to establish end-on microtubule attachment to kinetochores. *J Cell Sci*.

Appendix:

Chromosome Segregation: Keeping Kinetochores in the Loop

Reprinted from Cell Press:

Jens C. Schmidt and Iain M. Cheeseman. Chromosome Segregation: Keeping Kinetochores in the Loop. 2011. *Curr Biol.* 21(3):R110-2.

Copyright © 2011 with permission from Cell Press.

The Ndc80 complex is a key component of the kinetochore-microtubule interface. Two studies now demonstrate that a conserved loop region within the extended coiled-coil of Ndc80 plays an unexpected role in recruiting proteins to the kinetochore.

Chromosome segregation in eukaryotes requires that the macromolecular kinetochore complex, built on foundation of centromeric chromatin, interact with the microtubules from the mitotic spindle [1]. The four protein Ndc80 complex is a component of the conserved microtubule binding KNL-1/Mis12 complex/Ndc80 complex (KMN) network, which is a key player in the kinetochore-microtubule interface. The Ndc80 complex is essential for the formation of kinetochore-microtubule interactions by binding to microtubules directly [2]. The Ndc80 complex also plays other important roles in kinetochore function in addition to binding to microtubules, including the recruitment of components of the spindle assembly checkpoint [3]. Previous structural analyses have revealed that the Ndc80 complex is a rod-shaped molecule with an extended coiled-coil domain spanning ~55 nm with globular domains at either end of the coiled coil [2, 4, 5]. The binding of Ndc80 to microtubules requires its calponin homology (CH) domain and its positively charged N-terminal tail, which directly contact microtubules and contain key residues involved in the correction of erroneous kinetochore-microtubule interactions [2, 6, 7]. Previous structure-function analyses have focused primarily on the role of these two regions, and have assumed that the extended coiled-coil region functions exclusively as a linker

between the inner and outer kinetochore. Interestingly, the Ndc80 coiled-coil is not uniform, but instead contains a "kink" in its structure whose location coincides with a conserved "loop" inserted into the coiled-coil domain ([5, 8]; Figure 1A). Despite this conserved structural feature within the coiled-coil, no specific function had been associated with the loop-region of Ndc80. Now, two papers analyzing the fungal Ndc80 complex have defined protein-protein interactions with this loop that are critical for proper kinetochore-microtubule attachments.

To generate an interface with microtubules, Ndc80 does not function in isolation. Recent studies have demonstrated that the budding yeast Dam1 complex, which also binds to microtubules, associates with the microtubule-bound Ndc80 complex to generate a synergistic microtubule binding and plus end tracking unit [9, 10]. However, how two distinct microtubule binding activities could be coordinated in the context of microtubules was unclear. Importantly, although Ndc80 is present in all eukaryotes, Dam1 homologues have thus far only been identified in fungi. Since the presence of the Ndc80 loop region is also conserved, its function has likely diverged in higher eukaryotes. Work from the Tanaka and Toda labs now demonstrates that the loop region of Ndc80 is required to recruit the Dam1 complex in *S. cerevisiae* and the XMAP215/Stu2 homologue Dis1 in *S. pombe* respectively [11, 12].

To analyze the role of the Ndc80 loop, Maure and colleagues [12] took a targeted approach to generate mutations that specifically disrupt the loop region of Ndc80 in budding yeast. These mutants retain kinetochore targeting of the

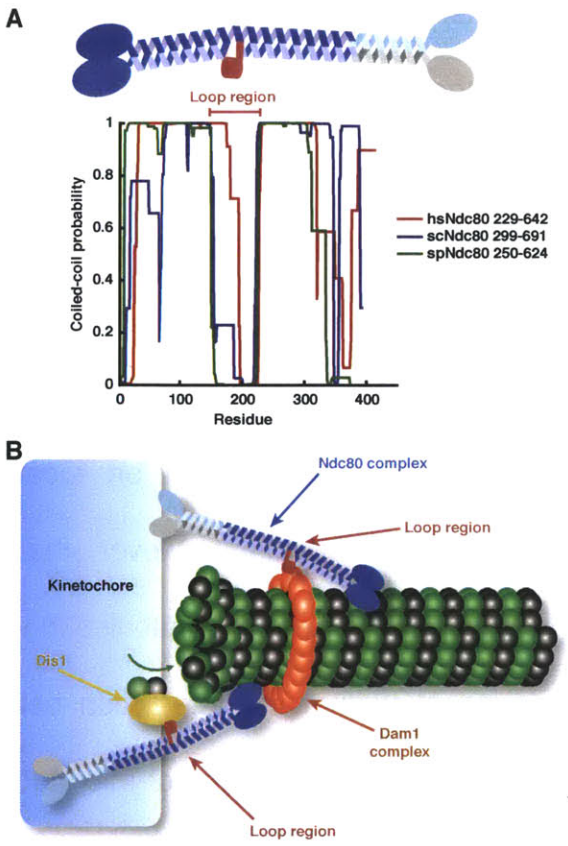

Figure 1. (A) Top, schematic model of the Ndc80 complex with the loop colored in red. Bottom, the position of the "loop" inserted in the Ndc80 coiled-coil is conserved throughout eukaryotes. Graph shows coiled-coil probability predicted from the Coils Server of Ndc80 from *S. cerevisiae*, *Homo sapiens* and *S. pombe* aligned by the start of the predicted coiled-coil. The dip in coiled-coil prediction corresponds to the "loop" region. (B) Schematic model for Ndc80 loop function showing contacts between the loop region and the Dam1 complex and Dis1. Connections between the Ndc80 loop and Dam1 may stabilize end on attachments, while binding of the loop to Dis1 may recruit the microtubule polymerizing activity of the Dis1/Stu2 family to kinetochores.

Ndc80 complex, indicating that the Ndc80 complex remains intact, but are temperature sensitive for growth. Phenotypic analysis of the these mutants revealed that chromosomes fail to achieve bi-orientation and only infrequently form end-on kinetochore-microtubule interactions in a chromosome recapture

assay, phenotypes reminiscent of defects in the Dam1 complex [13]. Based on the phenotypic resemblance between the *ndc80* loop mutants and loss of function mutations in the Dam1 complex, Maure *et al* [12] tested whether there is a loop-dependent interaction between Ndc80 and the Dam1 complex. Indeed, the Ndc80-Dam1 interaction is eliminated in the loop mutants based on yeast two hybrid analysis, and Dam1 less efficiently associated with kinetochores in cells expressing the Ndc80 loop mutants based on localization and chromatin immunoprecipitation (ChIP) experiments. However, the capacity of the Dam1 complex to recruit the Ndc80 complex to microtubules *in vitro* is unchanged in the *ndc80* loop mutants suggesting that the interaction between the Ndc80 loop-region and the Dam1 complex in the context of microtubules may involve more than the tested loop region. In total, Maure *et al* [12] conclude that the loop region of Ndc80 is required for the formation of stable end-on kinetochore microtubule interactions via the recruitment of Dam1 complex to kinetochores.

Taking a parallel approach in fission yeast, Hsu and Toda [11] identified mutations in the loop of Ndc80 by random mutagenesis followed by a screen for defects in spindle assembly. Mutations in the *S. pombe* Ndc80 loop lead to an unstable spindle phenotype, in which kinetochore microtubules are formed inefficiently and hence stable kinetochore-microtubule interactions are never established. The authors demonstrate that this phenotype can be suppressed by overexpression of Dis1, the *S. pombe* homologue of the microtubule polymerase Stu2/XMAP215. Dis1 localizes to kinetochores and is required for proper

microtubule dynamics, but has not been implicated in mediating kinetochore microtubule attachments directly [14, 15]. Consistent with a loop-dependent recruitment of Dis1, the localization of Dis1 to kinetochores is lost when the Ndc80 loop is mutated. In addition, based on several distinct approaches, Hsu *et al* [11] demonstrate Ndc80 and Dis1 interact directly in a manner that is dependent on the loop region of Ndc80. Interestingly, expression of an Ndc80 mutant lacking the N-terminal 95 amino acids, which are crucial for the Ndc80 microtubule interaction, was able to partially rescue the loop mutant phenotype, demonstrating a separation of function between the loop region and the microtubule binding activity of Ndc80. Strikingly, artificially localizing Dis1 to kinetochores by tethering it to the Ndc80 complex component Nuf2 was able to partially suppress the phenotypes associated with the loss of Ndc80 loop function, indicating that recruitment of Dis1 to the kinetochore is an important function of the Ndc80 loop in fission yeast. In total, Hsu *et al* [11] propose a model in which Ndc80 recruits Dis1 to kinetochores via its loop region to facilitate proper spindle formation.

Based on these two studies, it is now clear that the conserved loop region of Ndc80 plays a key role in controlling of spindle dynamics in fission yeast and the formation of proper end-on kinetochore microtubule interactions in budding yeast. Due to its elongated shape, the Ndc80 complex can associate with microtubules laterally, while spanning the dynamic end of the microtubule. A protein-protein interaction domain located within the coiled-coil stalk would

enable Ndc80 to specifically recruit other proteins into close proximity with the microtubule plus end (Figure 1B). Although the presence of this loop appears to be conserved throughout eukaryotes, the protein activity recruited by Ndc80 may depend on the specific requirements posed by the kinetochore architecture of each species. It is striking that the conserved loop region of Ndc80 has such different apparent functions in *S. cerevisiae* and *S. pombe*, raising important questions about their differential requirements for kinetochore-microtubule interactions. In addition, while homologues of the Dam1 complex have not been found in metazoans, the loop region of Ndc80 is conserved throughout eukaryotes. Since the Dam1 complex is present, but non-essential in fission yeast [16], it is tempting to speculate that fission yeast might be an evolutionary intermediate and the divergent function of the Ndc80 loop in this species reflects the adaptation to the requirements of multiple microtubule binding sites at a single kinetochore (budding yeast kinetochores, in contrast, interact with a single microtubule). Future work to define the contribution of the Ndc80 loop region in other species will be important to understand how kinetochore architecture is tailored to the functional requirements of kinetochore-microtubule attachment in different organisms.

In total, these studies provide significant insight into how the multiple microtubule binding activities at a kinetochore are integrated to facilitate kinetochore-microtubule interactions.

References

1. Cheeseman, I.M., and Desai, A. (2008). Molecular architecture of the kinetochore-microtubule interface. In Nat Rev Mol Cell Biol, Volume 9. pp. 33-46.
2. Cheeseman, I.M., Chappie, J.S., Wilson-Kubalek, E.M., and Desai, A. (2006). The conserved KMN network constitutes the core microtubule-binding site of the kinetochore. In Cell, Volume 127. pp. 983-997.
3. Santaguida, S., and Musacchio, A. (2009). The life and miracles of kinetochores. In EMBO J, Volume 28. pp. 2511-2531.
4. Ciferri, C., Pasqualato, S., Screpanti, E., Varetti, G., Santaguida, S., Dos Reis, G., Maiolica, A., Polka, J., De Luca, J., and De Wulf, P. (2008). Implications for kinetochore-microtubule attachment from the structure of an engineered Ndc80 complex. In Cell, Volume 133. pp. 427-439.
5. Wang, H.W., Long, S., Ciferri, C., Westermann, S., Drubin, D., Barnes, G., and Nogales, E. (2008). Architecture and flexibility of the yeast Ndc80 kinetochore complex. J Mol Biol *383*, 894-903.
6. Deluca, J.G., Gall, W.E., Ciferri, C., Cimini, D., Musacchio, A., and Salmon, E.D. (2006). Kinetochore microtubule dynamics and attachment stability are regulated by Hec1. In Cell, Volume 127. pp. 969-982.
7. Wilson-Kubalek, E.M., Cheeseman, I.M., Yoshioka, C., Desai, A., and Milligan, R.A. (2008). Orientation and structure of the Ndc80 complex on the microtubule lattice. In J Cell Biol, Volume 182. pp. 1055-1061.
8. Maiolica, A., Cittaro, D., Borsotti, D., Sennels, L., Ciferri, C., Tarricone, C., Musacchio, A., and Rappsilber, J. (2007). Structural analysis of multiprotein complexes by cross-linking, mass spectrometry, and database searching. Molecular & Cellular Proteomics *6*, 2200-2211.
9. Lampert, F., Hornung, P., and Westermann, S. (2010). The Dam1 complex confers microtubule plus end-tracking activity to the Ndc80 kinetochore complex. Journal of Cell Biology *189*, 641-649.
10. Tien, J.F., Umbreit, N.T., Gestaut, D.R., Franck, A.D., Cooper, J., Wordeman, L., Gonen, T., Asbury, C.L., and Davis, T.N. (2010). Cooperation of the Dam1 and Ndc80 kinetochore complexes enhances microtubule coupling and is regulated by aurora B. Journal of Cell Biology *189*, 713-723.
11. Hsu, K.-S., and Toda, T. (2011). Ndc80 internal loop interacts with Dis1/TOG to ensure proper kinetochore-spindle attachment in fission yeast. Current Biology.
12. Maure, J.-F., Komoto, S., Oku, Y., Mino, A., Pasqualato, S., Natsume, K., Clayton, L., Musacchio, A., and Tanaka, T.U. (2011). The Ndc80 loop region facilitates formation of kinetochore attachment to the dynamic microtubule plus end. Current Biology.

13. Tanaka, K., Mukae, N., Dewar, H., van Breugel, M., James, E.K., Prescott, A.R., Antony, C., and Tanaka, T.U. (2005). Molecular mechanisms of kinetochore capture by spindle microtubules. Nature *434*, 987-994.
14. Nakaseko, Y., Goshima, G., Morishita, J., and Yanagida, M. (2001). M phase-specific kinetochore proteins in fission yeast: Microtubule-associating Dis1 and Mtc1 display rapid separation and segregation during anaphase. Current Biology *11*, 537-549.
15. Al-Bassam, J., van Breugel, M., Harrison, S.C., and Hyman, A. (2006). Stu2p binds tubulin and undergoes an open-to-closed conformational change. Journal of Cell Biology *172*, 1009-1022.
16. Sanchez-Perez, I., Renwick, S.J., Crawley, K., Karig, I., Buck, V., Meadows, J.C., Franco-Sanchez, A., Fleig, U., Toda, T., and Millar, J.B.A. (2005). The DASH complex and Klp5/Klp6 kinesin coordinate bipolar chromosome attachment in fission yeast. Embo Journal *24*, 2931-2943.

The Ska1 microtubule-binding domain forms spirals around microtubules

Jens C. Schmidt, Elizabeth Wilson-Kubalek, Ron Milligan, Iain M. Cheeseman.
Elizabeth Wilson-Kubalek carried out electron microscopy.

Introduction

The Ska1 complex is essential for the formation of kinetochore-microtubule attachments (Raaijmakers et al., 2009; Welburn et al., 2009). The results presented in this thesis demonstrate that the C-terminal half of Ska1 is the microtubule binding domain (MTBD) of the Ska1 complex (see Chapter III). Furthermore, structural analysis of the ceSKA1 MTBD revealed two conserved basic surface areas, which are required for microtubule binding. It remains unknown, whether the Ska1 complex binds to microtubules in an ordered manner. Here, we present structural analysis of the Ska1 complex binding to taxol stabilized microtubules using negative stain electron microscopy. We demonstrate that while the full Ska1 complex does not seem to bind to microtubules in a well-ordered manner the MTDB of both ceSKA1 and hSka1 forms striking spiral like structures around microtubules.

Results

To structurally analyze the Ska1 complex binding to microtubules, we imaged taxol-stabilized microtubules decorated with various Ska1 complex constructs using negative stain electron microscopy. The full Ska1 complex readily decorates microtubules but does not form well-ordered repetitive structures (Fig. 1). Strikingly, both human and *C. elegans* Ska1 MTBD form highly repetitive spiral like structures around microtubules, indicating that it binds to microtubule in well-ordered fashion (Fig. 1).

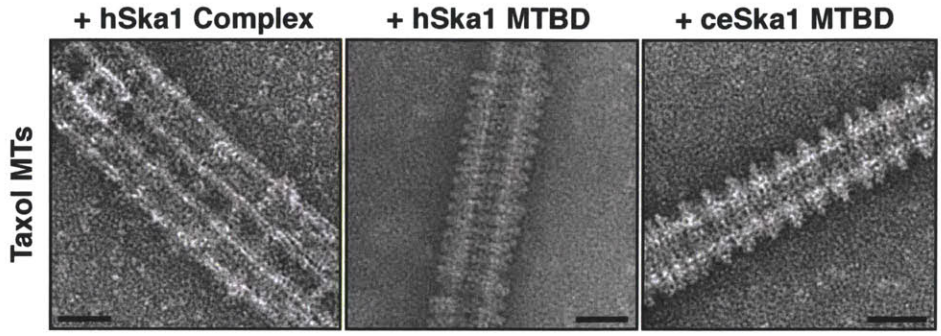

Figure 1. The Ska1 MTBD forms spirals around microtubules. Electron micrographs showing the various Ska1 complex constructs decorating taxol stabilized microtubules (Scale bars, 25 nm). The Ska1 MTBD but not the full complex forms highly repetitive spirals around microtubules.

Discussion

To understand the molecular details of the Ska1 complex binding to microtubules it is important to define its binding site on the microtubule. Here, we demonstrate that the Ska1 MTBD forms highly repetitive spirals around microtubules. Importantly, both human and *C. elegans* homologues of the Ska1 MTBD domain have this activity, indicating that the structural features underlying the formation of these spirals are evolutionarily conserved. In the context of the full Ska1 complex the tight packing if the MTBD is most likely sterically hindered by the presence of Ska2, Ska3 and the N-terminal half of Ska1, since the full Ska1 complex does not form these striking spirals. There are two alternative hypotheses to explain the spiral formation. First, the Ska1 microtubule-binding domain has a defined binding site on the microtubule surface and the spirals are a manifestation of the repetitive helical nature of the microtubule lattice.

Importantly, the spiral formations seems to be a cooperative process, since microtubule appear either fully covered by Ska1 MTBD spirals or are entirely undecorated (data not shown), indicating that the Ska1 MTBD domain might self-associate in the context of the spirals. Second, the spirals could be composed of a layer of Ska1 MTBD and a curved tubulin protofilament wrapped around this the Ska1 MTDB payer, perpendicular to the axis of the microtubule. The formation of such a structure has been demonstrated for the microtubule-binding domain of the kinesin-13 (Tan et al., 2008). Importantly, the additional density of the spirals on the microtubules is too large to be accounted for by merely the Ska1 MTBD, which has a diameter of approximately 4 nm (data not shown). Furthermore, there are additional parallels between kinesin-13 and the Ska1 MTBD domain: Both the Ska1 complex and kinesin-13's accelerate microtubule depolymerization (Chapter III, (Desai et al., 1999)), bind to dolastain-10 induced rings (Chapter III, (Moores and Milligan, 2008)), and have surfaces important for microtubule binding on opposite faces of their respective microtubule binding domain (data not shown, (Tan et al., 2008)). In total, these parallels lead me to favor the latter model and higher resolution electron microscopy data will be able to distinguish the two models.

Experimental Procedures

Electron Microscopy

Microtubules were assembled by incubating 45 μM tubulin (Cytoskeleton, Inc.) in 50 mM PIPES pH6.8, 4 mM $MgCl_2$, 12% (V/V) DMSO, 20 μM taxol, and 2 mM GTP at 34 C for 1 hour. Microtubules were diluted in BRB80 to 4.5 μM in the presence of equimolar amounts of hSka1 complex, hSka1 MTBD, or *C. elegans* MTBD and immediately added to glow discharged electron microscopy grids and stained with 1% uranyl acetate. Images were acquired using FEI Tecnai and FEI Spirit transmission electron microscopes equipped with Teitz (2k x 2k) and Gatan (4k x 4k) CCD cameras.

References

Desai, A., S. Verma, T.J. Mitchison, and C.E. Walczak. 1999. Kin I kinesins are microtubule-destabilizing enzymes. *Cell.* 96:69-78.

Moores, C.A., and R.A. Milligan. 2008. Visualisation of a kinesin-13 motor on microtubule end mimics. *Journal of molecular biology.* 377:647-654.

Raaijmakers, J.A., M.E. Tanenbaum, A.F. Maia, and R.H. Medema. 2009. RAMA1 is a novel kinetochore protein involved in kinetochore-microtubule attachment. *J Cell Sci.* 122:2436-2445.

Tan, D., W.J. Rice, and H. Sosa. 2008. Structure of the kinesin13-microtubule ring complex. *Structure.* 16:1732-1739.

Welburn, J.P.I., E.L. Grishchuk, C.B. Backer, E.M. Wilson-Kubalek, J.R. Yates, and I.M. Cheeseman. 2009. The Human Kinetochore Ska1 Complex Facilitates Microtubule Depolymerization-Coupled Motility. *Dev Cell.* 16:374-385.